General Disclaimer

One or more of the Following Statements may affect this Document

- This document has been reproduced from the best copy furnished by the organizational source. It is being released in the interest of making available as much information as possible.

- This document may contain data, which exceeds the sheet parameters. It was furnished in this condition by the organizational source and is the best copy available.

- This document may contain tone-on-tone or color graphs, charts and/or pictures, which have been reproduced in black and white.

- This document is paginated as submitted by the original source.

- Portions of this document are not fully legible due to the historical nature of some of the material. However, it is the best reproduction available from the original submission.

Produced by the NASA Center for Aerospace Information (CASI)

NASA CR 73260

AVAILABLE TO THE PUBLIC

EXOTECH
INCORPORATED

FACILITY FORM 602

N69 13357
(ACCESSION NUMBER) (THRU)

112 1
(PAGES) (CODE)

NASA-CR 73260 03
(NASA CR OR TMX OR AD NUMBER) (CATEGORY)

DEC 1969
RECEIVED
NASA STI FACILITY
INPUT BRANCH

FINAL REPORT

on the

Design, Development and Fabrication of a Precision Autocollimating Solar Sensor (PASS)

NASA CR 73260
AVAILABLE TO THE PUBLIC

Prepared Under Contract

NAS 2-4050

for the

National Aeronautics and Space Administration
Ames Research Center
Moffett Field, California 94035

by
D. L. Fain/J. M. Hall/ D. F. Johnson
EXOTECH INCORPORATED
12721 Twinbrook Parkway
Rockville, Maryland 20852

TR IC033

June 1968

DEC 1968
RECEIVED
NASA STI FACILITY
INPUT BRANCH

TABLE OF CONTENTS

SECTION			Page
	ILLUSTRATIONS		iii
	ABSTRACT		v
1.0	INTRODUCTION		1-1
	1.1	Summary	1-3
2.0	DESCRIPTION OF HARDWARE		2-1
	2.1	Sensor Unit	2-1
	2.1.1	Solar Aspect Sensing System	2-1
	2.1.2	Optical Design	2-4
	2.1.3	Knife Edge Reticle	2-4
	2.1.4	Filter	2-8
	2.1.5	Solar Cells	2-8
	2.1.6	Measurement Program	2-12
	2.1.7	Autocollimator Unit	2-14
	2.1.8	Mounting Assembly	2-14
	2.2	Sensor Amplifier Unit	2-18
	2.3	Signal Processor Unit	2-20
3.0	TEST AND CALIBRATION		3-1
	3.1	Optical Sensor Testing	3-1
	3.2	Signal Processor Testing	3-4
	3.2.1	Sensor Channel Transfer Curve Evaluation	3-4
	3.2.2	Autocollimator Channel Transfer Curves	3-4
	3.2.3	Summary	3-4
	3.3	Sensor Amplifier Testing	3-4
	3.3.1	Gain Evaluation	3-7
	3.3.2	Offset Control Evaluation	3-7
	3.3.3	Zero Drift Evaluation	3-7
	3.3.4	Noise	3-7
	3.3.5	Offset Control Stability	3-9
	3.4	Solar Cell Experiment Testing	3-9
	3.4.1	Electronics Testing	3-9
	3.4.2	Cell Calibration	3-9
	3.4.3	Thermistor Calibration	3-9
	3.4.4	Standard Cell Calibration	3-12
4.0	FLIGHT REPORT		4-1
	4.1	Preflight Checks	4-1
	4.2	Flight Chronology	4-3
	4.2.1	Flight Highlights	4-3
	4.3	Calibration	4-6
	4.4	Pointing	4-8

			Page
4.0	FLIGHT REPORT (cont'd)		
	4.4.1	Absolute Pointing	4-14
	4.4.2	Pitch Axis	4-14
	4.4.3	Yaw Axis	4-15
	4.5	Solar Cell Experiment	4-16
5.0	CONCLUSIONS		5-1
	5.1	Optical Components	5-1
	5.2	Electronics	5-1
	5.3	Flight Report	5-3
	5.4	Solar Cell Experiment	5-4
APPENDIX			A-1

ILLUSTRATIONS

FIGURE		Page
1-1	PASS System	1-6
2-1	PASS Block Diagram	2-2
2-2	PASS Sun Sensor Optical Layout	2-3
2-3	Completed Reticle Block	2-6
2-4	Solar Cell Equivalent Circuit	2-9
2-5	Solar Cell Relative Spectral Response-Production Limits	2-11
2-6	Detector Test Set-Up	2-13
2-7	Pre-flight Output Change vs Temperature Data, Solar Simulator With Filter A, Exotech	2-15
2-8	Autocollimator Reticle Assembly	2-16
2-9	Sensor Assembly	2-17
2-10	Signal Processor Unit	2-21
2-11	Solar Sensor Channel Transfer Characteristics	2-22
2-12	Solar Cell Experiment After Recovery	2-26
2-13	Solar Cell Experiment Assembly	2-27
2-14	Solar Cell Experiment Telemetry Format	2-29
3-1	Pitch Sun Sensor Transfer Curve ATP 101 7.2.1.2	3-2
3-2	Pitch Autocollimator Transfer Curve ATP 101 7.12	3-3
3-3	Thermistor Calibration System #1	3-11
4-1	Yaw Axis Check	4-2
4-2	Pitch Axis Check	4-2
4-3	Sensor Connections	4-4
4-4	Sensor Mounting	4-5
4-5	PASS Flight Data	4-13
4-6	Solar Cell Experiment Flight Records	4-17
4-7	PASS Flight Record	4-21 - 4-34

ILLUSTRATIONS (Cont'd)

FIGURE		Page
5-1	Solar Cell Experiment #1, Flight Data	5-5
5-2	Solar Cell Experiment #1, Flight Data	5-6
5-3	Filter Characteristics	5-7
A-1	General Characteristics Of The Spectral Irradiance Function For The Sun And A Tungsten Simulator	A-6
A-2	Spectral Characteristics Of Space Sun And Filtered Tungsten Light	A-7
A-3	Transmission Characteristics of Four Interference Filter Types and Spectral Response Of Matched N/P Solar Cells	A-11
A-4	Effect of Temperature On Solar Cell Current	A-12

ABSTRACT

This report summarizes the design, development, calibration, test and flight of the PASS (Precision Autocollimating Solar Sensor) for the SPARCS (Solar Pointing Aerobee Rocket Control System) program. The PASS concept was conceived and executed as a means of measuring the real-time solar pointing error of the first two SPARCS flights in order to assess the performance of the attitude control system. In order to accomplish this to the required accuracy (better than 5 arc second), this unique sensor combined a high resolution solar sensor with an integral electronic readout autocollimator in a monolithic quartz structure permitting precise measurement of the angle between the solar vector and a reflective (reference) mounting surface independent of mounting errors and deflections induced by the launch and flight environment.

The concept development, the design, testing and calibration program and flight history are discussed in detail, including the results of an additional flight experiment designed to evaluate the enhancement of matched solar cell pair performance through the use of properly selected bandpass filters. The solar experiment also yielded a standard block of cells/filters which have been calibrated against space sun data for use in the calibration and evaluation of future solar detectors.

Two flights, using PASS systems for attitude control system evaluation, were made aboard Aerobee 150 rockets launched from White Sands Missile Range, New Mexico in December 1967 and March 1968. Flight data from both of these flights is presented and discussed, most significantly, that from the highly successful second flight. A malfunction of the attitude control system prevented fine pointing during the first mission. Information acquired by the PASS during the flight contributed to the failure analysis leading to the ultimate success of subsequent flights.

1.0 INTRODUCTION

In late 1966 Exotech began a Research and Development program for NASA, Ames Research Center to determine the feasibility of a new concept for a precision optical sensor which would have particular application to the Performance Payload portion of the SPARCS (Solar Pointing Aerobee Rocket Control System) program. A sensor was required to measure the real-time solar pointing error of the first two SPARCS flights in order to assess the performance of the attitude control system. The SPARCS goals included pointing accuracy and limit cycles in the 10 to 30 arc second range and the performance payload sensor which would measure the system performance required an accuracy in the 1-5 arc second range. Conventional approaches could not meet the specifications needed for the measurement sensor.

It is very difficult if not practically impossible to mount two or more optical devices on a spacecraft such as solar aspect sensors or space experiments which will maintain a relative boresight accuracy within 5 arc seconds after being subjected to the launch environment and the thermal stresses encountered during the mission. The optical components within the sensor or experiment must be located rigidly with respect to each other and must maintain a constant alignment to the experiment or sensor mounting surface. The sensor or experiment mounting surface must furthermore maintain a constant alignment to the spacecraft mounting surface. Lastly, the spacecraft structure itself must not deflect between the locations of the sensors and/or experiments. Sensors having intrinsic accuracies in the 1-5 arc second range cannot be effectively utilized unless some means is established to either maintain all alignments in a rigid and constant manner over all environmental conditions or a technique is used to accurately measure the deflections caused by the launch and flight regime.

Exotech's PASS (Precision Autocollimating Solar Sensor) concept was conceived as a means of achieving the desired accuracy. This sensor combines a solar sensor with an integral electronic readout autocollimator in a monolithic quartz structure. Since the optical axes of the solar sensor and the autocollimator

could be rigidly maintained the device had the capability of measuring the angle between the solar vector and a reflective mounting surface to a precision which was independent of minor mounting errors and deflections induced by the launch environment. Providing that PASS and the control system Fine Sun Sensor (FSS) were mounted on the same reflecting surface this approach would provide the needed information on vehicle performance.

By March of 1967 the preliminary results of the PASS research and development program indicated that the basic concept was sound and that a flight sensor could be fabricated which would be useful for the SPARCS Performance Payload mission. Accordingly, Exotech commenced development of two flight sensor packages which included signal conditioning electronics which would permit the high resolution signals obtained with the PASS unit to be transmitted over relatively low resolution telemetry channels.

During the Summer of 1967 it became apparent that the critical nature of matching the silicon photovoltaic cells used in both the autocollimating and solar sensing portions of PASS required certain assumptions of spectral response variations with temperature which could not be adequately verified in the laboratory to permit positive prediction of the space sensing error relative to the sensing error measured in the test chambers. A solar cell experiment package was added to the flight payload complement to measure the actual cell response under space solar conditions as an internal heater raised the temperature of the cells. Lockheed Missiles and Space Company, Sunnyvale, California, the prime contractor to NASA, Ames Research Center for SPARCS, participated with Exotech in the solar cell experiment by providing matched cells and filters similar to those used in the SPARCS FSS. In this manner, the same experiment would provide useful data on two cell matching methods and filter combinations.

Final testing of the two flight sensor packages, including separate yaw and pitch sensors, preamplifiers, signal processing electronics and the solar cell experiment was successfully concluded in October 1967. These were promptly integrated with the rest of the SPARCS payload at NASA, GSFC. The first flight

occurred in December 1967 from White Sands, New Mexico, but a malfunction of the attitude control system prevented fine pointing. The PASS system however, provided useful information regarding the solar acquisition problem through an analysis of the telemetry record as the SPARCS swung across the solar disc several t'mes during the mission.

The second flight was launched in March 1968 on a highly successful mission. A significant portion of this report is concerned with a detailed analysis of the time history obtained with PASS of the control system performance during this second flight.

The results of the solar cell experiment were very interesting and clearly demonstrated that the cell selection method used by both Lockheed and Exotech in combination with their respective spectral filters was adequate for both the FSS and PASS. The data also indicated that if the proper spectral filter is used less rigorous cell selection methods may be used in future solar sensors.

A noteworthy output of the PASS program was the validation of the bi-directional sensor concept for precision attitude determination without reliance on rigid mounting structures for high accuracy. Exotech, under contract to NASA, Ames Research Center is currently applying these principles in the development of SEAS (Solar Experiment Alignment Sensor), a device which may be integrally mated with most solar experiments to obtain high precision offset pointing capability.

1.1 Summary

Although solar sensors may be fabricated which will have a resolution better than a fraction of an arc second it is extremely unlikely that an absolute accuracy better than ten arc seconds is obtainable using conventional techniques, over a typical rocket launch and flight regime. The difficulty lies with changes in the angle between the sensor axis and the mounting surface because of vibration, shock and thermal stresses.

To achieve an absolute accuracy in the 1 to 5 arc second range, Exotech utilized the PASS approach to overcome the accuracy limitation imposed by the sensor mounting alignment variations.

The solar aspect sensing portion of PASS consists of a two inch long, by one-half inch square cross section quartz bar with a lens ground on one end to focus collimated light onto the rear flat surface. A quartz reflecting prism type energy splitting reticle is cemented onto the rear surface of the quartz block and a pair of matched silicon photovoltaic cells are mounted onto the reticle block. In operation the lens forms a solar image on the reticle and the solar cell pair measures the relative energy incident on each half of the reticle. At null, i.e., when the sensor optical axis is coincident with the solar vector, equal currents will flow in both cells (connected in opposition) to produce zero output. To minimize drifts and sensitivity variations due to temperature changes, a thin film spectral filter is included at the quartz block/reticle interface to limit system response to those wavelengths (a narrow band of wavelengths centered at approximately 0.75 microns) where the thermal effects are essentially nil.

The autocollimating portion of the PASS unit is almost identical to the solar sensing portion with the important inclusion of a tungsten light source in the reticle block. The central region of the reticle is clear, permitting the light from the lamp to reach the front lens where it is directed in a collimated beam to the reflective mounting surface. The returning rays re-enter the lens and are focused onto the reticle to illuminate the silicon cells, depending on the relative angle between the mirror surface and the autocollimator axis. When the autocollimator is exactly normal to the mirror, equal energy falls on both cells producing a null condition. In order to avoid system drifts and sensitivity to stray light, the light source is modulated at approximately 2 cps, producing a square wave modulation of the output signal whose peak to peak amplitude contains the autocollimator error information.

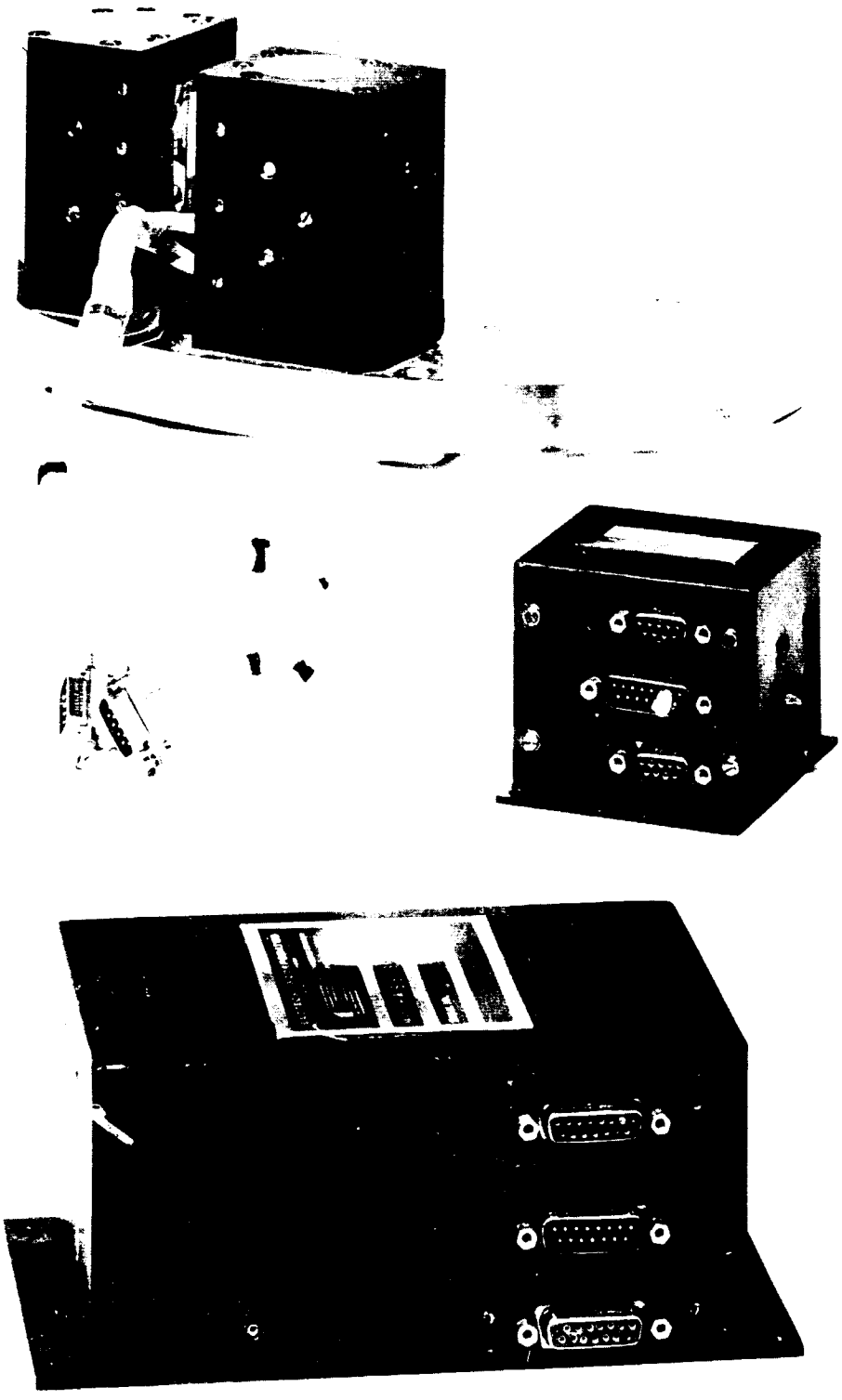
To complete a single axis assembly, the autocollimator and the solar sensor are cemented together along their long dimension, facing in opposite directions. The sensitive axes of the two components are coincident and the completed structure comprises a single axis PASS unit. Unless extremely large mechanical stresses are placed across the unit, both quartz blocks will bend equally and will remain in exact relative alignment. Furthermore, the use of fused quartz with its extremely low thermal expansion virtually eliminates thermal stresses from the error considerations. The resulting sensor is highly stable and almost insensitive to environmental variations.

Exotech solved the problem of mounting the low thermal expansion sensor block within a relatively high thermal expansion aluminum block through the use of spring loaded plungers bearing opposite to optically lapped mating surfaces between the sensor block and steel pads located on the mounting block. Relative expansion between the aluminum and the quartz caused the pads to slip over each other without disturbing the optical alignment. Five spring plungers are used to locate the block within the mount. The spring tensions are selected so that the springs are not compressed by the most extreme conditions of shock and vibration loading, maintaining a constant contact between mating pads. This technique exceeded all expectations, resulting in extremely small alignment changes (which could be easily measured with the integral autocollimator) under vibration and shock testing as well as during the actual space flights.

The final configuration included a quartz wedge window mounted in the front cover of the aluminum block. This window was rotated during assembly to boresight the axes of the solar sensor and the autocollimator to each other. A pair of single axis sensor assemblies was mounted on an aluminum mirror to provide yaw and pitch information. Figure 1-1, taken after flight recovery shows the two PASS units mounted on the aluminum mirror. In the payload, the FSS was mounted adjacent to the PASS units on the same mirror.

A four channel preamplifier using operational amplifiers in the current amplification mode was included to bring the output signals of the solar sensors and the autocollimators to a usable level. This item is the small black box shown in Fig. 1-1.

Power supplies and the autocollimator lamp drive circuits are included in the Signal Processing Unit (the large black box in Fig. 1-1) as well as electronic circuits to process the outputs of the solar sensors, autocollimators and the solar cell experiment. Very high resolution data was required of the PASS system over a wide dynamic range. To obtain fractional arc second resolution over a range encompassing over one arc minute with telemetry which is limited to two per cent resolution requires that the signal dynamic range be broken into several ranges, each using the entire range of the telemetry output. The signal processing unit



performs this function, providing 12 ranges for each solar sensor output and appropriate signals to indicate which range is being utilized. In essence, the signal processing unit operates as a "signal accurizer" and is an approach which may be very useful for other purposes requiring a highly accurate wide dynamic range signal to be transmitted by a low accuracy data link.

One, single axis PASS unit and a preamplifier package, signal processing unit and solar experiment package were subjected to qualification level tests. The remaining items were subjected to reduced, acceptance level testing. In both cases, the environmental tests were preceeded by extensive optical measurements using the Exotech Model 5-T Precision Solar Simulator and auxiliary equipment to determine the transfer curves of the sensors and autocollimators. New measurement techniques had to be developed to achieve the required arc second accuracy.

After environmental testing the units were re-tested in the solar simulator facility to measure any system changes. In addition, thermal testing was performed in the solar simulator beam. The worst case error from pre-environmental to post-environmental testing in any unit was 4.6 arc seconds, primarily associated with thermal effects. The thermal tests encompassed a wide range of temperature (-20°C to +55°C) in order to assure the system would accomodate the wide range in launch temperature. It was recognized that once the launch began the temperature would not change significantly during the flight. Available data on the second SPARCS flight indicates an almost room temperature condition at launch and throughout the flight. Considering the results of the testing program the probable error which would occur under these conditions is well below the maximum value indicated above.

Data regarding solar sensor calibration and spectral matching of the silicon cells was needed to provide increased confidence in the design approach being used by Exotech in the PASS program and in the development of the FSS for SPARCS. Highly precise matching of the solar cells is required for arc second sensor accuracy even when the sensors incorporate spectral filters.

Currently available solar simulators which have sufficiently accurate geometrical and optical properties to permit their use in testing and calibrating precision solar aspect sensors do not have spectral properties which correspond closely to that of space sunlight. Ground testing using sunlight is not satisfactory either since the atmosphere acts as a selective filter as well as a variable attenuator causing the sunlight reaching the ground to have a very different spectral content from that in space. Therefore, the design of the solar sensors and the detector matching procedures must take these factors into consideration and a basis for extrapolation must be derived.

Errors in any of the above procedures and extrapolations may result in boresight errors when the sensors view space sunlight and/or when their temperature varies under space sunlight conditions. The SPARCS and PASS programs required very high accuracy sensors and thus extreme detector matching accuracies. An experiment to establish the drift and boresight error potential of the SPARCS and PASS sensors in space was developed to increase the confidence in the extrapolation techniques and provide accuracy limit data for the PASS units (aiding evaluation of vehicle performance, especially with regard to absolute pointing accuracy).

Extensive calibrations and matching were performed on a number of solar cells, and matched cells were selected from each group of the SPARCS type and the PASS type. Three of each type were flown in each spaceborne experiment package and the remaining cells were mounted for future use as calibrated standards.

The flight package consisted of six cells with their respective spectral filters mounted on an insulated substrate. The substrate was electrically heated in flight to provide data points over a wide temperature range. The output of the cells were commutated, amplified and telemetered using precision offset techniques to provide 0.5 per cent accuracy with the vehicle tememetry equipment.

An analysis of the first flight telemetry records showed that although SPARCS failed to acquire the sun, the vehicle swept past the sun several times during acquisition attempts. Finally it came to rest several degrees from the sun. This

data, in conjunction with other data obtained during the flight, was useful in determining the problems in the control system which were solved prior to the next flight.

The second SPARCS flight was successful, both for the control system and PASS. Based on pre-flight alignment data the absolute pointing error of SPARCS as measured by PASS was 3.3 arc seconds in pitch and 8.3 arc seconds in yaw. In addition, the yaw axis drifted 11.7 arc seconds during the flight. Limit cycles were 11.0 arc seconds peak to peak (3.2 arc seconds rms) in pitch and 16.5 arc seconds peak to peak (4.8 arc seconds rms) in yaw.

The solar cell experiment yielded data which verified the anticipated thermal drifts of the matched cells under space sun conditions. Close examination of the data shows that the drift directions were opposite for the Lockheed cells/filter and the Exotech cells/filter. In addition, all cells in a group drifted in the same direction. It can be concluded that a filter having characteristics midway between the Lockheed and Exotech filters would virtually eliminate all thermally induced drift. This knowledge now permits one to greatly reduce the time and effort needed to match cells for future solar sensors. Finally, the data obtained is closely in agreement with expected results, providing the validity of the cell matching techniques in conjunction with the spectral filters used in the PASS program. Therefore, we are highly confident that thermal variations have negligible effect on PASS accuracy.

It was decided early in the program that a set of cells and filters would be calibrated for "space sun" conditions using data acquired prior to and during the solar experiment flights. These cells would then be used as standards for laboratory evaluation of future solar sensors. To accomplish this, an additional set of six (three Exotech and three Lockheed) cells/filters were selected, matched to those to be flown, and mounted on a standard block. Sufficient comparative measurements of all cells were made using laboratory spectral sources to insure that, given the solar experiment cell's in-flight output data, correction factors could be determined to adjust

the cell's laborat ory performance to that to be experienced in space. After completion of the two flights the solar cell experiment data for cell/filter output under space sun illumination were compared with those data obtained during the pre-flight calibrations, and the laboratory-to-space sun correction factors determined for the standard cell. This cell is now available for and is being used for the selection and calibration of new sun sensor elements.

In conclusion, the PASS program provided useful and important data for evaluation of the SPARCS Performance Payload. It paved the way for a new generation of space sensors by providing the bi-directional sensor concept, and contributed generally to the body of knowledge concerned with space sensors.

2.0 DESCRIPTION OF HARDWARE

The PASS system is composed of four basic assemblies shown in Fig. 1-1. There are two optical sensor units, each consisting of a solar aspect sensor and attached autocollimator, housed within an aluminum structure. The remaining units consist of a sensor-amplifier package and a signal-processor unit.

For the SPARCS mission the sensor units were bolted to a polished reference plate which also supported the SPARCS control sensor. Sensor outputs were fed to the sensor amplifier through shielded cables and after amplification were routed to the signal processor which conditioned them for telemetry transmission. This package also contained power supplies and regulators for the entire PASS system and for a solar cell experiment package which made up part of the SPARCS payload. A block diagram is shown in Fig. 2-1.

The following section describes the design features of each unit, along with special component testing programs such as the solar cell matching process and life tests on the autocollimator light source.

2.1 Sensor Unit

For ease of discussion, the following description of the sensor unit is separated into two parts, one relating to the solar aspect sensing portion and the other to the autocollimator portion of the unit. These parts may be treated separately although in the final unit they are integrated into a monolithic structure incapable of physical separation and/or relative motion.

2.1.1 Solar Aspect Sensing System

The solar aspect sensing section of the overall sensor unit consists of a two inch long, quartz bar having a lens ground on one end and a knife edge detector assembly mounted on the opposite end. Figure 2-2 shows the optical assembly in detail.

"REPRODUCIBILITY OF THE ORIGINAL PAGE IS POOR."

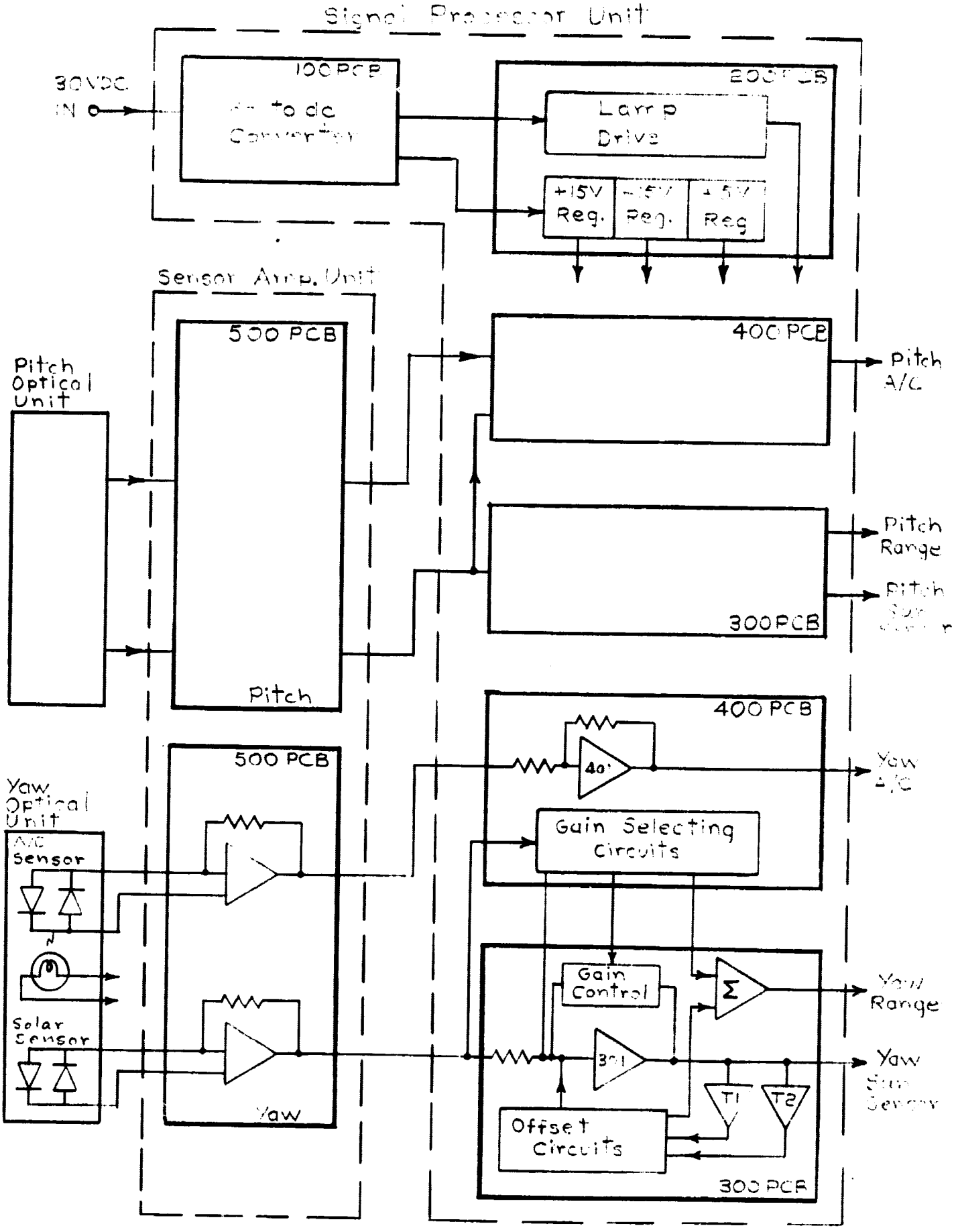


Figure 2-1 PASS Block Diagram

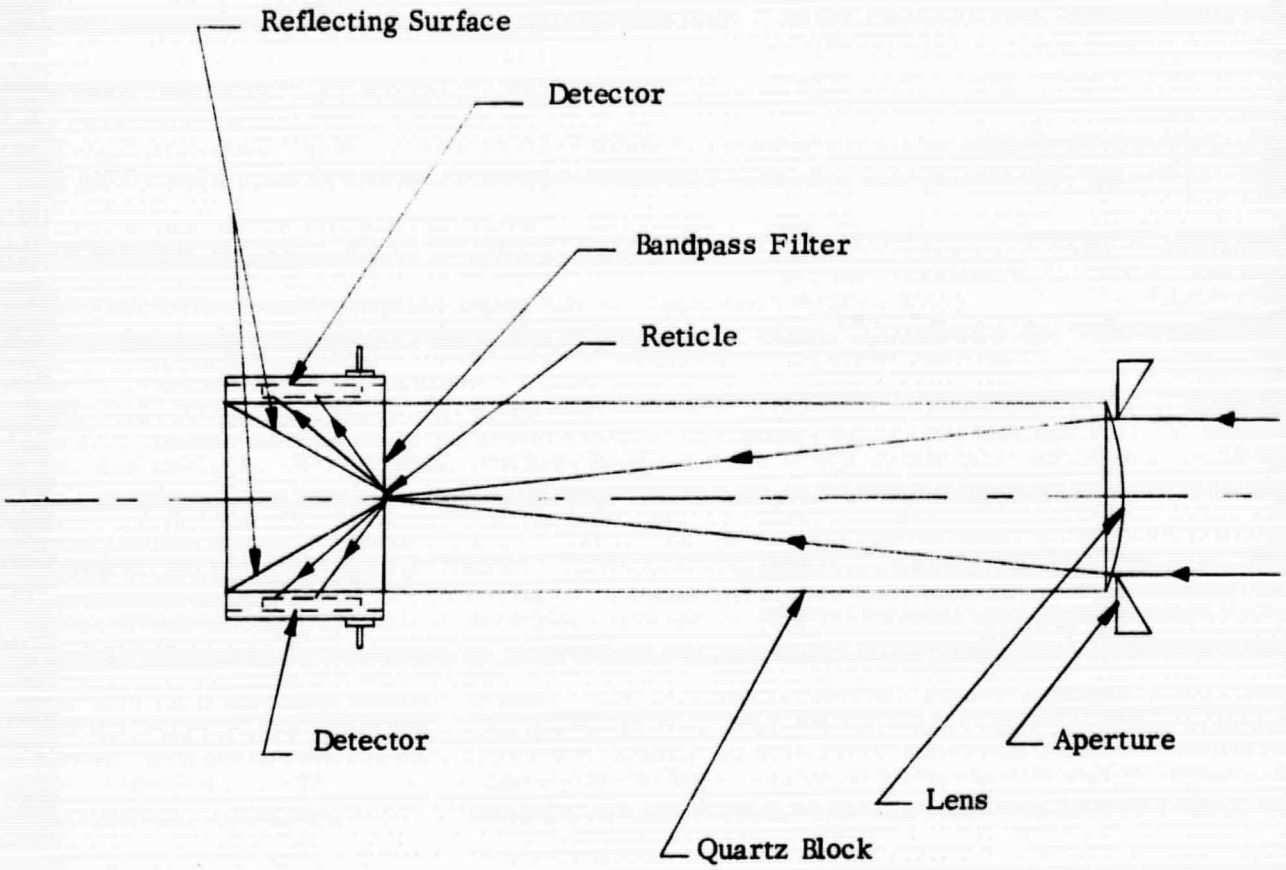


Figure 2-2 PASS Sun Sensor Optical Layout

2.1.2 Optical Design

The front surface of the fused quartz bar is optically ground and polished to form a spherical lens, 0.5 inch in diameter having a radius of curvature of 0.623 inch to focus collimated light at a wavelength of 0.8 microns on the rear surface of the bar, 1.960 inches from the lens surface. The material is isotropic, has a thermal coefficient of expansion of 0.56 parts/millions per degree Centigrade, and is transparent to the wavelength region of solar cell sensitivity. Prolonged exposure of Ultrasil to ultraviolet radiation will not cause darkening. The refractive index of 0.85 microns is 1.4525, varying only in the fourth significant figure over a wide temperature range. This material is an excellent choice for the application in terms of its mechanical, thermal and optical properties.

The basic concept of maintaining the autocollimator and the solar aspect sensor in one monolithic structure does not necessarily imply that the two devices must be machined and polished in a single quartz block. This approach was investigated and found to have certain drawbacks from a fabrication viewpoint. Furthermore, it is desirable to include a light shield between the sensor and autocollimator sections, a difficult design problem if the two are contained in a single piece of quartz. The approach followed was to fabricate the sensor and autocollimator separately, out of identical, 0.5 inch by 0.5 inch by 2.0 inch long, Ultrasil bars. After fabrication of the two sections was completed, they were cemented together along one of their long faces using American Optical AO 805 cement. An analysis of the thermal distortion problems which might have been encountered with the cemented approach, clearly indicated that these problems are negligible providing the cement remains stable.

2.1.3 Knife Edge Reticle

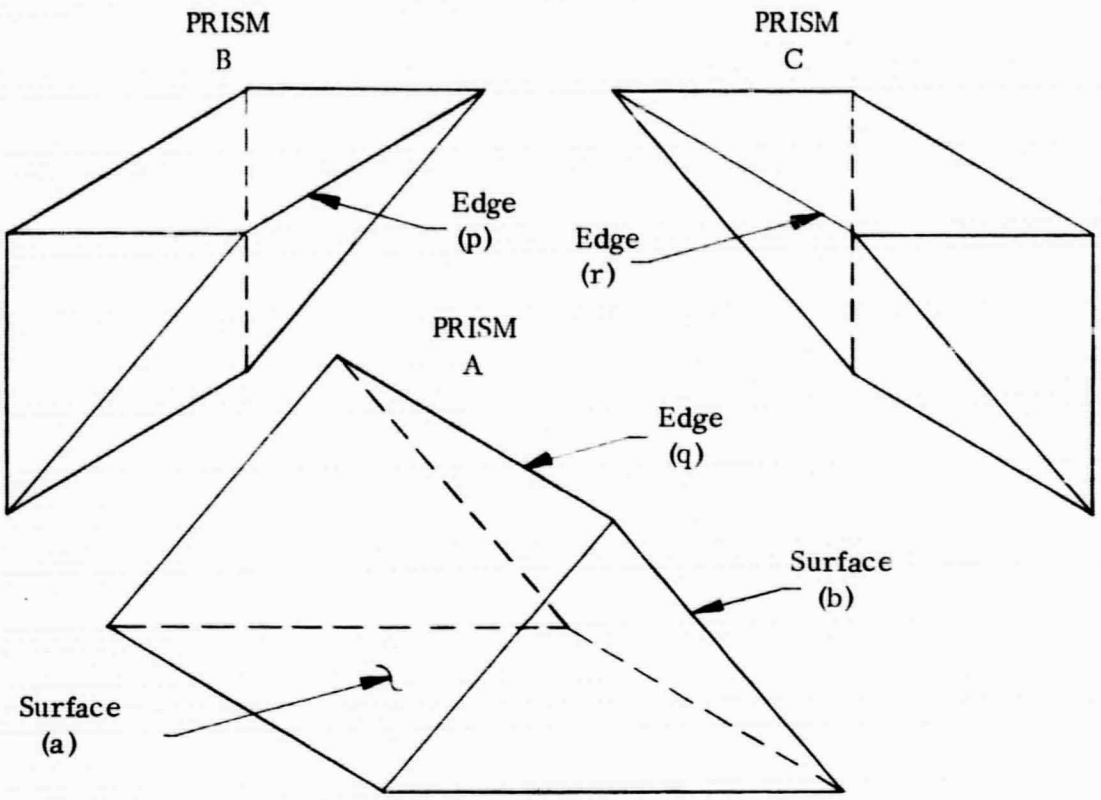
The solar aspect sensor is based on the principle of splitting the energy contained in the solar image between a pair of silicon solar cell detectors in such a manner that when the solar vector is co-incident with the optical axis of the solar sensor, equal energy falls on the two detectors. Electrically, the cells are connected in parallel, with opposing polarities. This results in a zero signal condition under

the above circumstances. A single solar sensor unit is only sensitive to angular motion in one axis (requiring a pair of sensor packages for two axis information) and should be entirely insensitive to small (several arc minutes) angular motions in the orthogonal axis. Careful attention to this ensures that cross-coupling between sensors is within tolerable limits.

The PASS design utilizes a reticle with a central occulting strip. This occulting region has a width which is 80 per cent of the diameter of the effective solar image at the rear surface of the aspect sensor unit for best linearity and low drift at null. The length of the occulting region is 1/2 inch although only the central region is used under normal circumstances.

The reticle comprises a double knife edge system, allowing the energy from the outer portions of the solar image to fall on the two sensors. In order to eliminate cross coupling effects the knife edges must be extremely straight and free from irregularities. Several approaches have been applied to this problem in the past including the use of vacuum deposited section of aluminum or other opaque material. This technique has a good ability to form reproducible, microscopically smooth edges. If the reticle knife edge is deposited directly on the quartz surface all requirements for rigidity and stability will be satisfied. However, this approach is not compatible with the autocollimator.

The Exotech approach satisfies design goals of both the sun sensor and autocollimator in a reticle block which is cemented directly to the rear surface of the sensor. The reticle block design is illustrated in Fig. 2-3 which also shows the fabrication technique. Three prisms were fabricated of Ultrasil fused quartz with special attention being given to the flatness of faces (a) and (b) on prism A. Great care was taken to maintain edges (p), (q) and (r) straight and unbroken(edges (p) and (r) may be broken up to 0.005 inch without causing subsequent difficulties). After polishing surfaces (a) and (b) were aluminized. The three prisms were then cemented as shown to form a solid block, Finally, the block was remounted in an



Components Of Reticle Block

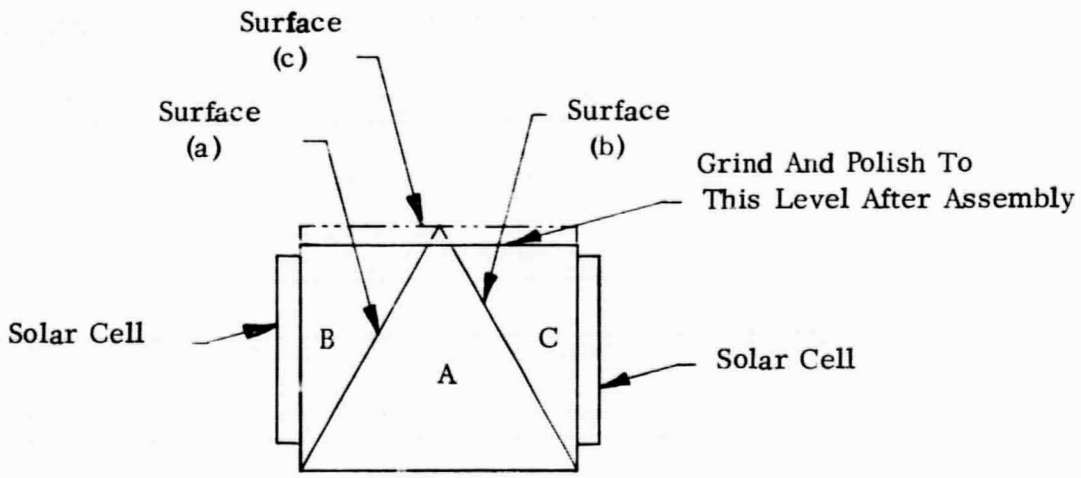


Figure 2-3 Completed Reticle Block

optical grinding machine and surface (c) ground down and polished to expose 0.0108 inch of prism A. If one looks into face (c) he sees directly through prism A in the exposed region of that prism. The edge irregularities of the boundary between this portion and the adjacent portions are several millionths of an inch (the typical flatness of optically ground surfaces). On either side of the straight, parallel central region he sees whatever scene is reflected from the aluminized faces of prism A. Non-uniformities in cement thickness do not have any effect on performance. The solar cells are mounted on a Kovar substrate which is cemented directly to the outside faces of prisms B and C. Note that at this distance a significant amount of image spread has occurred, making the system relatively insensitive to localized "hot spots" on the detectors.

The PASS reticle design has very significant advantages for use in autocollimators. The use of this concept for both sensors results in lower costs and high reliability. The only potential problem with this approach is the physical separation of the cells (0.5 inch). Small thermal gradients may occur across this distance and unless both cells have essentially zero sensitivity variations with temperature, errors may result. The PASS design, which uses a spectral filtering, cell matching and a high thermal conductivity, symmetrical mounting configuration effectively overcomes this objection.

2.1.4 Filter

As will be discussed in Section 2.1.5, restriction of the wavelengths falling on the solar cells to a 0.2 micron band centered approximately 0.75 microns greatly improves the stability of the solar sensor with respect to operation over a wide temperature range. Furthermore, since the incoming solar radiation passes through three layers of cement a filter is required to prevent darkening of the cement by ultraviolet transmission properties removes all doubt as to the need of an ultraviolet blocking filter for long term missions.

Thin film, multilayer filter technology permits the deposition of stable, efficient filters directly on the rear surface of the quartz lens. Having practically no absorption, the filter either reflects the incoming solar power back out of the system or transmits it toward the detectors. Available filters made by Optical Coating Laboratories, Inc. have been used extensively in spacecraft and were entirely satisfactory for the PASS system. The transmission through the filter within the selected bandpass was greater than 80 per cent. Transmission outside this region was less than 0.1 per cent.

2.1.5 Solar Cells

Silicon solar cells are the best detector for energy splitting solar sensors because of their simplicity, ruggedness, stability and low noise characteristics. The equivalent circuit of a silicon solar cell is shown in Fig. 2-4 where the current I_o, generated by incident light is a linear function of light intensity for radiation of a given spectral distribution. If the cell is open circuited, current flows through R_{SH} and diode D, which limits the output voltage to about 500 millivolts. Very little current flows through R_{SH} which is a large value and may be neglected. Because the diode characteristics vary with temperature, V_o is very dependent upon temperature and is an unreliable indicator of I_o. If the cell is short circuited, most of I_o flows through R_S which is in the order of 1 ohm, and the diode conducts very little current because of the low voltage across it. Thus I_{sc} is an accurate indication of I_o at low levels where the drop across R_S is small and the diode current is virtually zero.

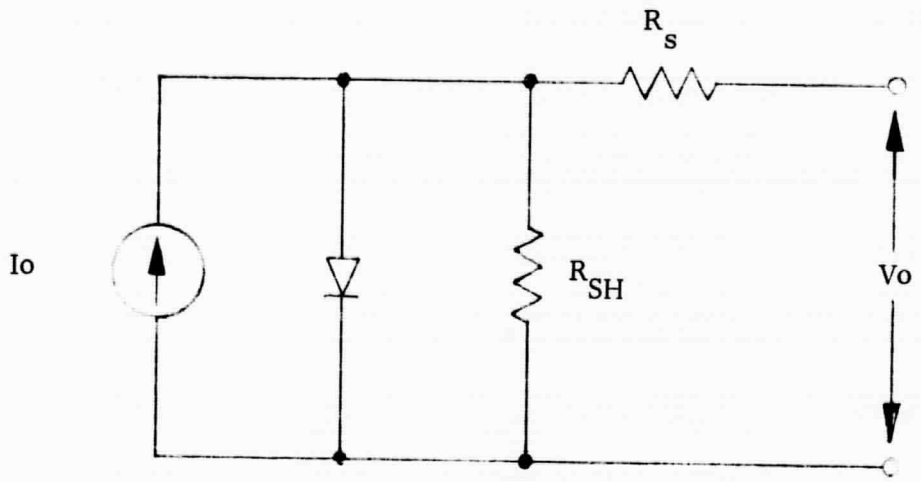


Figure 2-4 Solar Cell Equivalent Circuit

I_0, and therefore I_{sc}, is also a function of incident light wavelength and cell temperature, two parameters which are independent as illustrated in Figure 2-5 where I_{sc} is shown as a function of temperature for a number of wavelength regions.[1] Increased minority carrier lifetime is responsible for the enhancement of red response with increasing temperature while anti-reflection coating effects account for reduced blue response with increasing temperature sensitivity occurs in the spectral range 0.7 to 0.85 microns.

In selecting a pair of cells for an energy splitting detector, two cell parameters must be considered. First is the absolute stability of cell responsivity which effects the sensor gain, and the second is relative stability which effects the boresight of null stability. The latter can generally be kept within closer limits than absolute responsivity, over a wide temperature range.

It may be noted from typical manufacturer's curves (Fig. 2-5) on the relative responsivity of a batch of solar cells that minimum deviation occurs in a wavelength region around 0.8 microns. This is roughly the region where minimum temperature sensitivity may be realized so that choosing a matched pair of silicon solar cells was facilitated by restricting the operating wavelength region to around 0.8 microns, in keeping with the selected filter bandpass.

In order to more accurately define the important solar cell requirements, an analysis of the general case for sun sensors is presented in Appendix A. A summary of this analysis is presented in the ensuing material for convenience.

1. E. L. Ralph, "Preflight Calibration and Matching Of Solar Cells for A Band-Pass Filter Experiment", Proceedings of the Fifth Photovoltaic Specialists Conference, Vol. III, 1965.

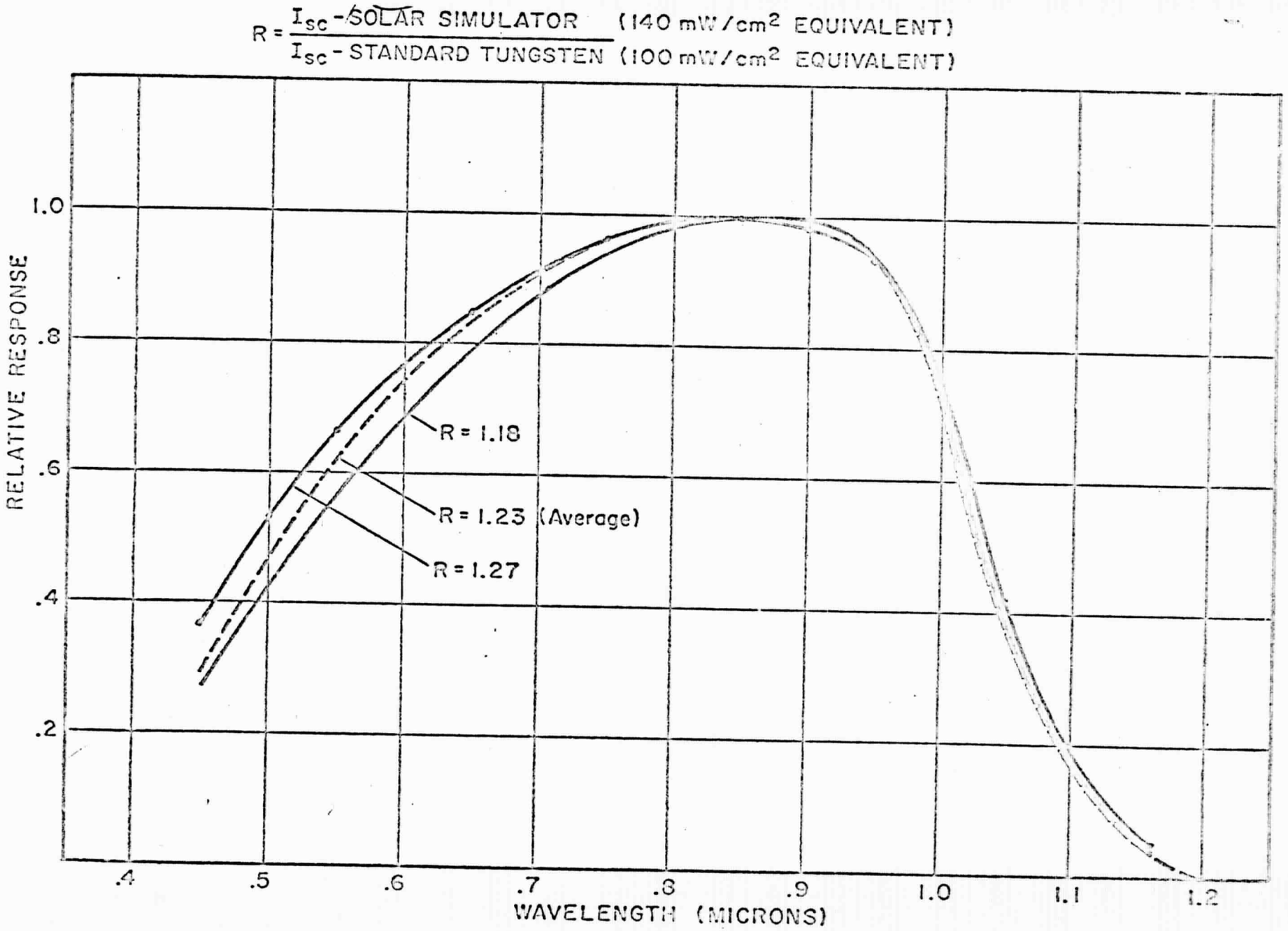


Figure 2-5 SOLAR CELL RELATIVE SPECTRAL RESPONSE - PRODUCTION LIMITS

"REPRODUCIBILITY OF THE ORIGINAL PAGE IS POOR."

2.1.6 Measurement Program

In Section 2.1.5 it was determined that the two significant detector parameters to be matched were the short circuit currents and the tracking of these currents with temperature. From an inspection of Fig. A-2 in Appendix A it can be seen that the filtered tungsten spactral characteristics differs significantly from the solar spectrum only in the ranges 0.65 μ to 0.7 μ and 0.75 μ to 0.875μ. Therefore, these ranges are the more critical regions of detector spectral match.

In this section the detector matching scheme is discussed. The objectives of the program were as follows:

1. develop a technique for testing solar detectors in simulated sunlight which results in adequately matched detectors.
2. using the matching program in (1) above test and select pairs of detectors for the sun sensor, autocollimator, solar experiment, and reference standards.
3. demonstrate the validity of the procedure using the solar experiment and establish absolute reference standards for predicting space performance of subsequent systems.

The matching procedure developed consisted of testing each detector against a common reference detector under a variety of radiant input spectrums and a wide range of temperatures. A thermoelectric unit was used to provide the thermal environment while a tungsten solar simulator in conjunction with a series of filters was used to provide the different spectral characteristics of the incident light. Figure 2-6 schematically illustrates the test setup. The detectors were tested under raw tungsten illumination, tungsten filtered by a Corning #1-59 filter, and tungsten filtered by the Corning filter and the PASS sensor narrow band filter. Tests were performed at +30, +50, +70, +90, +110 and +130°F.

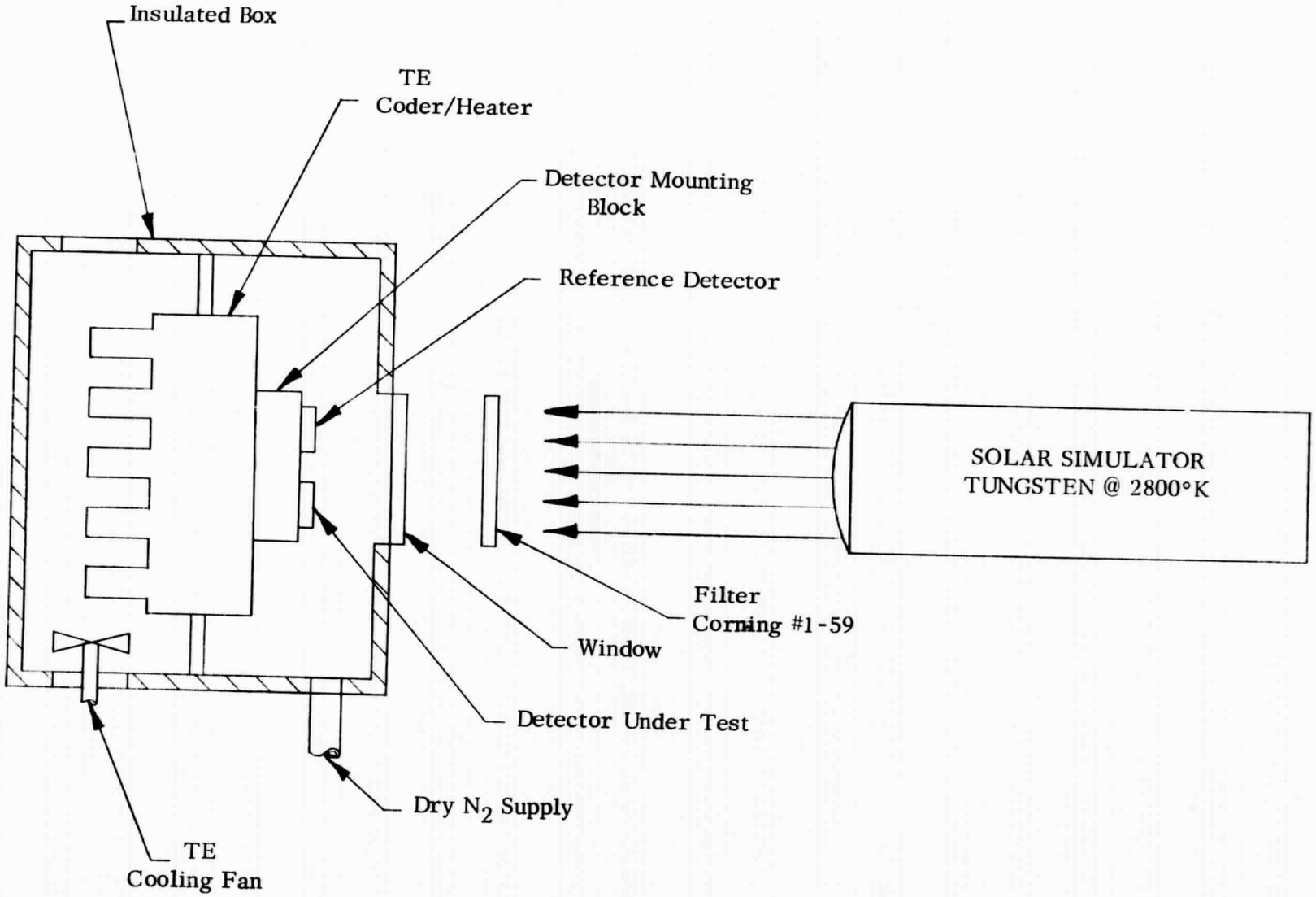


Figure 2-6 Detector Test Set-Up

Twenty-two cells were tested in two lots. The detectors in each lot were divided into two batches after testing on the basis of whether they had a higher or lower temperature coefficient than the reference cell. The detectors within each batch were selected on the basis of relative match in filtered or unfiltered tungsten depending on whether they were to be used in the sun sensor and solar experiment or the autocollimator. Figure 2-7 illustrates a typical matching curve for a group of three cells used in one of the flight solar experiments.

2.1.7 Autocollimator Unit

Except for the use of a built-in light source and the location of the spectral filter the autocollimator unit was identical in all respects to the solar aspect sensor unit. Figure 2-8 illustrates the changes in the reticle block to incorporate the source and spectral filter. The source used was a Pinlight #30-30.

The spectral filter was relocated to prevent light from the source being reflected down the glue line between the reticle assembly and the lens block thereby swamping the detector. The filters were cemented to the reticle block directly in front of the detectors in the final configuration thus eliminating the swamping problem.

2.1.8 Mounting Assembly

The most critical requirements of the mechanical structure are (1) to avoid mechanical distortion of the optical line of sight relative to the spacecraft reference surface by more than 15 arc seconds, which would exceed the highly linear field of view of the system, and (2) to avoid distortion of the optical line of sight of the sun sensor relative to the autocollimator.

Figure 2-9 shows the mechanical assembly and packaging of the sensor. In order to avoid thermal distortion of the quartz assembly during inflight heating of the case and transient heating of the quartz, it is desirable to minimize temperature

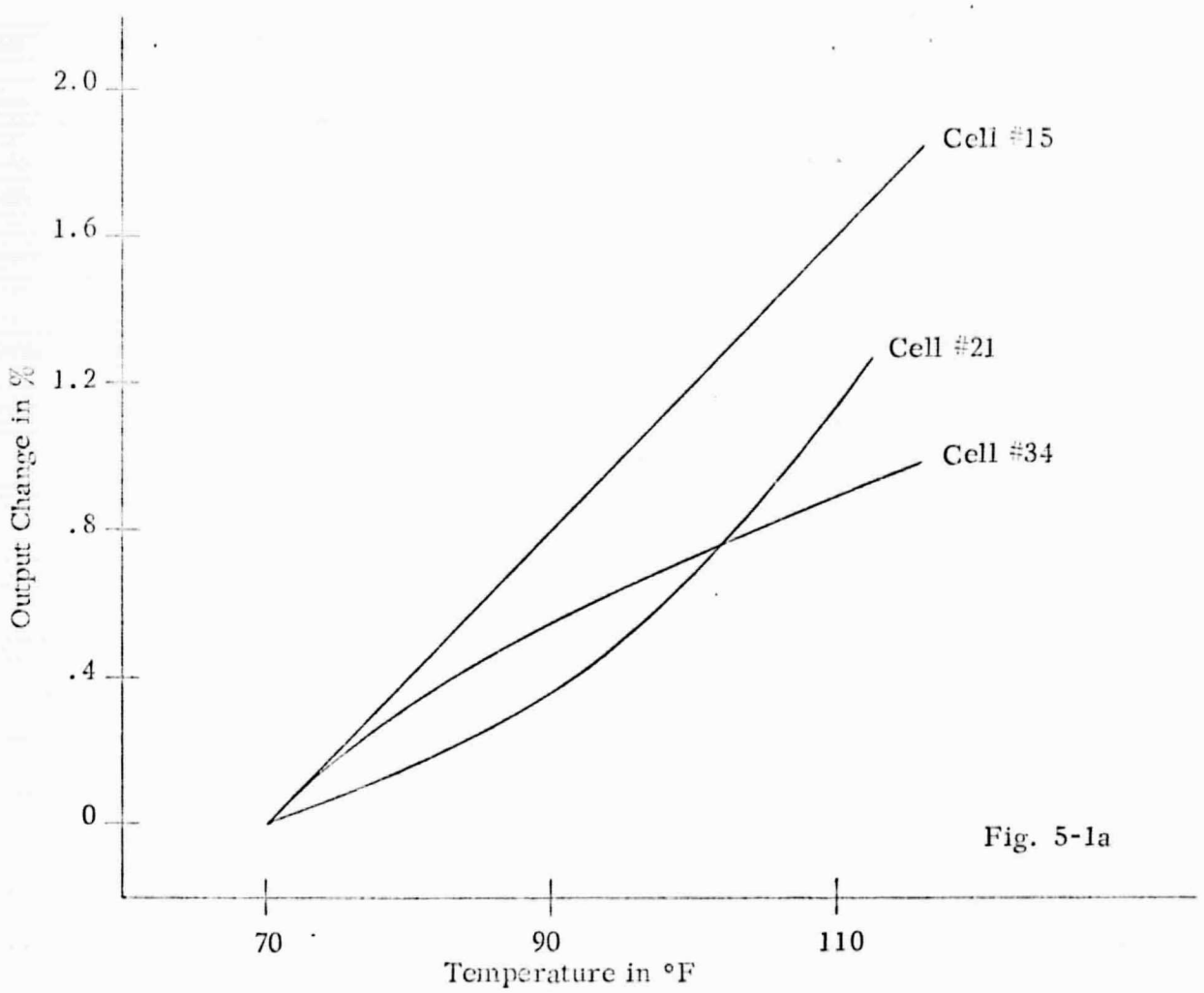


Figure 2- 7 Pre-flight Output Change vs Temperature Data
Solar Simulator With Filter A Exotech

"REPRODUCIBILITY OF THE ORIGINAL PAGE IS POOR."

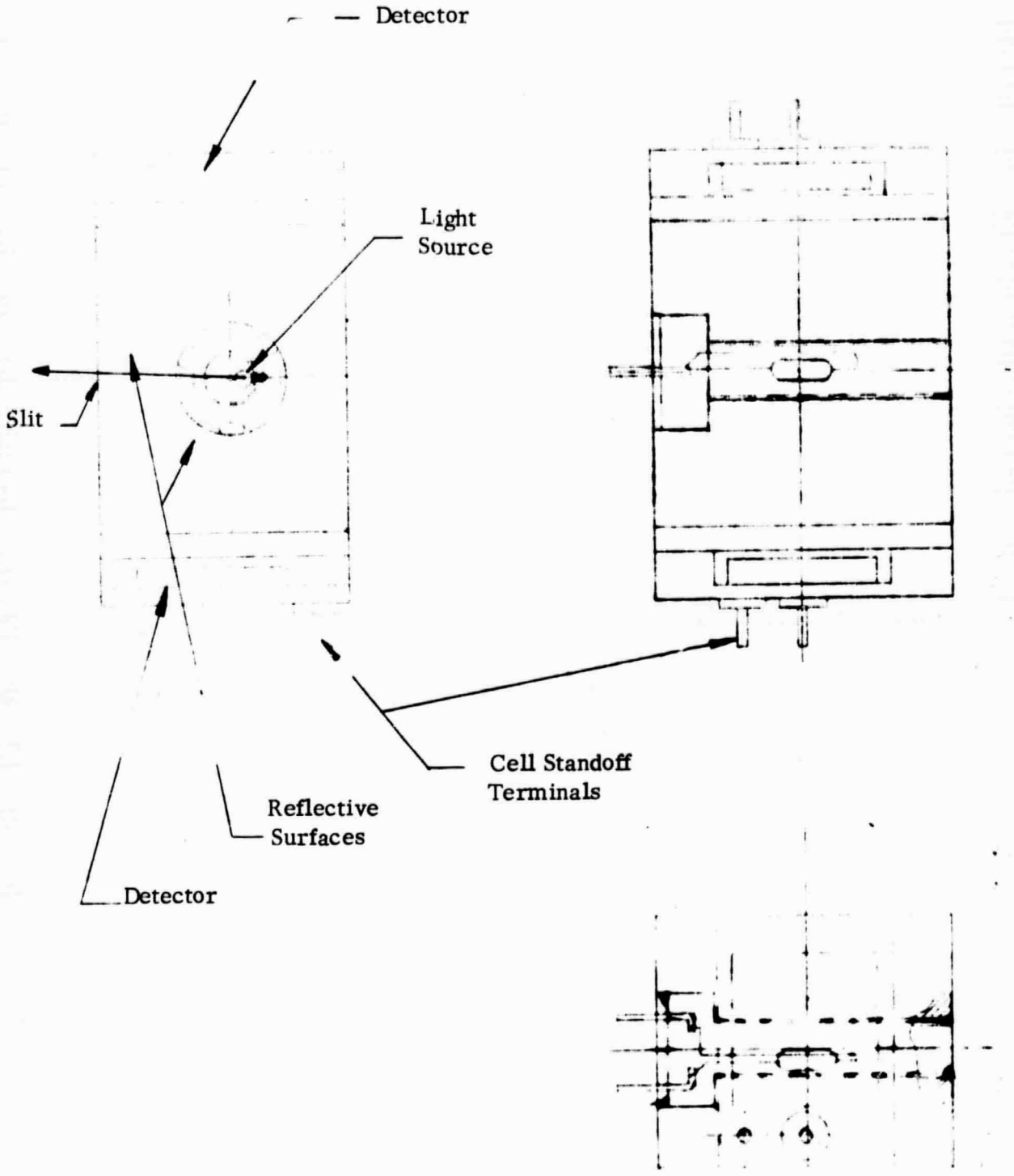


Figure 2-8 Autocollimator Reticle Assembly

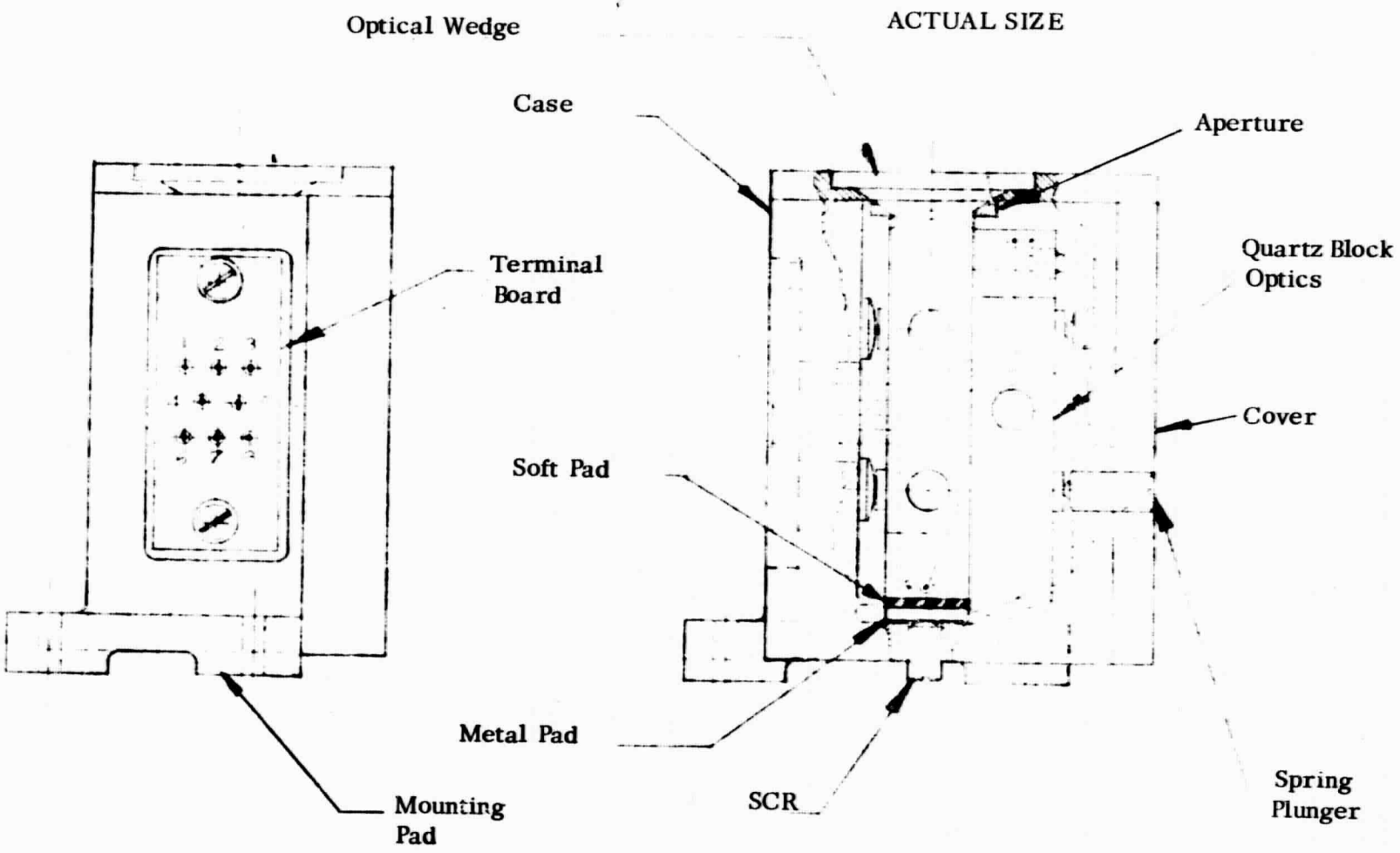


Figure 2-9 Sensor Assembly

"REPRODUCIBILITY OF THE ORIGINAL PAGE IS POOR"

gradients across the quartz blocks. In order to minimize this transverse temperature gradient, the quartz assembly was supported with three supports on one side which are rigidly attached to an aluminum housing and serve to define the mounting plane of the system. The three supports on the opposite side are symmetrically located and contain springs to force the quartz assembly against three rigid pads. Each spring support is directly opposite a rigid support to avoid bending stresses in the quartz.

All rigid pads and spring-loaded pads are located near the ends of the quartz blocks in order to define the optical axis most accurately and to assure that most of the conductive heat transfer is fed into the ends of the blocks and then flows toward the mid-point of the blocks. This minimizes transverse temperature gradients except in a small region near the two ends of each block. Since conduction predominates over radiation heat transfer, the isothermal planes are approximately perpendicular to the optical axis throughout most of the quartz volume. Therefore "bowing" of the blocks is minimized. In any case, any bowing of the sun sensor block is approximately the same as for the autocollimator block because they are cemented together. It is only any differential bowing which would lead to an uncorrectable error.

The quartz assembly is supported in the plane of the autocollimator slit (perpendicular to the measurement axis) by two rigid pads on one side and two spring-loaded pads on the opposite side. All rigid and spring-loaded pads are polished and permit the quartz to expand and contract axially with temperature differences between the aluminum housing and the quartz.

2.2 Sensor Amplifier Unit

During the initial design phase of the PASS program it was not apparent just where the PASS electronics would be located so it was decided to provide a small package containing preamplifiers which could be located in close proximity to the optical sensors and avoid the possibility of a long cable run with low level sensor

signals. These preamplifiers are contained within the sensor amplifier unit which houses two identical printed circuit boards, each one being associated with a particular optical unit. A single board contains one amplifier for the solar sensor and a second for the autocollimator making a complete one axis unit.

Both the solar sensor and autocollimator employ silicon solar cells in a back to back configuration as detectors. Since silicon cells may be considered as incident-radiation dependent current sources, shunted by diodes, the most reliable way to measure their output is to determine their short circuit current while keeping the voltage across the detectors low. This was achieved by the amplifier circuits in which the sensor outputs were fed into the inverting output of an operational amplifier with a feedback resistor. The input impedance of this circuit is given approximately by

$$Z \text{ input} \approx \frac{Z \text{ feedback}}{\text{Open Loop Amplifier Gain}}$$

which is very low (i.e. about 0.005 ohm for the solar sensor amplifier). A Burr Brown, Model 1901, operational amplifier was selected for this circuit because of its high gain (100 db) and low input offset voltage (0.3 mv). It also featured low input current drift (0.3 na/°C) and input offset voltage drift, and was manufactured to high reliability specifications.

In the case of the solar aspect sensor which has a nominal sensitivity in space sun of about 6μA/arc seconds, the input current drift of the sensor amplifier was negligible and dc coupling was used throughout the solar sensor channel. The amplifier gain was established after the solar sensor associated with it had been tested for gain, by choosing a feedback resistor to give a nominal output of 3 mv/arc second.

In the case of the autocollimator sensor which had a nominal sensitivity of 1 na/arc second, the current drift of the associated amplifier was significant so the autocollimator light source was chopped at about 1.5 cps to overcome drift problems. Because of the low chopping frequency, which was limited by the

commutation rate of the telemetry, it was decided to retain dc coupling throughout the autocollimator channel and determine the error signal by observing the difference in the chopped signal levels. This allowed some dc drift in the output (equivalent to about 10 arc seconds for a 30°C temperature change) but did not affect measurement accuracy and eliminated the need for large coupling capacitors.

Also included with each amplifier was an offset control pot which allowed adjustment of dc output levels.

2.3 Signal Processor Unit

The signal processor unit shown in Fig. 2-10 houses five printed circuit boards plus a shielded dc-to-dc converter which supplies power for the complete PASS system. One circuit board contains three regulator circuits plus an oscillator and switched regulator which drives the autocollimator light sources. Two circuit boards per axis contain the amplifiers that supply 0-5 volt signals to telemetry, for the autocollimator channel, sun sensor channel and sun sensor range channel.

The signal processor was designed primarily to permit transmission of sun sensor signals over standard 0-5 volt telemetry channels while permitting a dynamic range of about ± 1600 arc seconds with an absolute accuracy and resolution near null, of better than one arc second. This capability was obtained by dividing the input signal continuum into a number of discrete ranges, and expanding each range to give a full 0-5 volt output to telemetry channel. Information specifying the range is transmitted on a separate channel. Thus information capability was increased at the cost of a wider bandwidth.

The transfer characteristic of a single sun sensor channel is shown in Fig. 2-11, where the high resolution range is comprised of eight separate ranges having a gain of 33, and cover a range of about four arc minutes. Output to telemetry in this range corresponds to roughly 100 mv/arc second, to give fractional arc second resolution through the relatively low resolution telemetry. For larger offsets a low gain region provides coverage over most of the dynamic range of the solar sensor. Gain in this region is typically 0.9 yielding a telemetry signal of about 2.7 mv/arc second depending on the slope of the sensor transfer curve.

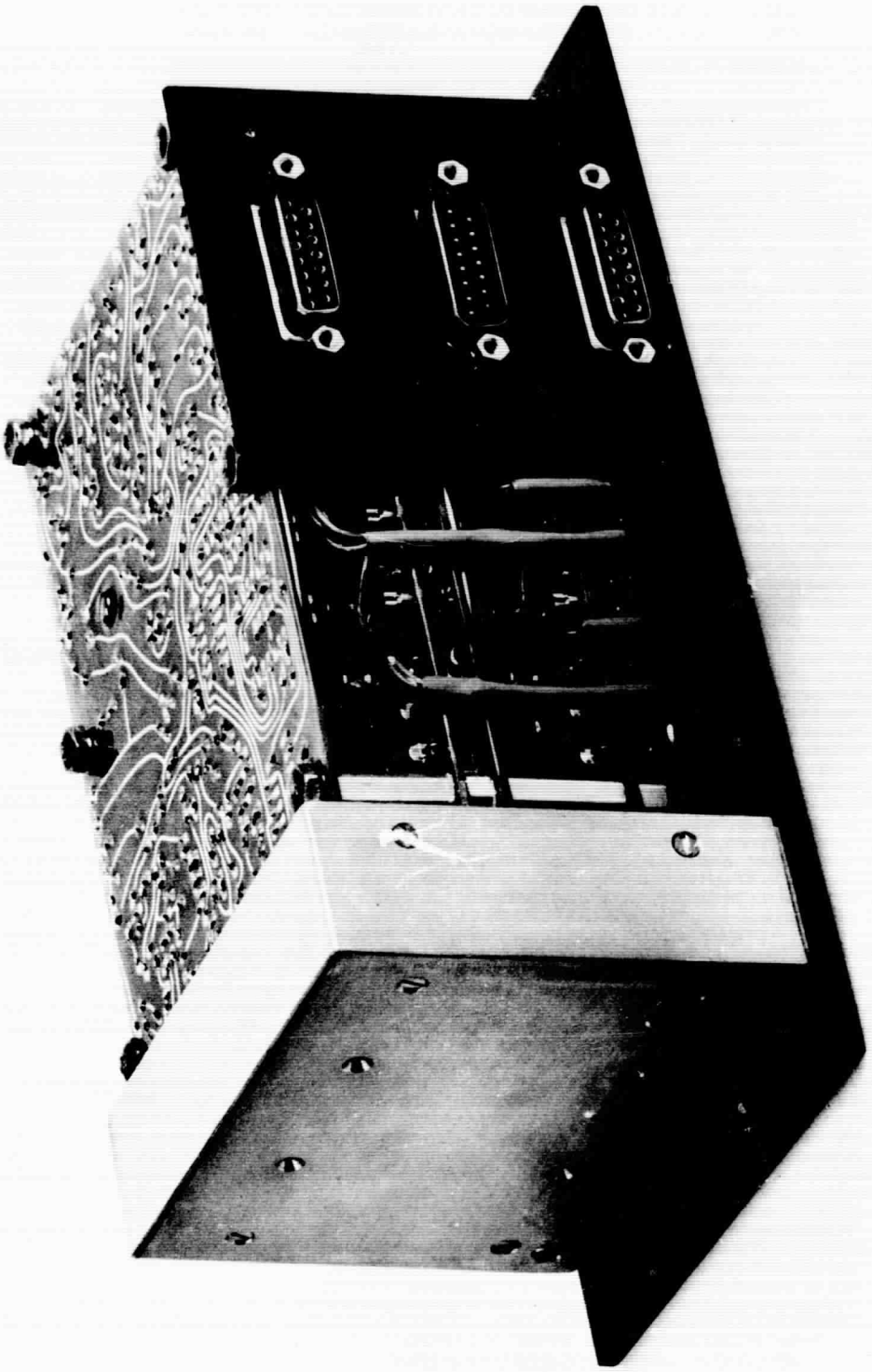


Figure 2-10 Signal Processor Unit

"REPRODUCIBILITY OF THE ORIGINAL PAGE IS POOR"

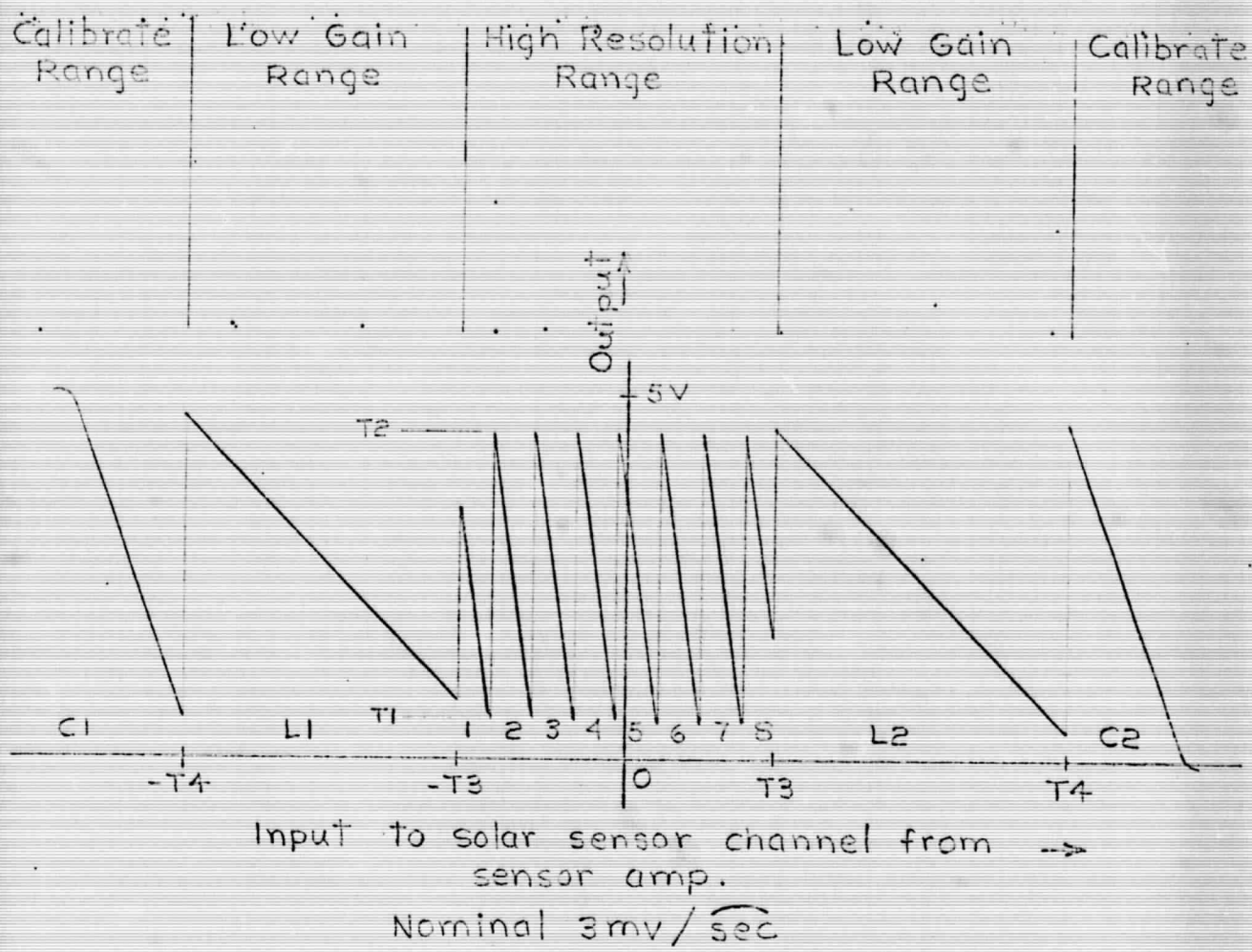


Figure 2-11 Solar Sensor Channel Transfer Characteristics

Finally, a higher gain, calibration-range was provided to give accurate information on the peak output of each sensor as the payload approached null during capture. This permitted accurate establishment of the sensor space-gain.

Operation of the sun sensor channel may be described with reference to the PASS block diagram, Fig. 2-1. In the high resolution range a signal from the solar sensor amplifier is fed to the signal processor unit where it is routed to an operational amplifier. The output of this amplifier which goes directly to telemetry is sensed by two comparator circuits having threshholds of approximately 0.2 volts and 4.7 volts, respectively. When the output reaches either of these values the comparators cause an offset of the correct value to be inserted by stepping a d/a converter which adds a current at the amplifier summing junction. A second output from the offset circuits is fed to a summing amplifier which gives a range indication.

The solar sensor signal is also monitored by comparator circuits on the Series 400 printed circuit board. Whenever the absolute value of the signal exceeds a threshhold the gain selecting circuits in the signal processor disable the offset circuits and change the amplifier gain to a lower value by switching in a new feedback resistor. This is the low gain region. Whenever the absolute value of the signal exceeds another threshold one of a second pair of comparators is activated, causing a third gain control resistor to be switched in for the calibration range. Appropriate offset currents are also injected into the amplifier. The comparator circuits consist basically of complementary Schmitt-trigger circuits with a differential input configuration to minimize temperature drift in the triggering level. Input resistors introduce a small amount of hysteresis in the Schmitt circuit which is essential for stable operation and noise immunity. The comparator circuit outputs are fed through level shifters to a reversible three-stage binary counter based on Fairchildμ L900 series integrated circuits.

Depending on which comparator is activated, a clock pulse is gated to cause the counter to count up or down. The counter outputs operate three transistor gates which supply +15 volts to three resistors which supply relative currents of 1, 2 and 4, respectively to the summing junction of the amplifier, so that eight different offset currents are supplied to the sun sensor amplifier corresponding to the eight binary counter states and the eight high resolution ranges.

Also located on this circuit board is a simple amplifier which sums weighted outputs from the counter gates to give eight output levels corresponding to the eight high resolution ranges. It also accepts inputs from the comparator circuits on the Series 400 board to generate four additional levels corresponding to ranges C1, C2, L1 and L2. Separation between levels is nominally 0.4 volts.

Amplifier A401 functions as a final amplifier for the autocollimator channel, with frequency and voltage limiting provided by external components. The remaining circuitry is associated with the low gain and calibration ranges of the solar sensor channel.

System power is supplied through a dc-to-dc converter located on the Series 100 printed circuit board which is housed in a shielded enclosure. It supplies four voltages, two at 10 volts and two at 18 volts, to regulators on the Series 200 board. Voltages for the amplifiers and precise offset circuits are regulated at +15 volts and -15 volts by two NSC LM100's which provide regulation and thermal stability in the order of 0.3 per cent. A simple emitter follower with a compensated zener reference provides +5 volts for the integrated circuits.

A clock circuit which provides pulses at a rate of about 500 pps to the binary counter circuits is made up of a Unijunction transistor pulse generator. The remaining circuit consists of an astable multivibrator which switches an LM100 regulator to provide a chopped voltage to the autocollimator light sources, which consist of Pinlight type 30-30 lamps drawing 30 Ma with an excitation of 3.0 volts, and having a rated

life of 1000 hours at these levels. To ensure that no new failure mode was introduced by cycling the lamps on and off, two lamps were selected from the batch received (Lot #6789) and placed on a cycle test in which they were operated at a 50 per cent duty cycle at one cps for a period of 245 hours, at rated voltage (3.0 volts). The lamp voltage was then increased by 20 per cent for 90 hours and reduced to 3.0 volts for an additional 73 hours, at which point the lamps were still operating. Since lamp life is inversely proportional to the 12th power of the applied voltage the equivalent time at increased voltage could be considered as 90×1.2^{12} which is approximately 810 hours. Thus, the total equivalent time was 1128 hours at a 50 per cent duty cycle. This was felt to be sufficient indication that no new failure mode was introduced by cycling the lamps, and that reasonable life could be expected.

2.4 Solar Cell Experiment Package

The solar cell experiment package shown in Figs. 2-12 and 2-13 is divided into two sections; one half being occupied by the solar cells, filters and heated mounting block, while the second half contains the processing electronics to sequentially monitor cell output and mounting block temperature.

The electronics for the solar cell experiment are contained on three printed circuit boards (Series 600, Series 700 and Series 800). The Series 800 board contains filters and regulators for the various supply voltages required by the electronics, while the Series 600 board contains a commutator drive system consisting of a unijunction pulse generator operating at about 3 pps, a driver, a three-stage binary counter made up of integrated circuits, and three relay drivers which function as saturated switches. The Series 700 circuit board holds an eight channel commutator using two pole double throw relays connected so that each state of the binary counter defines a unique path through the relay tree. Its output is fed to a conditioning amplifier whose output is proportional to the product of the feedback resistor, and the difference between a particular cell current and an offset current. This technique is permitted the determination of cell current to better than one per cent because accuracy depended primarily on the offset current which was measured prior to flight. Limiter circuits are provided to limit the output of A701 between 0 and 5 volts.

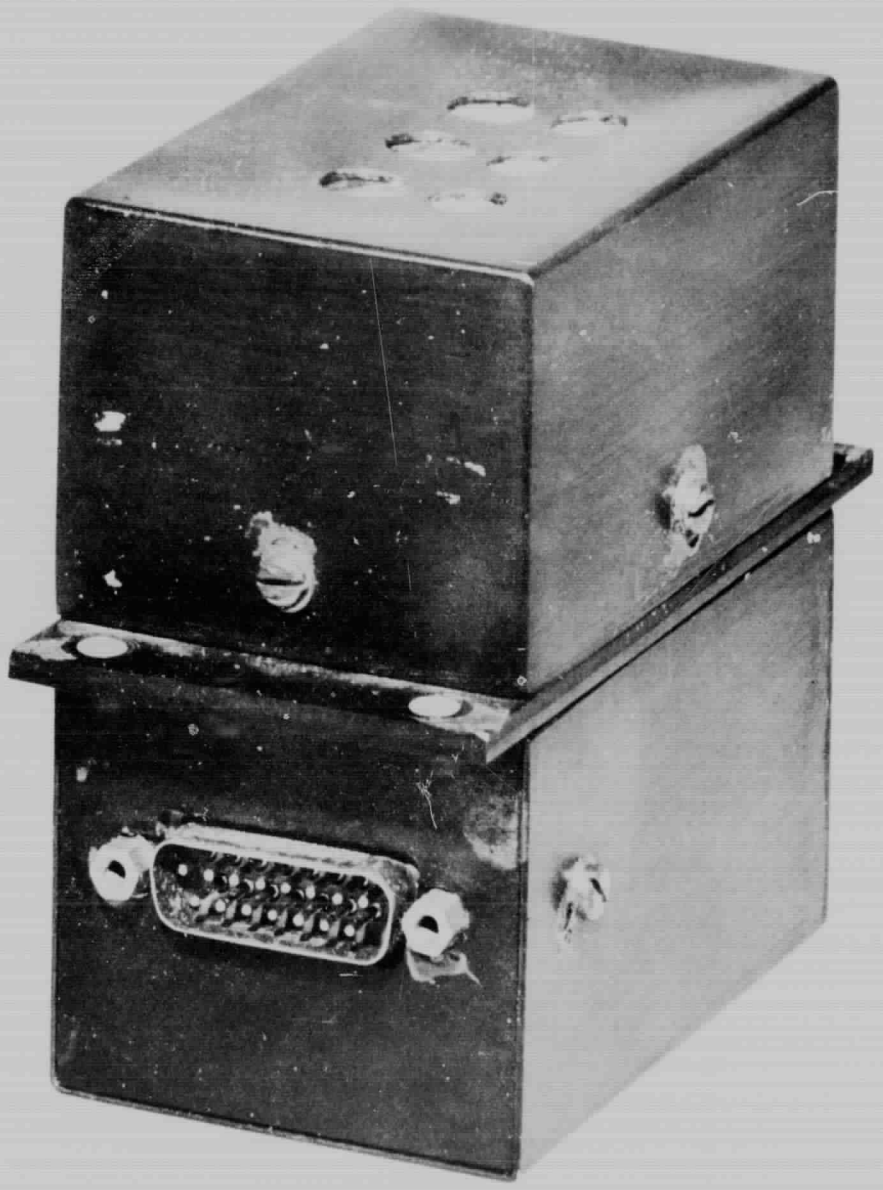


Figure 2-12 Solar Cell Experiment
After R[illegible]y

"REPRODUCIBILITY OF THE ORIGINAL PAGE IS POOR."

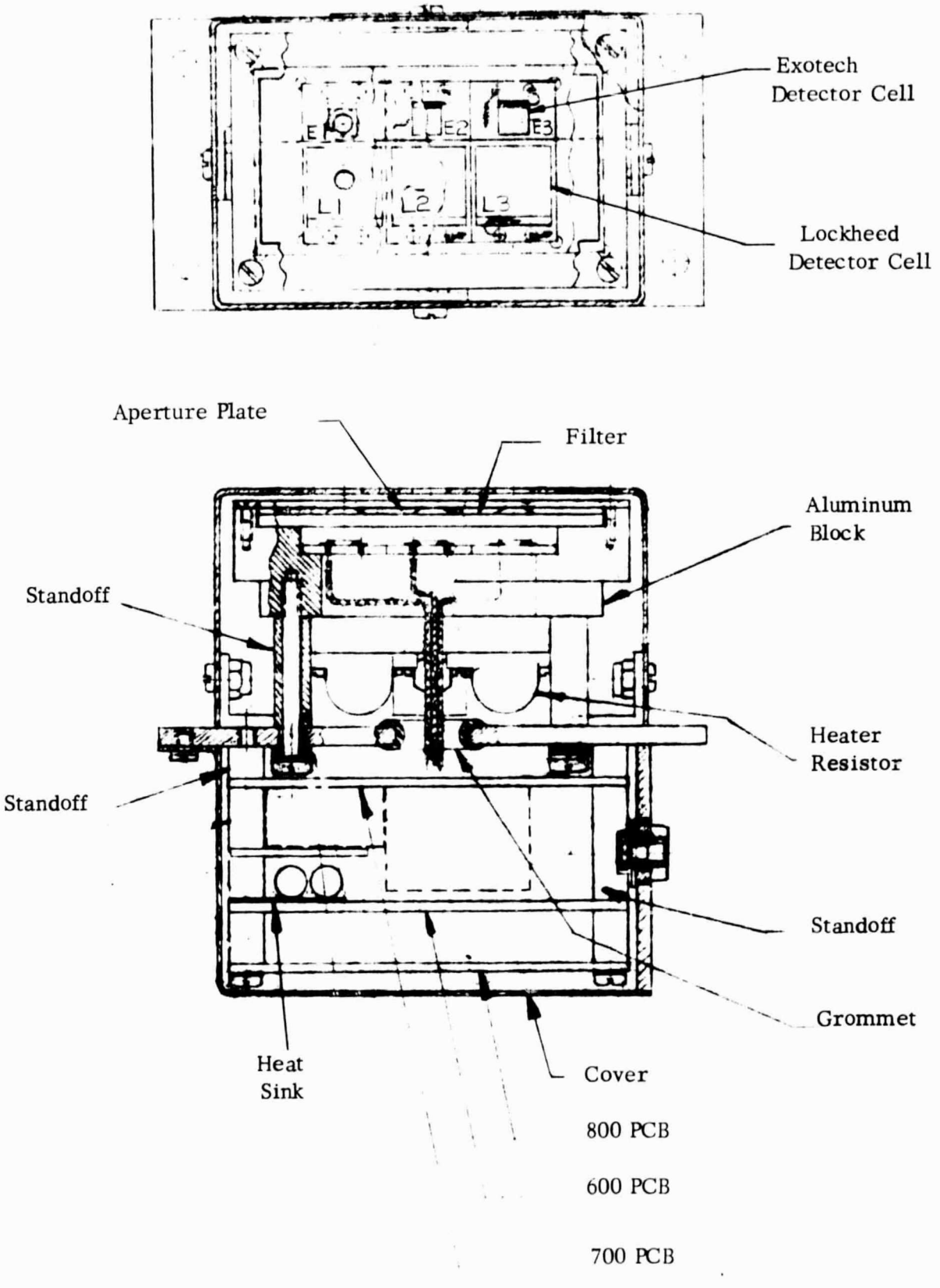


Figure 2-13 Solar Cell Experiment Assembly

In addition to the six cell currents, two other commutated signals are generated, the temperature of the block and a sync pulse.

An actual telemetry record showing the complete output format is shown in Figure 2-14.

"REPRODUCIBILITY OF THE ORIGINAL PAGE IS POOR"

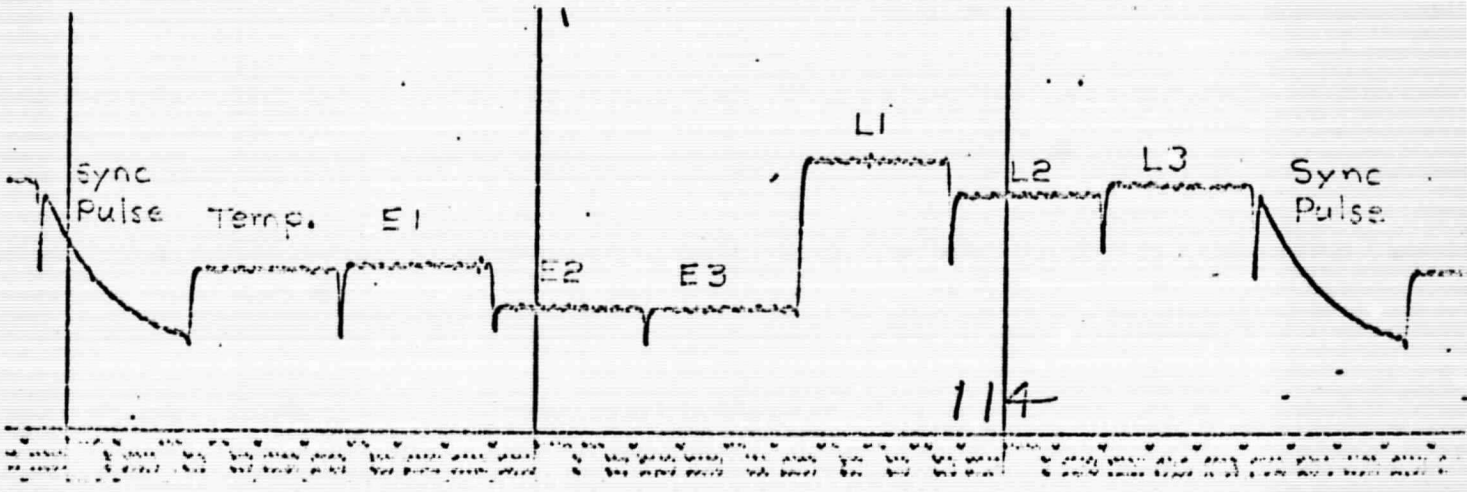


Figure 2- 14 Solar Cell Experiment Telemetry Signal Format

3.0 TEST AND CALIBRATION

An extensive test and calibration program was carried out in connection with the PASS system in order to establish the validity of information obtained during subsequent operation as a performance payload. Tests were performed under environmental conditions anticipated in an Aerobee flight regime, including shock, vibration, temperature variation and supply voltage fluctuation. In addition, an elaborate solar cell test program was undertaken to provide information for the solar cell experiment package.

3.1 Optical Sensor Testing

The optical sensors were carefully calibrated using an Exotech Model 5-T Solar Simulator and subjected to qualification or acceptance tests in conformance with Aerobee 150 specifications. Measurements were performed during and subsequent to these tests to determine the extent of uncertainty in the calibration due to the launch and operating conditions. A complete calibration of the sensor transfer function was performed prior to and subsequent to the test sequence. Operational tests of the sensor absolute accuracy were performed during the thermal tests. A summary of the significant results is given in Table 3-1 and Figs. 3-1 and 3-2 which are typical examples of the sensor transfer functions.

TABLE 3-1

	PITCH	YAW
Change in Sensor Absolute Pointing + 25° C to +55°C	+ 5. 8 Sec	- 4. 4 Sec
Change in Sensor Absolute Pointing +25°C to -5°C	+ 2. 0 Sec	- 2. 6 Sec
Total Change in Sensor Absolute Pointing At 25°C Due to Shock, Vibration, and Permanent Thermal Effects	- 2. 7 Sec	- 4. 6 Sec

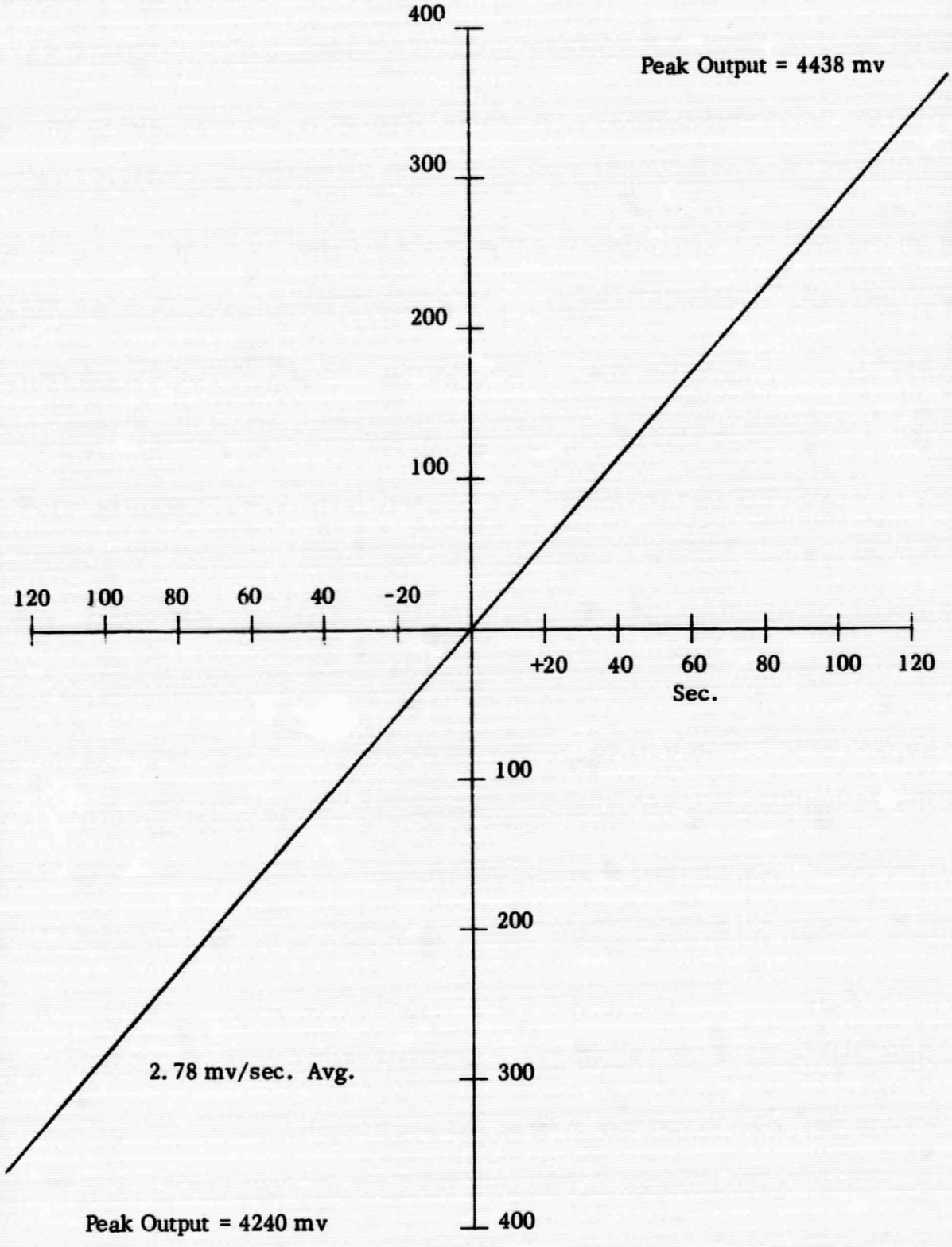


Fig. 3-1 Pitch Sun Sensor Transfer Curve ATP 101 7.2.1.2

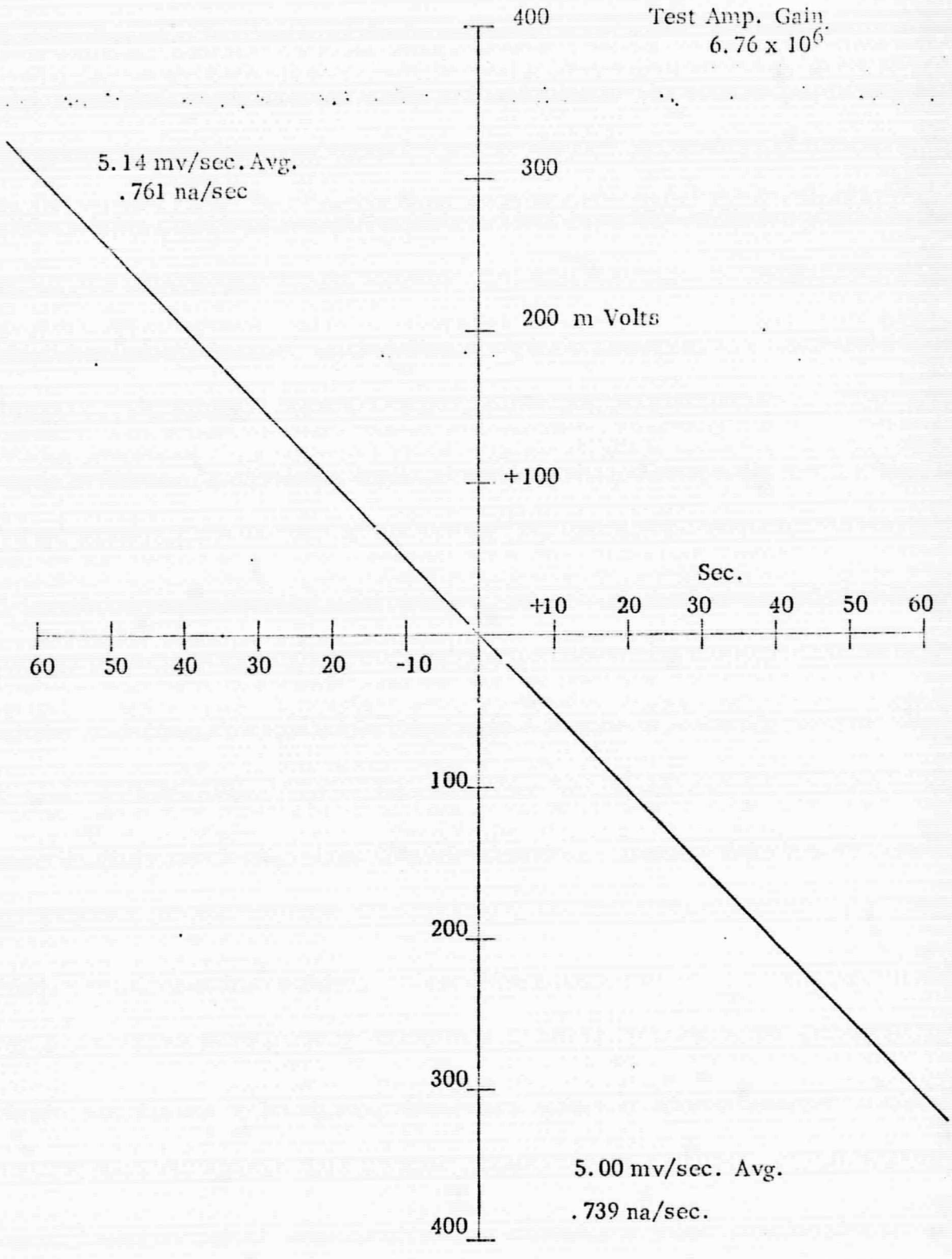


Fig. 3-2 - Pitch Autocollimator Transfer Curve ATP 101 7.1.2

3.2 Signal Processor Testing

The signal processor was tested according to the procedures specified in the Acceptance Test Procedure (ATP) and a summary of the important results is given in the ensuing material.

3.2.1 Sensor Channel Transfer Curve Evaluation

For the sensor channel transfer curves the maximum output change in the high resolution range was -0.07 volts in the pitch channel (See Tables 3-2 and 3-3). Based on an output sensitivity of 0.09 volts/arc second this was equivalent to 0.77 arc seconds.

For the low gain region, the maximum shift was 0.01 volts in the output with a gain of 0.834 and a full scale input of 3.0 volts. This corresponds to an accuracy of (0.01/3 x 0.834) x 100= 0.4% of full scale.

For the calibration range the maximum output change was 0.1 volts with an input of 5.0 volts and a gain of 2.91, corresponding to an accuracy of (0.1/5 x 2.91) x 100=0.69% of full scale.

3.2.2 Autocollimator Channel Transfer Curves

For the autocollimator channels, the maximum gain change was 0.63% which occurred in the pitch channel at 55°C. Limiting took place at nominal levels of +5.0 volts and -0.3 volts.

3.2.3 Summary

All of the above results are within the limits specified in the ATP.

3.3 Sensor Amplifier Testing

The sensor amplifier was tested according to the procedures specified in the ATP and a summary of the results is given in Table 3-4. The only major change in the ATP was to make the amplifier zero-drift test more realistic by substituting the actual sensor cells for a fixed input resistor. Since the sensor

TABLE 3-2

PITCH SENSOR CHANNEL TRANSFER CURVE VARIATIONS

RANGE	MAXIMUM SHIFT +	-
High Resolution	+0.04 Volts	-0.07 Volts
Calibration	+0.10 Volts	-0.05 Volts
Low Gain	+0.01 Volts	-0.00 Volts

*Supply Input Range 28 to 32 Volts

Temperature Range -6°C to 55°C

****

TABLE 3-3

YAW SENSOR CHANNEL TRANSFER CURVE VARIATIONS

RANGE	MAXIMUM SHIFT +	-
High Resolution	+0.06 Volts	-0.06 Volts
Calibration	+0.03 Volts	-0.04 Volts
Low Gain	+0.00 Volts	-0.01 Volts

*Supply Input Range 28 to 32 Volts

Temperature Range -6°C to 55°C

****

TABLE 3-4

SENSOR AMPLIFIER GAIN

AMPLIFIER	MEASURED GAIN	FEEDBACK RESISTOR
Yaw Sun Sensor	612	611
Pitch Sun Sensor	586	589
Yaw Autocollimator	829,000	823,000
Pitch Autocollimator	828,000	823,000

impedance tended to fall rapidly at high temperatures, the effect of amplifier offset voltages was more apparent.

3.3.1 Gain Evaluation

Measured gains and predicted gains based on the specified feedback resistor are given in Table 3-4. All are in agreement within 0.8%.

3.3.2 Offset Control Evaluation

From inspection of the test records, the offset resolution was better than one arc second for both solar sensor and autocollimator amplifiers.

The minimum peak offset was 100.5 for the pitch solar sensor amplifier, corresponding to 33.5 arc seconds, which confirms an offset range capability of at least ±33.5 arc seconds.

In the case of the autocollimator amplifier the actual voltage offset was undirectional with a minimum value of -36.3 millivolts or about 60 arc seconds nominal. This was sufficient to ensure that the autocollimator reference or 0 level could be adjusted to +2.5 volts at the output, assuming the signal processor autocollimator channel had a gain of -79 as confirmed by previous tests.

3.3.3 Zero Drift Evaluation

From Table 3-5 the maximum solar sensor amplifier zero drift was equivalent to 0.087 arc seconds, while the maximum autocollimator zero drift was equivalent to seven arc seconds. The latter figure of course is a dc shift that affects both levels of the chopped autocollimator signal equally and does not cause an error in the autocollimator signal.

3.3.4 Noise

From the test records, noise levels were below 0.5 arc sec. peak to peak.

TABLE 3-5
SENSOR AMPLIFIER ZERO DRIFT

AMPLIFIER	T= -5°C	T= +55°C
Yaw Sun Sensor	-0.063 sec	-0.087 sec
Pitch Sun Sensor	+0.023 sec	-0.070 sec
Yaw Autocollimator	-7.0 sec *	+6.8 sec *
Pitch Autocollimator	+4.5 sec *	+4.7 sec *

*Shifts refer to center of chopped waveform and do not result in error

3.3.5 Offset Control Stability

This test was added to the ATP after the first system had been tested (System No. 2) and only data from System No. 1 are available. An offset was set on each amplifier prior to environmental testing and rechecked after testing. The maximum shift in the solar sensor channels was 0.5 millivolts corresponding to about 0.17 arc seconds. The autocollimator channel shifts were negligible.

3.4 Solar Cell Experiment Testing

3.4.1 Electronics Testing

From the electronics test results it is possible to generate a formula for computing cell current, I_c, from output voltage, V_o. At 25°C this is:

$$I_o = 0.861 + \frac{(Vo - 2.69)}{21.2} \text{ milliamps}$$

3.4.2 Cell Calibration

The output currents of the cells were adjusted to a uniform sun predicted output by adjusting the size of the apertures in front of each cell. The standard cells were used to set up the intensity of a filtered quartz-iodine lamp to simulate space sun irradiances and a preflight calibration run was performed. The data from this calibration is included as Table 3-6.

3.4.3 Thermistor Calibration

Thermistor calibration data is shown in Fig. 3-3 which also shows the heating rate of the cell mounting block to be about 5.7°C/min, at room temperature.

EXOTECH INCORPORATED ROCKVILLE, MD.		PARAMETER: SOLAR CELL EXPERIMENT PREFLIGHT CALIBRATION PRODUCT: PASS SYSTEM #1			
CELL		Lamp 92.1V Load 10 Ω Millivolts	Lamp 99.4V Load 10 Ω Millivolts	Experiment Output Volts	Cell Current Milliamps
Lamp Voltage 92.1V					
Lockheed	#15	59.3			5.93
	# 9	59.8			5.98
	# 3	59.0			5.90
L1	#20			3.03	.877
L2	#16			2.55	.854
L3	# 1			2.75	.864
Lamp Voltage 99.4V					
Exotech	# 3		27.0		2.70
	#25		28.1		2.81
	#13		26.4		2.64
E1	#15			2.85	.869
E2	#21			2.28	.842
E3	#34			1.95	.826

TABLE 3-6

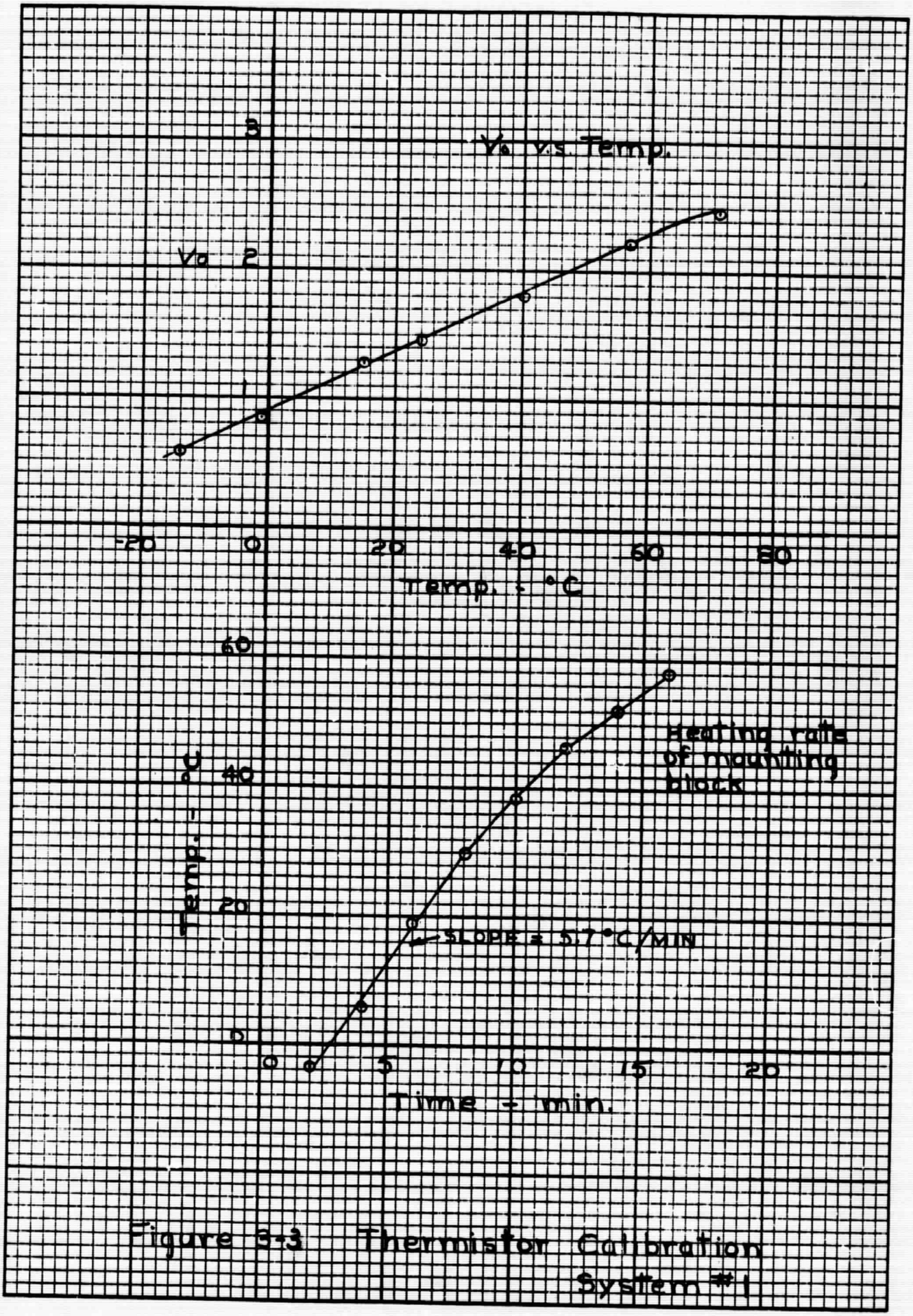


Figure 3-3 Thermistor Calibration System #1

3.4.4 Standard Cell Calibration

In order to provide a standard for space sun performance evaluation of future solar detectors under laboratory conditions, a set of six solar cells/filters were prepared, matched, and calibrated along with the two cell/filter sets to be flown on the solar cell experiment. Output data was taken for each of three Exotech cell/filter pairs and three Lockheed cell/filter pairs along with those to be flown while being illuminated by the Exotech Model 5-T solar simulator. These data were filed with the standard cells so that after flight data indicating cell output under space conditions is available, correction factors can be calculated to equate the laboratory measurements with the values to be expected in flight, making possible judicious cell selection and output level adjustments.

4.0 FLIGHT REPORT

The flight report is based on playback number nine of the telemetry record of NASA rocket flight 4.202, launched from White Sands, New Mexico, in March, 1968.

PASS System No. 1 was aboard as a performance payload, in which the PASS sensors were mounted on an optical reference plate along with the SPARCS control sensor, the purpose of the PASS system being to monitor SPARCS control performance.

Also included in the payload was a solar cell experiment package, containing three PASS type solar cells and filters and three SPARCS type solar cells and filters. Its purpose was to provide information on solar cell stability in space sun conditions with varying cell temperatures.

4.1 Preflight Checks

Several preflight checks were made on the PASS system to verify system performance on a functional level, and to check sensor output polarities. A record of these tests is included in Figs. 4-1 and 4-2, whose results may be summarized as follows:

1. A positive going pitch solar sensor error gives positive going telemetry output.
2. A positive going yaw solar sensor error gives positive going telemetry output.
3. If the pitch sensor is forced to pitch up in a positive pitch error position, the pitch autocollimator telemetry output is positive or in-phase with the lamp drive signal.
4. If the yaw sensor is forced to yaw right in a positive yaw error position, the yaw autocollimator telemetry output is positive or in-phase with the lamp drive signal.

"REPRODUCIBILITY OF THE ORIGINAL PAGE IS POOR."

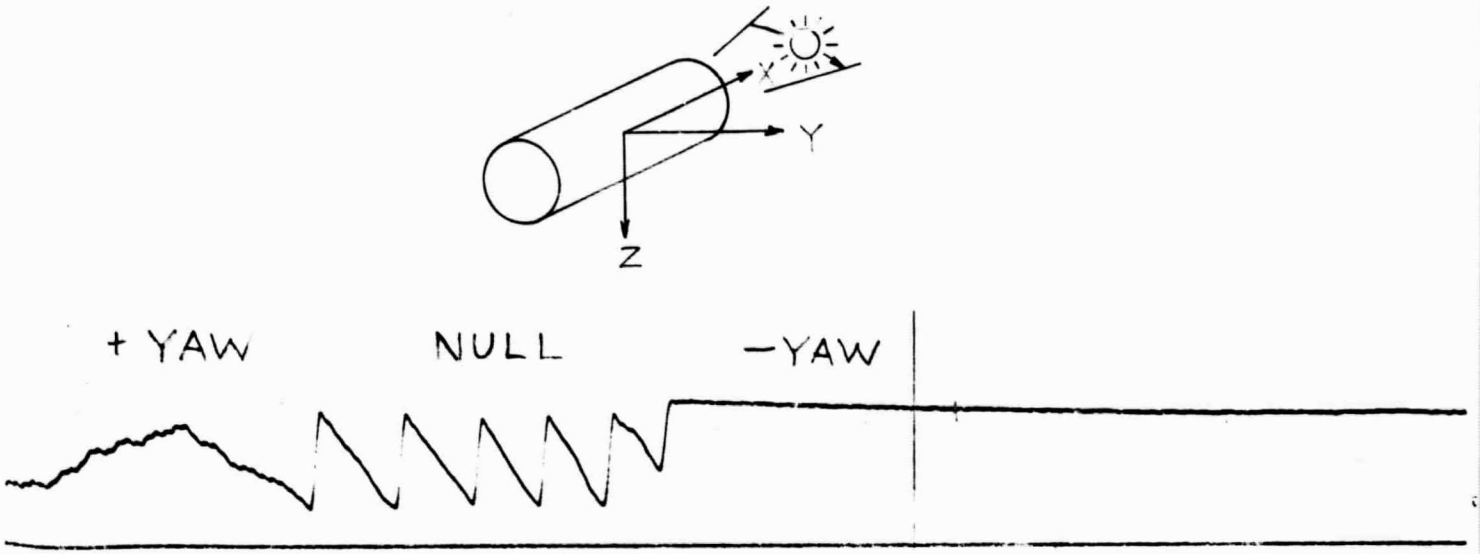


Figure 4-1 Yaw Axis Check

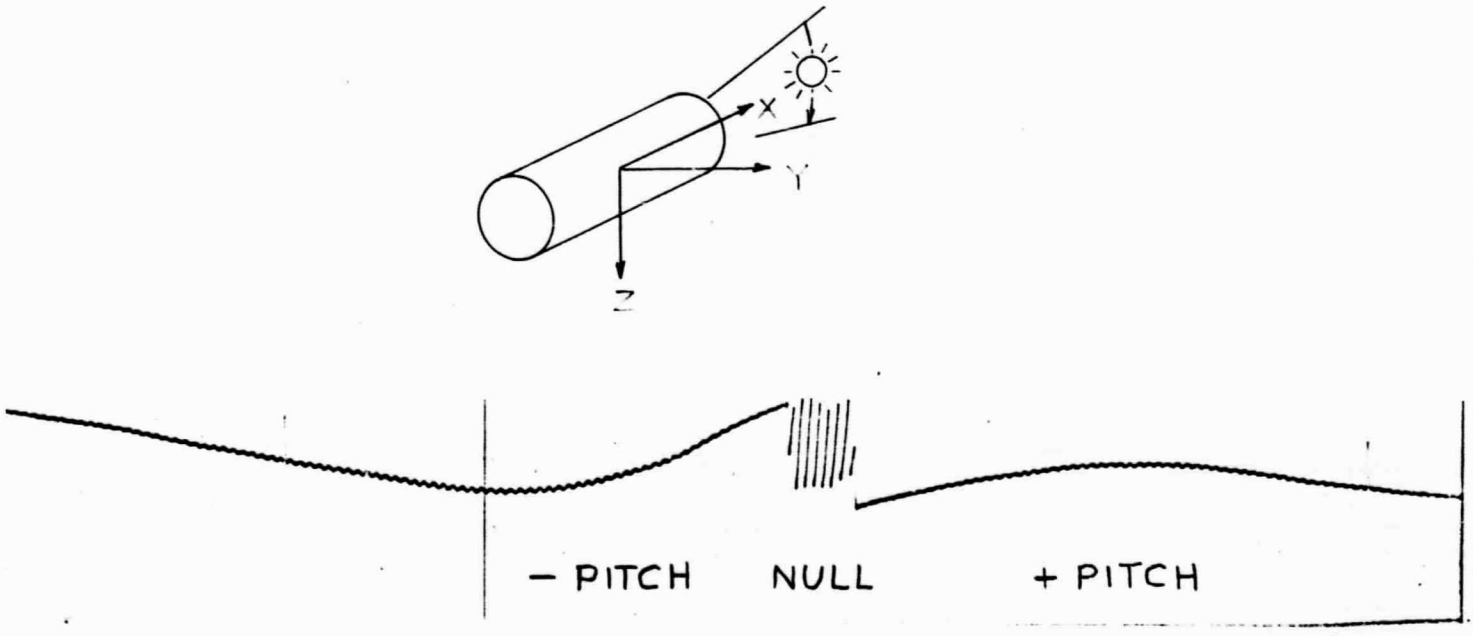


Figure 4-2 Pitch Axis Check

For reference purposes, a diagram of the sensor connections and the orientation of the sensors in the mounting plate are included in Figs. 4-3 and 4-4, respectively.

4.2 Flight Chronology

Segments of the flight telemetry record are included to support the following discussion of the flight. Times indicated on each section are relative to the launch time.

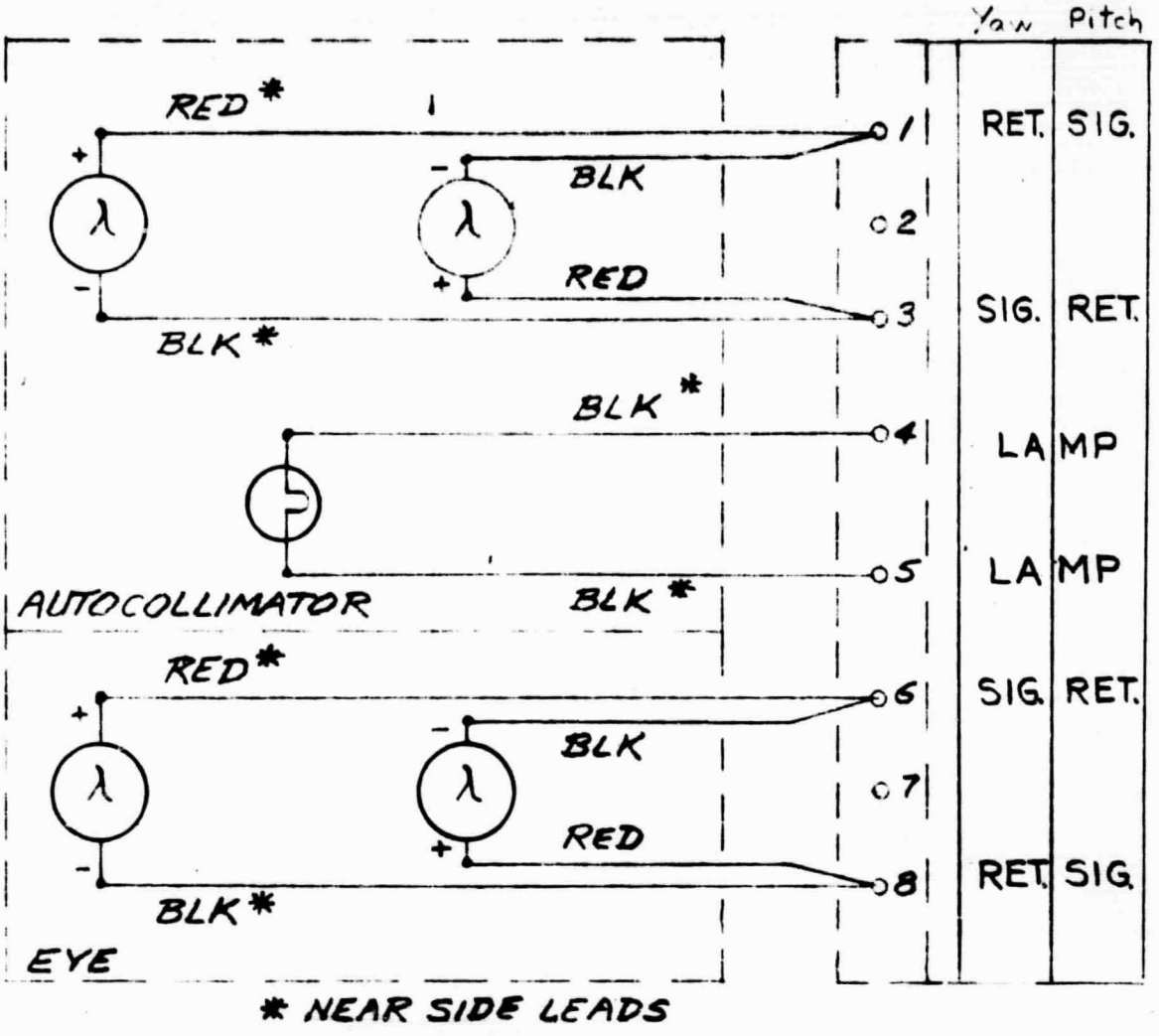
4.2.1 Flight Highlights

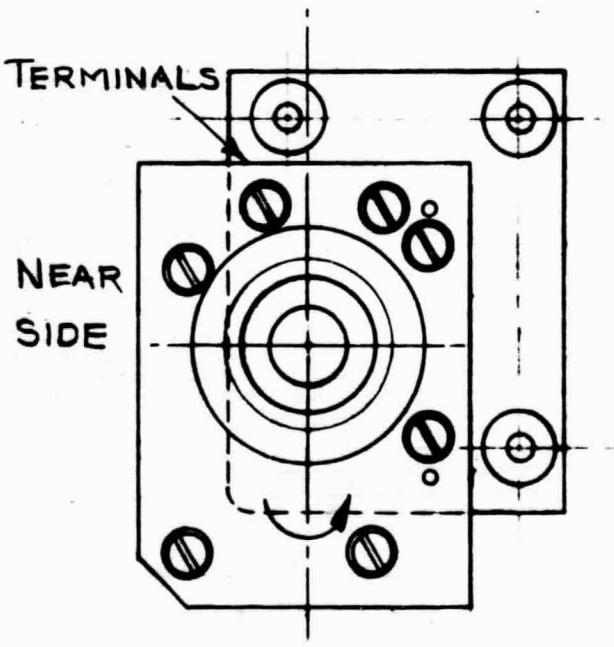
4.2.1.1 Pre-Launch (t= -9)

A record of all PASS outputs is shown prior to launch. The voltage levels noted compare closely to those measured during set-up by Exotech in November, 1967, which illustrates the inherent long-term stability of the system.

	March 1968 Output Volts	Nov. 1967 Output Volts
Pitch Range	2.0 (Range 4)	2.04
Pitch Sun Sensor	0.61	0.62
Yaw Sun Sensor	4.10	4.10
Yaw Range	2.8 (Range 6)	2.80
Pitch A/C 0	2.9 Δ = +.48V	2.80 Δ = -.42V
Yaw A/C 0	2.4 Δ = +.37V	2.20 Δ = +.40V

"REPRODUCIBILITY OF THE ORIGINAL PAGE IS POOR."





ROTATION
SHOWN

+ O/P FROM PIN 1

+ O/P FROM PIN 8

Figure 4-3 Sensor Connections

"REPRODUCIBILITY OF THE ORIGINAL PAGE IS POOR."

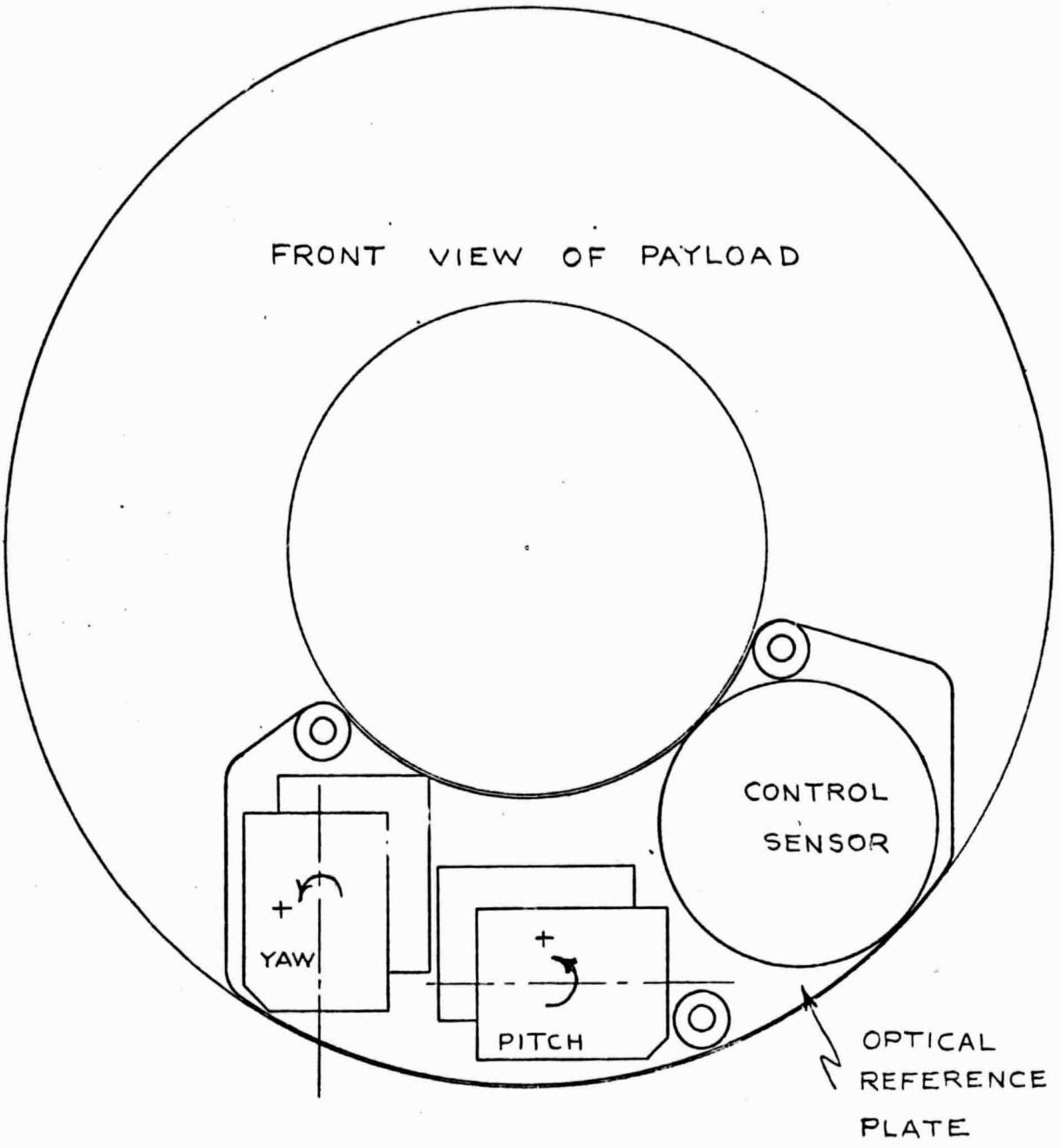


Figure 4-4 Sensor Mounting

4.2.1.2 Launch (t= 0)

During the boost phase of the launch the pitch autocollimator output shifted about ten arc seconds which may have been due to deflection of the reference mirror or to a small tilt in the optical housing. In any case the output returned to its preflight value by t = 4 seconds.

4.2.1.3 Acquisition (t = 114 to t = 126)

Acquisition of the sun occurred from t= 114 to t = 126 during which time both solar sensor outputs went through the calibration ranges as noted on the accompanying records. From peak outputs, accurate calibration constants could be calculated for sensor gain. It is also possible to see transitions through the high resolution ranges as noted on the records.

4.2.1.4 Initial Limit Cycle (t =130)

A portion of the record near t = 130 shows the initial limit cycle which is about 16 arc seconds peak-to-peak in yaw and nine arc seconds peak-to-peak in pitch.

4.2.1.5 Yaw Drift (t = 224)

A slow drift occurred in the yaw sun sensor channel output throughout the flight, culminating in switching back and forth between ranges 6 and 5 of the high resolution range.

4.2.1.6 Loss of Lock (t= 347)

Loss of lock is indicated at about t=347, when the pitch channel output again went through calibration range C2 giving a peak output of 3.30 volts, corroborating the 3.31 volts obtained during acquisition.

4.3 Calibration

The first essential piece of information to be obtained is the calibration of the solar sensors from their peak space output, as indicated by peak readings in the calibration ranges.

PAGE 4-7 MISSING FROM ORIGINAL DOCUMENT.

The Space Gain at the sensor amplifier output may be determined from:

$$G_{space} = \text{Test Gain} \times \frac{\text{Space Peak}}{\text{Test Peak}}$$

	From + Peak Space Gain millivolts/sec	From -Peak Space Gain millivolts/sec	Mean Space Gain
Pitch	$4.49 \times \frac{2.780}{4.438} = 2.82$	$4.34 \times \frac{2.780}{4.240} = 2.84$	2.83 mv/sec
Yaw	$4.31 \times \frac{2.380}{4.000} = 2.56$	$4.65 \times \frac{2.380}{4.318} = 2.56$	2.56 mv/sec

Space Gain at the telemetry output may be computed for the fine ranges of the signal processor through multiplying the above results by the fine range gain constants obtained from tests on the signal processor.

Pitch Space Gain = 2.83 x 33.4 = 94.5 mv/sec for range 4 at 25°C

Yaw Space Gain = 2.56 x 33.3 = 85.3 mv/sec for range 6 at 25°C

4.4 Pointing

After fine pointing control was established, the solar sensor outputs were determined to be in ranges 4 and 6 for the pitch sensor and yaw sensor respectively. This was determined from the pitch and yaw range signals, which were somewhat noisy due to decommutation problems with the telemetry record. However, these range values were verified by keeping track of the ranges on the high resolution channels during acquisition. Ranges are noted on the telemetry records from t = 120 to t = 126.

Data from the fine sun sensor channels were recorded at 10 second intervals, for maximum and minimum points in the limit cycle as noted on the records. From these data mean pointing position and peak-to-peak limit cycle information were computed (Tables 4-1 and 4-2).

EXOTECH INCORPORATED PARAMETER: PITCH AXIS SOLAR SENSOR FLIGHT DATA

ROCKVILLE, MD.

Time	Limit Cycle Solar Sensor +Peak Volts	Limit Cycle Solar Sensor -Peak Volts	Mean Range 6 Volts	Difference D Volts	Peak to Peak Limit Cycle D/.00945 Arc Sec.	Deviation From Initial Mean Volts	Deviation Arc Sec.
t= 130	3.15	2.25	2.68	.85	9.0	0.00	0.0
140	3.45	2.35	2.90	1.10	11.6	.22	2.3
150	3.60	1.95	2.78	1.65	17.5	.10	0.9
160	3.55	2.20	2.88	1.35	14.3	.20	2.1
170	3.40	2.50	2.95	.90	9.5	.27	2.9
180	3.25	2.10	2.68	1.15	12.2	0.00	0.0
190	3.60	2.00	2.80	1.60	16.9	.12	1.3
200	3.20	2.15	2.68	1.05	11.1	0.00	0.0
210	3.35	2.05	2.70	1.30	13.8	.02	.2
220	3.50	2.30	2.90	1.20	12.7	.20	2.1
230	3.00	2.15	2.73	1.15	12.2	.05	.5
240	3.05	2.70	2.88	.35	3.7	.20	2.1
250	3.30	2.35	2.83	.95	10.1	.15	1.6
260	3.25	2.45	2.85	.80	8.5	.17	1.8
270	3.40	2.25	2.83	1.15	12.2	.15	1.6
280	3.60	2.40	3.00	1.20	12.7	.32	3.4
290	3.00	2.35	2.68	.65	6.9	0.00	0.0
300	2.95	2.45	2.70	.50	5.3	.02	.2
310	3.10	2.25	2.68	.85	9.0	0.00	0.0
320	3.00	2.00	2.50	1.00	10.6	-.18	-1.9

TABLE 4-1

EXOTECH INCORPORATED
ROCKVILLE, MD.

PARAMETER: YAW AXIS SOLAR SENSOR FLIGHT DATA

Time	Limit Cycle Solar Sensor + Peak Volts	Limit Cycle Solar Sensor -Peak Volts	Mean Range 6 Volts	Difference D Volts	Peak to Peak Limit Cycle D/.0853 Arc Sec.	Deviation From Initial Mean Volts	Arc Sec.
t = 130	4.05	2.65	3.35	1.40	16.4	0.00	0.0
140	4.10	2.75	3.43	1.35	15.8	.08	.9
150	4.25	2.75	3.50	1.50	17.6	.15	1.8
160	4.45	2.90	3.68	1.55	18.2	.33	3.9
170	4.40	2.90	3.65	1.50	17.6	.30	3.5
180	4.35	2.95	3.65	1.40	16.4	.30	3.5
190	4.35	3.00	3.68	1.35	15.8	.33	3.9
200	4.45	3.00	3.73	1.45	17.0	.38	4.5
210	4.50	3.05	3.78	1.45	17.0	.43	5.0
220	4.40	3.05	3.73	1.35	15.8	.38	4.5
230	0.40 (R5)	3.15	3.88	1.45	17.0	.53	6.2
240	.35	3.40	3.98	1.15	13.5	.63	7.4
250	.45	3.30	3.98	1.35	15.8	.63	7.4
260	.50	3.35	4.03	1.35	15.8	.68	8.0
270	.45	3.25	3.95	1.40	16.4	.60	7.0
280	.45	3.30	3.93	1.35	15.8	.58	6.8
290	.55	3.35	4.05	1.40	16.4	.70	8.2
300	.65	3.50	4.18	1.35	15.8	.83	9.7
310	.70	3.50	4.20	1.40	16.4	.85	10.0
320	.85	3.35	4.20	1.70	19.9	.85	10.0

TABLE 4-2

Autocollimator information was obtained at less frequent intervals, primarily beacuse of noisy decommutation which caused the record to have frequent jumps. However, autocollimator shifts were small so that data were taken whenever the decommutation appeared regular and several points were averaged near the beginning and end of the flight. Autocollimator gains were obtained from the autocollimator transfer characteristics and the composite autocollimator channel gains. This is summarized below, and in Table 4-3.

	+O/P -∠ Gain na/sec	-O/P + ∠ Gain na/sec	Preamp Gain ohms	Signal Proc. Gain	+O/P Gain -	-O/P Gain +
Pitch	0.761	0.739	8.28×10^3	79.0	49.8mv/sec	48.4mv/sec
Yaw	0.684	0.823	8.29×10^3	79.2	44.7mv/sec	53.8mv/sec

For the output polarities of the PASS System No. 1

Pitch A/C Gain = 48.4 mv/sec for negative outputs
49.8 mv/sec for positive outputs

Yaw A/C Gain = 53.8 mv/sec for positive outputs
44.7 mv/sec for negative outputs

From Tables 4-1 and 4-2 plots of peak-to-peak limit cycle and mean pointing position relative to initial position were made. These are shown in Fig. 4-5 which has several features of interest. For example, the yaw axis limit cycle appears to be very constant in amplitude with an average value of roughly 16 arc seconds peak-to-peak and 13.5 arc seconds peak-to-peak. The pitch axis limit cycle is somewhat smaller in amplitude, averaging about 11 arc seconds peak-to-peak but the amplitude varies from a maximum of 17.5 arc seconds peak-to-peak, to a minimum of 3.7 arc

EXOTECH INCORPORATED
ROCKVILLE, MD.

PARAMETER: AUTOCOLLIMATOR FLIGHT DATA

Time From Launch	Pitch A/C Output Volts ptop	(G=48.4) (mv/sec) Arc Sec.	Means Arc Sec.	Yaw A/C Output Volts ptop	(G=53.8) (mv/sec) Arc Sec	Means Arc Sec
-9	-.40	-8.3	-8.3	+.37	6.9	6.9
120	-.30	-6.2	-7.3	.40	7.4	8.1
165	-.40	-8.3		.47	8.7	
190	-.25	-5.2	-5.2	.35	6.5	6.5
270	-.28	-5.8		.34	6.3	
290	-.36	-7.4	-5.9	.37	6.9	6.4
300	-.22	-4.6		.29	5.4	
330	-.28	-5.8		.37	6.9	
Shift during launch +1 Sec				Shift during launch +1.2 Sec		

TABLE 4-3

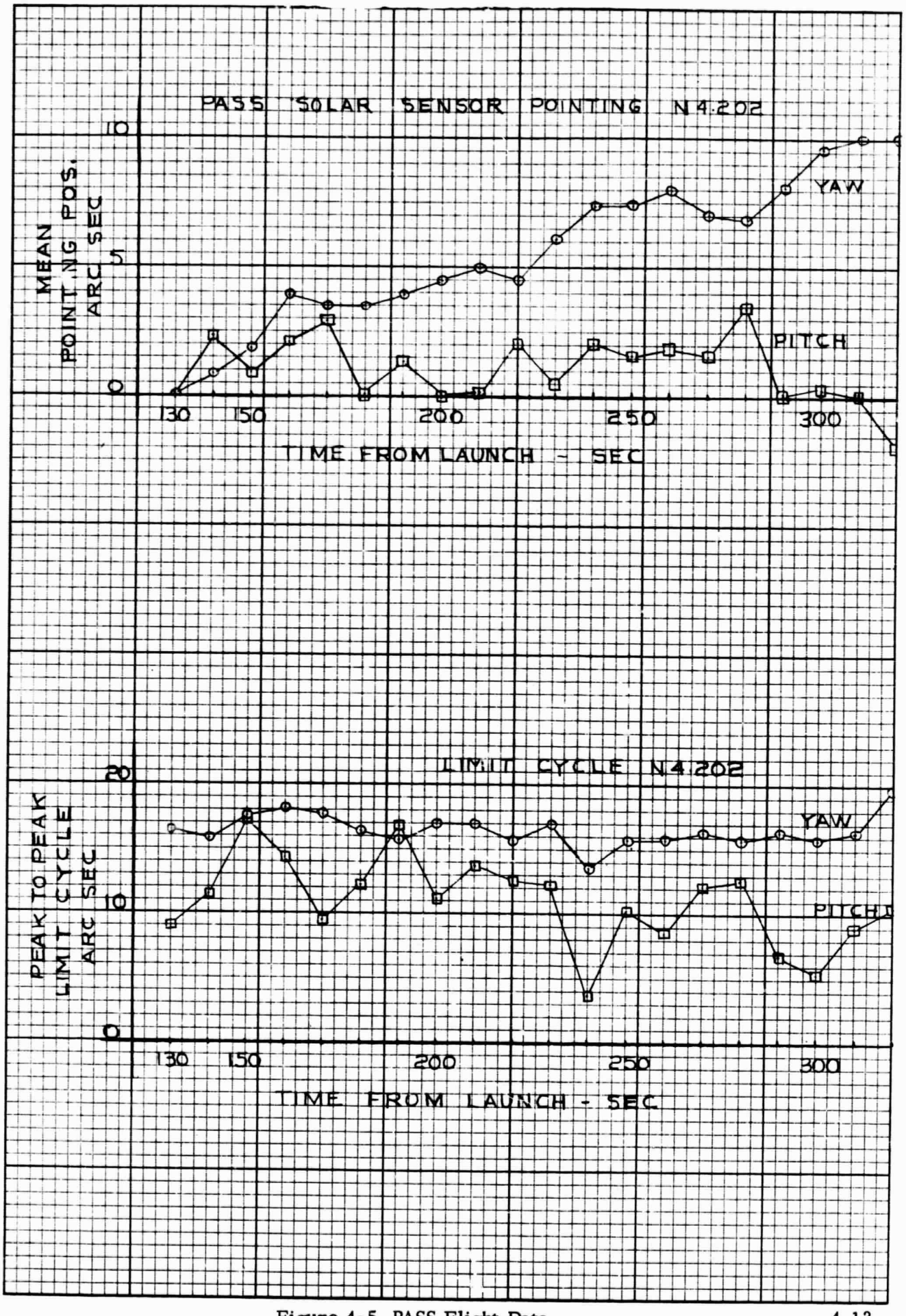


Figure 4-5 PASS Flight Data

seconds peak-to-peak.

In the case of the mean pointing position relative to the initial pointing position as indicated by the solar aspect sensor alone, both pitch and yaw axes may be characterized by relatively constant pointing for periods of about 40 seconds, followed by rapid transitions to new mean pointing positions. These jumps were quite small in the case of the pitch axis, being about 1.5 arc seconds and occurred in both directions. However, the yaw axis jumps were unidirectional so that a total drift of about 10 arc seconds was accumulated over the flight.

4.4.1 Absolute Pointing

Absolute pointing information must be determined separately for each axis since initial offsets, gains and sensor alignment calibrations vary.

4.4.2 Pitch Axis

Prior to launch, pitch output = 0.61 volts in range 4 with zero light input (section 4.2.1, t = -9).

After acquisition pitch output was still in range 4.

The angle between solar vector and sun sensor axes for any voltage, V_{ps}, in range 4 is given by:

$$\angle \text{ss-sv} = \frac{V_{ps} - 0.61}{0.0945} \quad \text{arc seconds}$$

where 0.945 is the pitch channel gain obtained from space calibration.

The angle between sun sensor and autocollimator axes was obtained during preflight testing ATP 101, and is +16.3 arc seconds.

$$\angle \text{ss-ac} = +16.3 \text{ arc seconds}$$

The angle between the autocollimator axis and a normal to the reference surface is given for any voltage, V_{pa}, by

$$\angle \text{n-ac} = \frac{V_{pa}}{0.484} \quad \text{arc seconds.}$$

The angle between the normal and the solar vector, i.e. the pointing error, E_p, is given by

$$E_p = \angle \text{n-sv} = \angle \text{n-ac} - \angle \text{ss-ac} + \angle \text{ss-sv}$$

$$E_p = -\frac{V_{pa}}{0.0484} - 16.3 + \frac{V_{ps} - 0.61}{0.0945}$$

After initial pointing at t=130, the mean pitch signal is given by

$$V_{psm} = 2.68 \text{ volts}$$

and

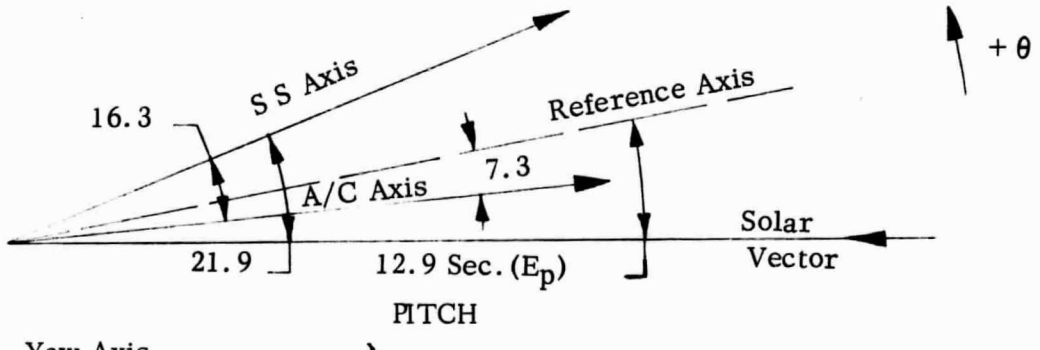
$$\frac{V_{pa}}{0.0484} = 7.3 \text{ arc sec.}$$

$$E_p = +7.3 - 16.3 + \frac{2.68 - 0.61}{0.0945}$$

$$= +7.3 - 16.3 + 21.9$$

$$E_p = 12.9 \text{ arc seconds}$$

This is illustrated below:



PITCH

4.4.3 Yaw Axis

Prior to launch yaw output = 4.10 volts in range 6 with 0 light input (section 4.2.1, t = -9).

After acquisition pitch output was still in range 6.

The angle between sun sensor and autocollimator axes is -38.4 arc seconds.

$\angle$ss-ac = 38.4 arc sec.

The sun sensor and autocollimator gains are 0.0853 volts/arc second and 0.0538 volts/arc second, respectively.

Using a development similar to that for the pitch axis, the pointing error is given by:

$$E_y = -\frac{V\,ya}{0.0538} + 38.4 - \frac{Vys - 4.10}{0.0853}$$

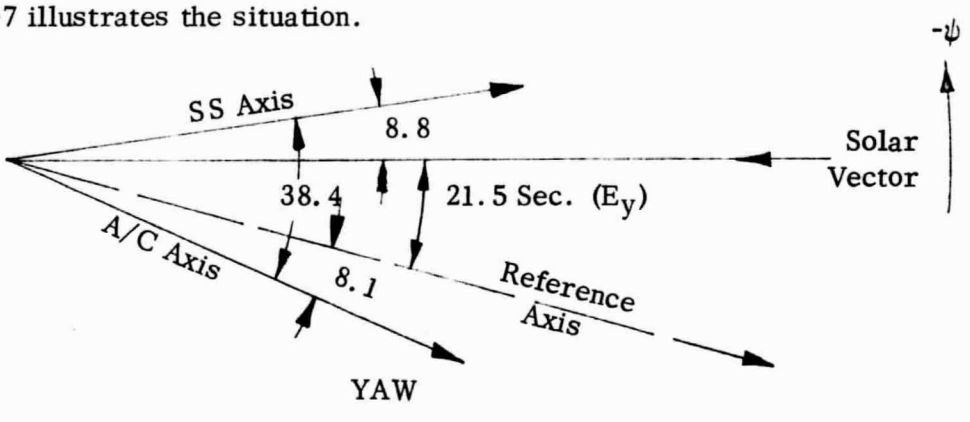
Initial pointing error at t= 130 is given by:

$$E_y = -8.1 + 38.4 + \frac{3.35 - 4.10}{0.0853}$$

$$= -8.1 + 38.4 - 8.8$$

$$= +21.5 \text{ arc seconds}$$

Figure 4-7 illustrates the situation.



4.5 Solar Cell Experiment

Two segments of the solar cell experiment flight record are shown in Figure 4-6 while a record of flight data is given in Table 4-4.

The solar cell mounting block functioned as expected, having a temperature rise of about 5.7°C/minute throughout the flight. Starting from an initial temperature of 19°C at t=130 a final temperature of 41°C was achieved at t = 340, just prior to the end of solar pointing.

"REPRODUCIBILITY OF THE ORIGINAL PAGE IS POOR."

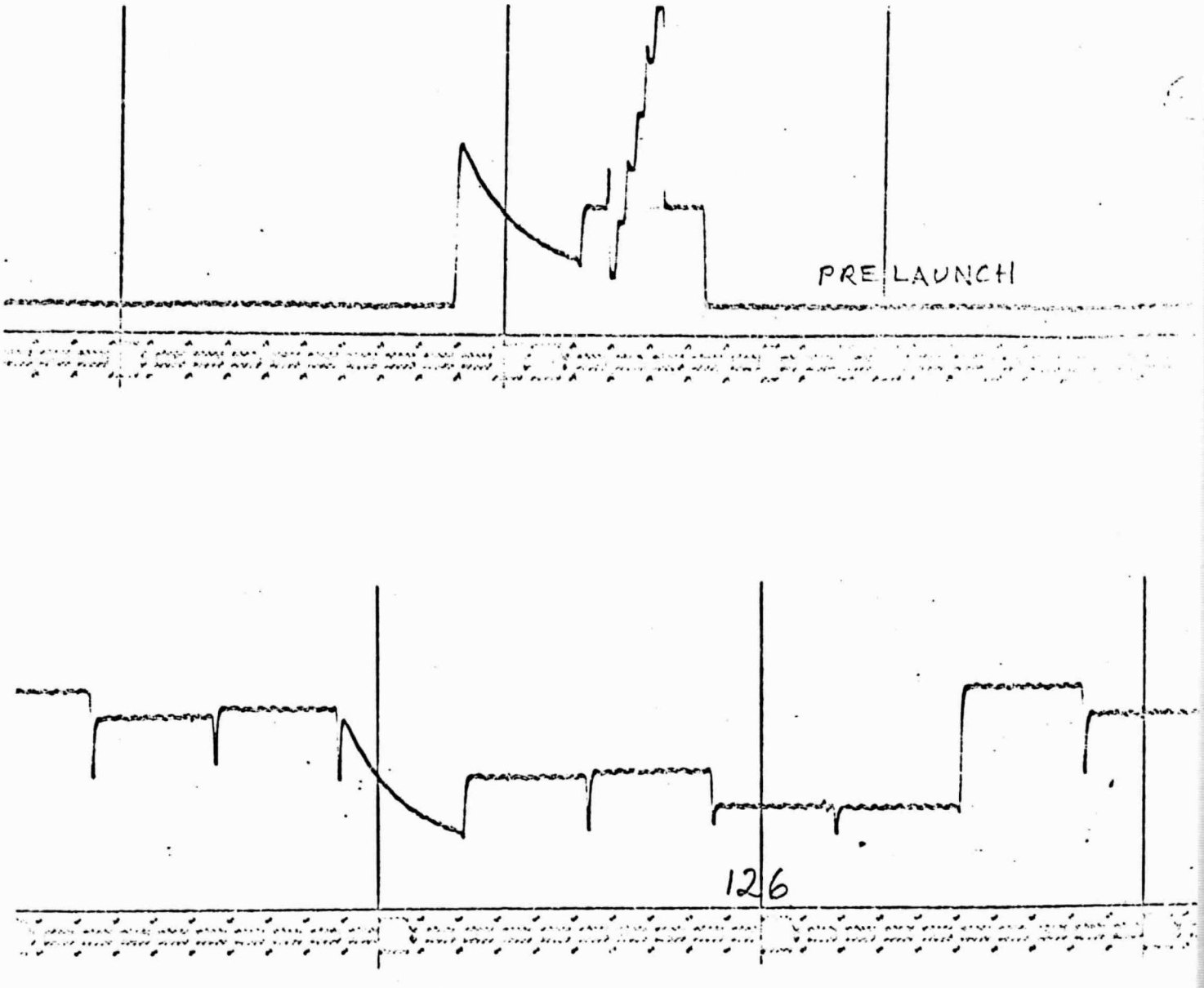


Figure 4-6 Solar Cell Experiment Flight Records

EXOTECH INCORPORATED ROCKVILLE, MD.	PARAMETER: SOLAR CELL EXPERIMENT FLIGHT DATA PRODUCT: PASS SYSTEM #1							
Time	E1 Volts	E2 Volts	E3 Volts	L1 Volts	L2 Volts	L3 Volts	Temp V_o	°C
t = 130	1.45	.80	.75	3.05	2.50	2.65	1.35	19.0
150	1.40	.80	.75	3.05	2.50	2.65	1.40	21.0
170	1.45	.80	.75	3.05	2.50	2.65	1.45	23.5
190	1.50	.80	.75	3.05	2.50	2.65	1.50	25.5
210	1.50	.80	.75	3.05	2.50	2.65	1.60	29.5
230	1.50	.85	.75	3.05	2.50	2.65	1.60	29.5
250	1.50	.85	.80	3.05	2.45	2.65	1.65	32.0
270	1.55	.85	.75	3.00	2.50	2.60	1.70	34.0
290	1.45	.90	.80	3.00	2.45	2.60	1.75	36.0
310	1.55	.90	.80	3.00	2.45	2.60	1.80	38.5
340	1.60	.85	.80	3.00	2.50	2.55	1.85	41.0

TABLE 4-4

Data was taken from the telemetry record at 20 second intervals as shown in Table 4-4, and from these, three pairs of data groups were selected for averaging and cell current computation. These pairs contained the first two groups and last two groups and a pair in the middle, as shown in Table 4-5. It may be noted that cell current changes are less than 1.0 per cent for all cells over the temperature range. This is discussed fully in the conclusion.

The complete PASS flight telemetry record is reproduced in Fig 4-7 for reference purposes.

EXOTECH INCORPORATED ROCKVILLE, MD.	PARAMETER: SOLAR CELL EXPERIMENT SUMMARY						
Cell	Mean Output t=130-150 Volts	Cell Current Ma.	Mean Output t=230-250 Volts	Cell Current Ma.	Mean Output t=310-340 Volts	Current Ma.	Cell Current During Ground Cal. Ma.
E1 #15	1.430	.802	1.500	.805	1.570	.809	.869
E2 #21	.800	.772	.850	.774	0.870	.775	.842
E3 #34	.750	.769	.775	.770	0.800	.771	.826
L1 #20	3.050	.878	3.050	.878	3.00	.876	.877
L2 #16	2.500	.852	2.470	.851	2.47	.851	.854
L3 # 1	2.650	.859	2.650	.859	2.57	.855	.864
Temperature	1.37	20°C	1.630	30.7°C	1.83	40°C	
				1 in =	.861 +	$(\frac{V_o - 2.69}{21.2})$	Ma.
	30°C Change Ma.	%	40°C Change Ma.	%		For Exotech Cells Space Correction for standards .924	
E1	+.003	.37	+.007	.87			
E2	+.002	.26	+.003	.39			
E3	+.001	.13	+.002	.26			
L1	.000	.00	-.002	-.23		For Lockheed Cells Space Correction for standards .998	
L2	-.001	-.12	-.001	-.12			
L3	.000	.00	-.004	-.47			

TABLE 4-5

"REPRODUCIBILITY OF THE ORIGINAL PAGE IS POOR."

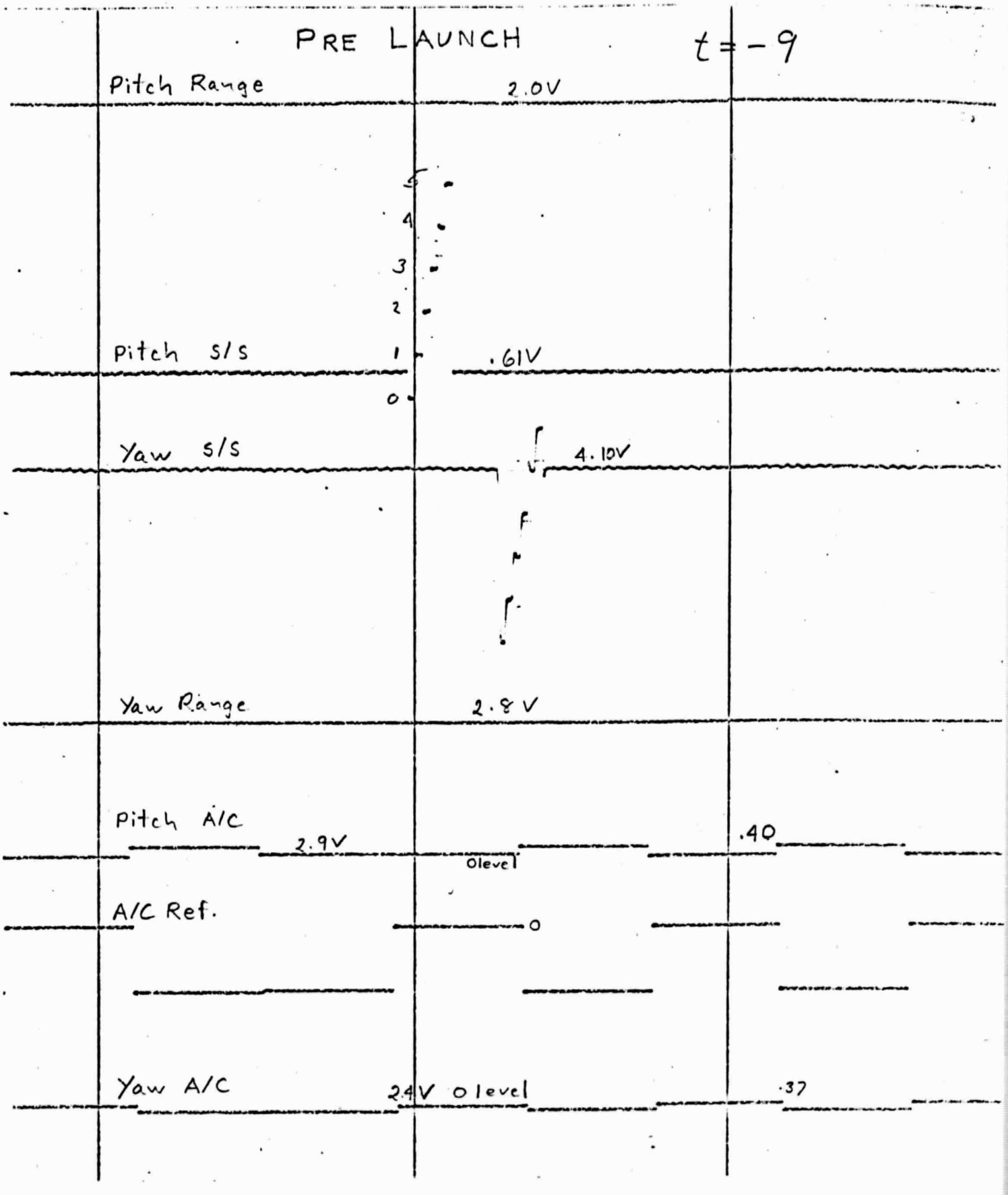
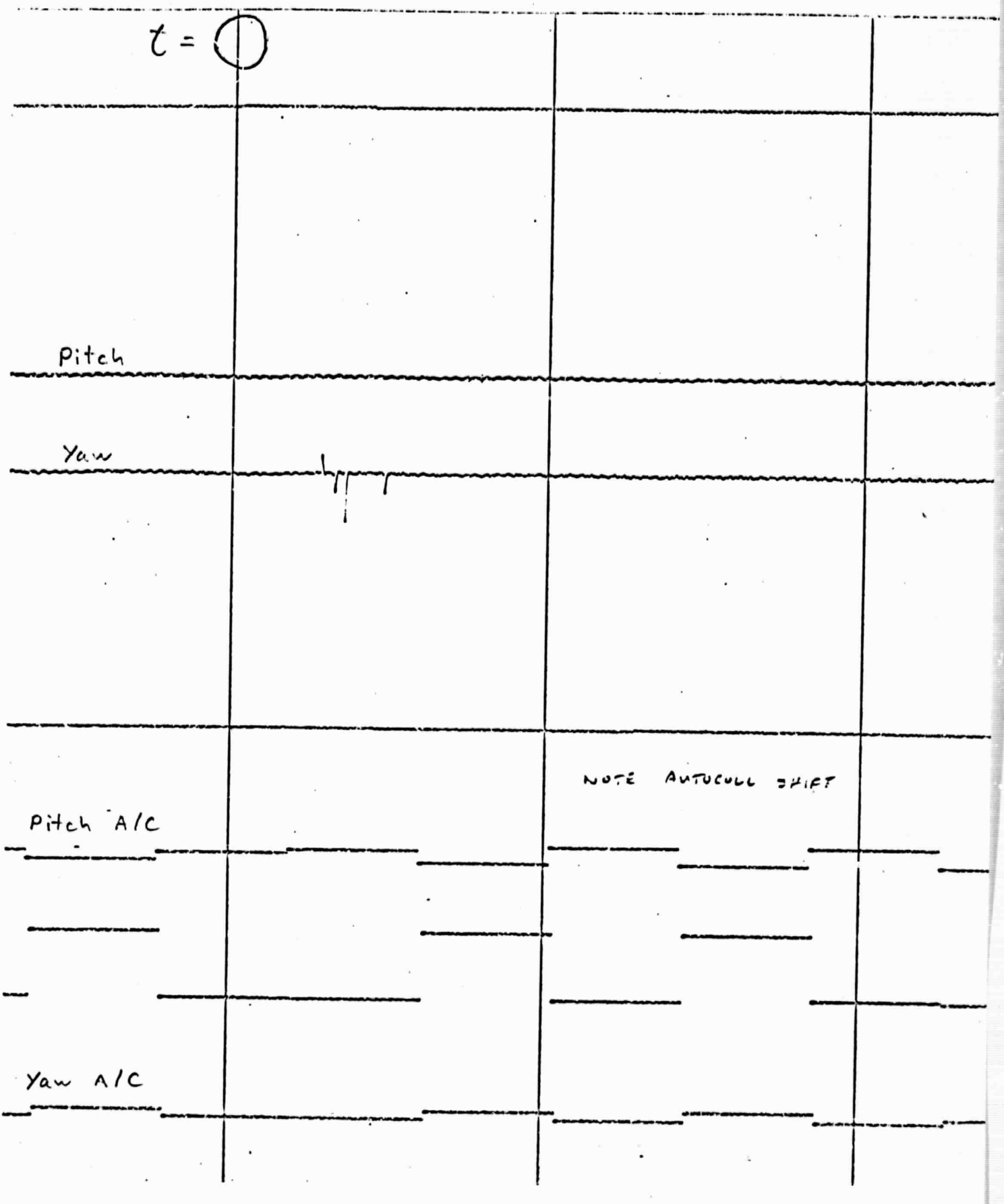
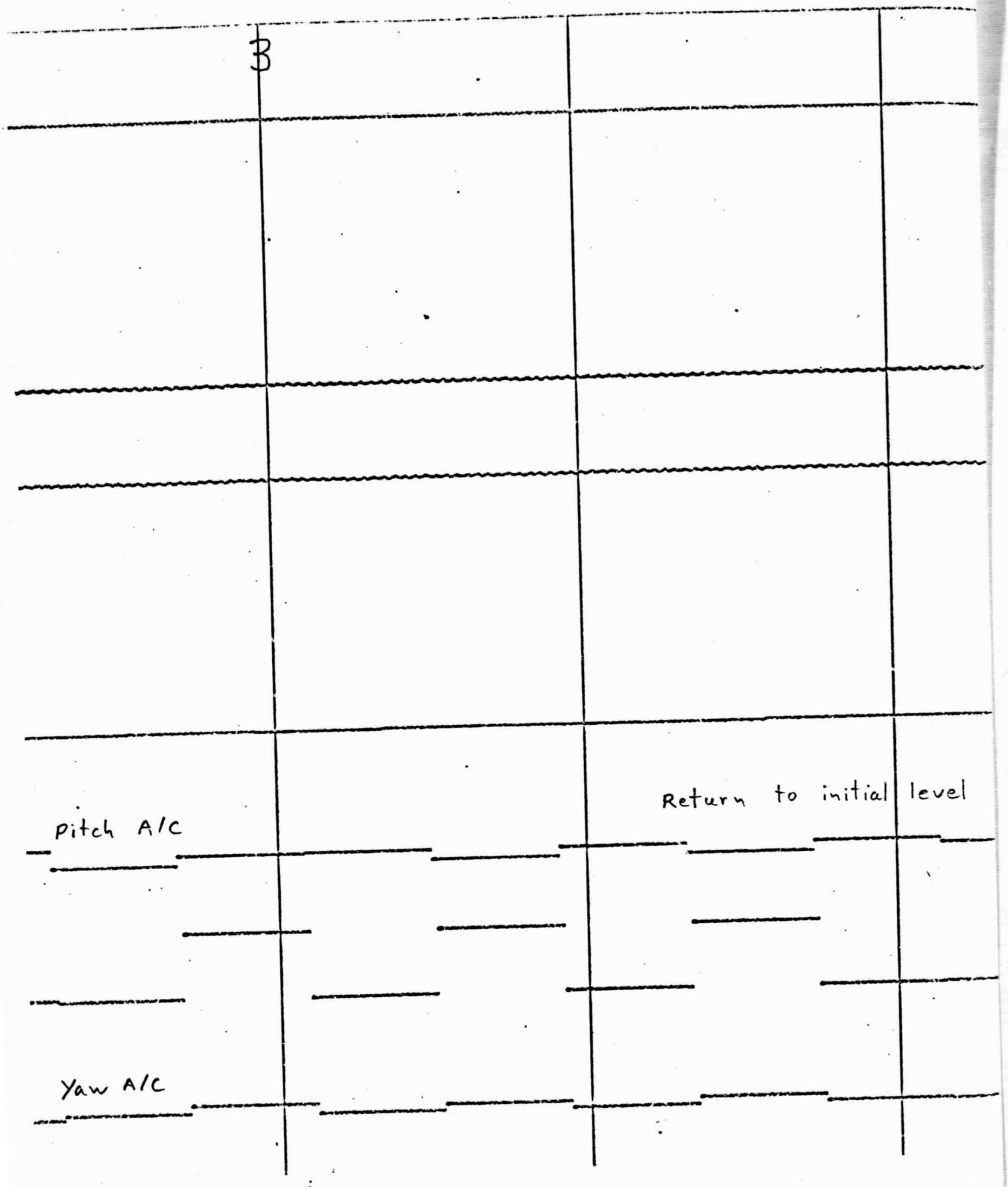


FIGURE 4-7 PASS Flight Record

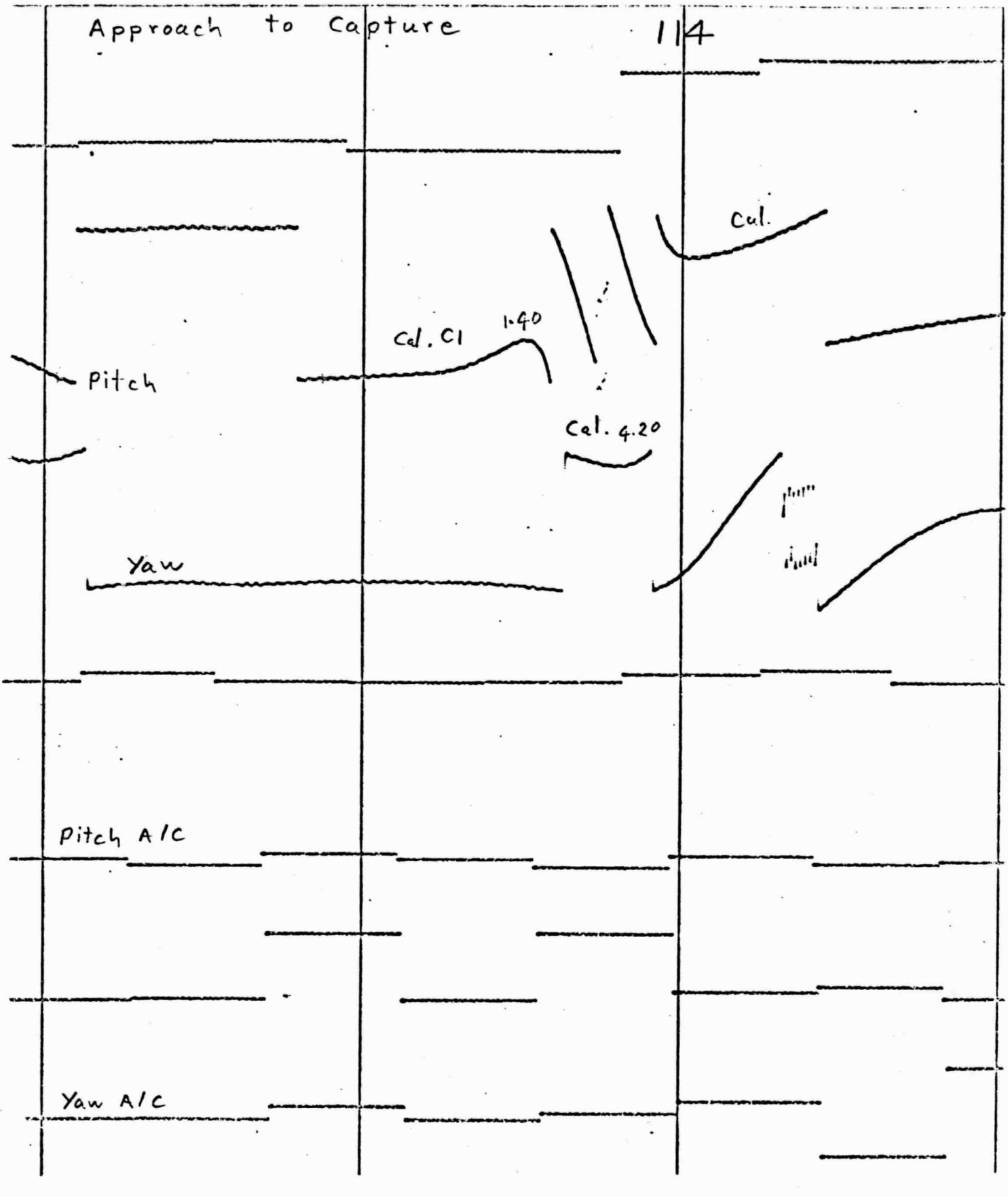
"REPRODUCIBILITY OF THE ORIGINAL PAGE IS POOR."



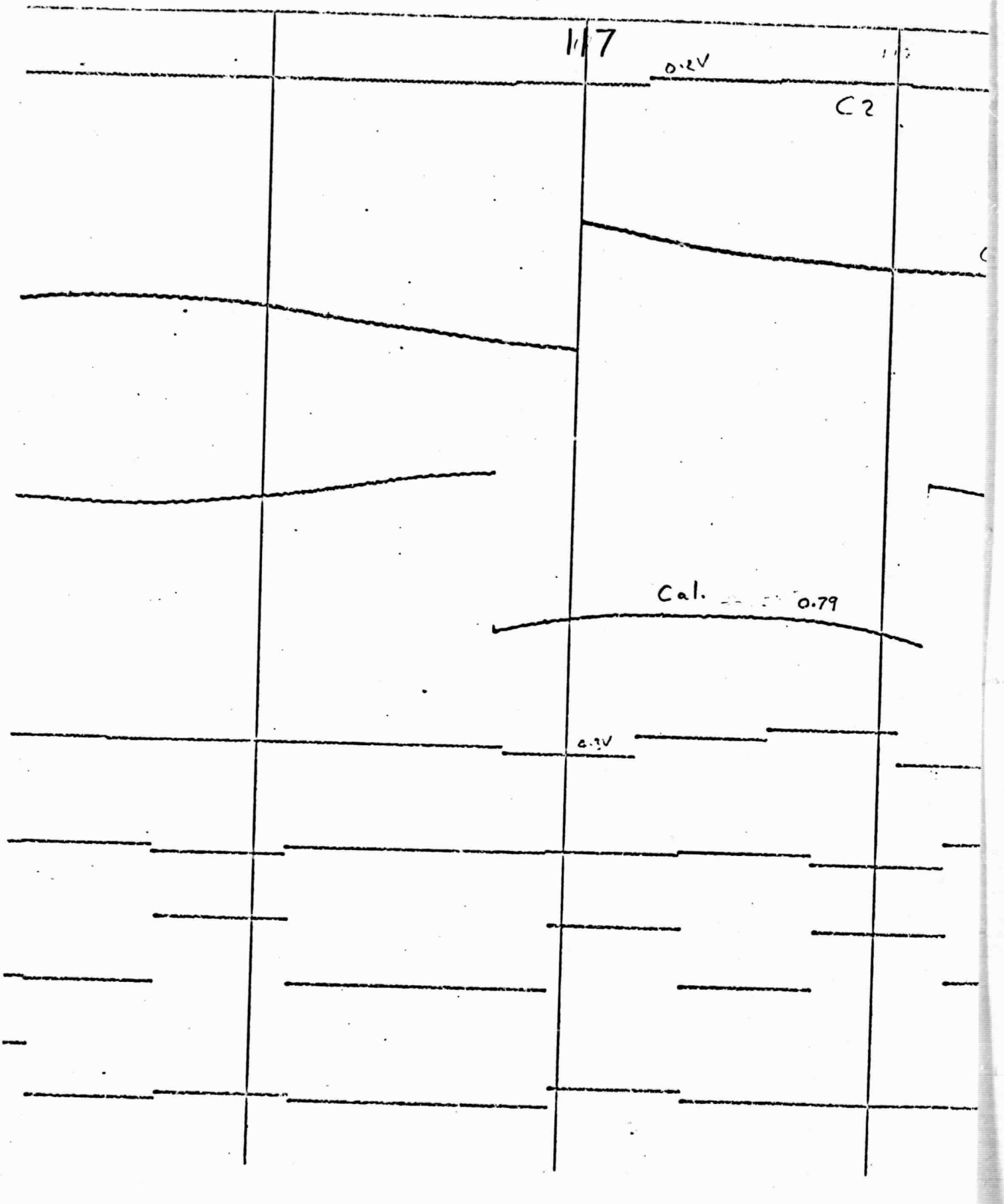
"REPRODUCIBILITY OF THE ORIGINAL PAGE IS POOR."



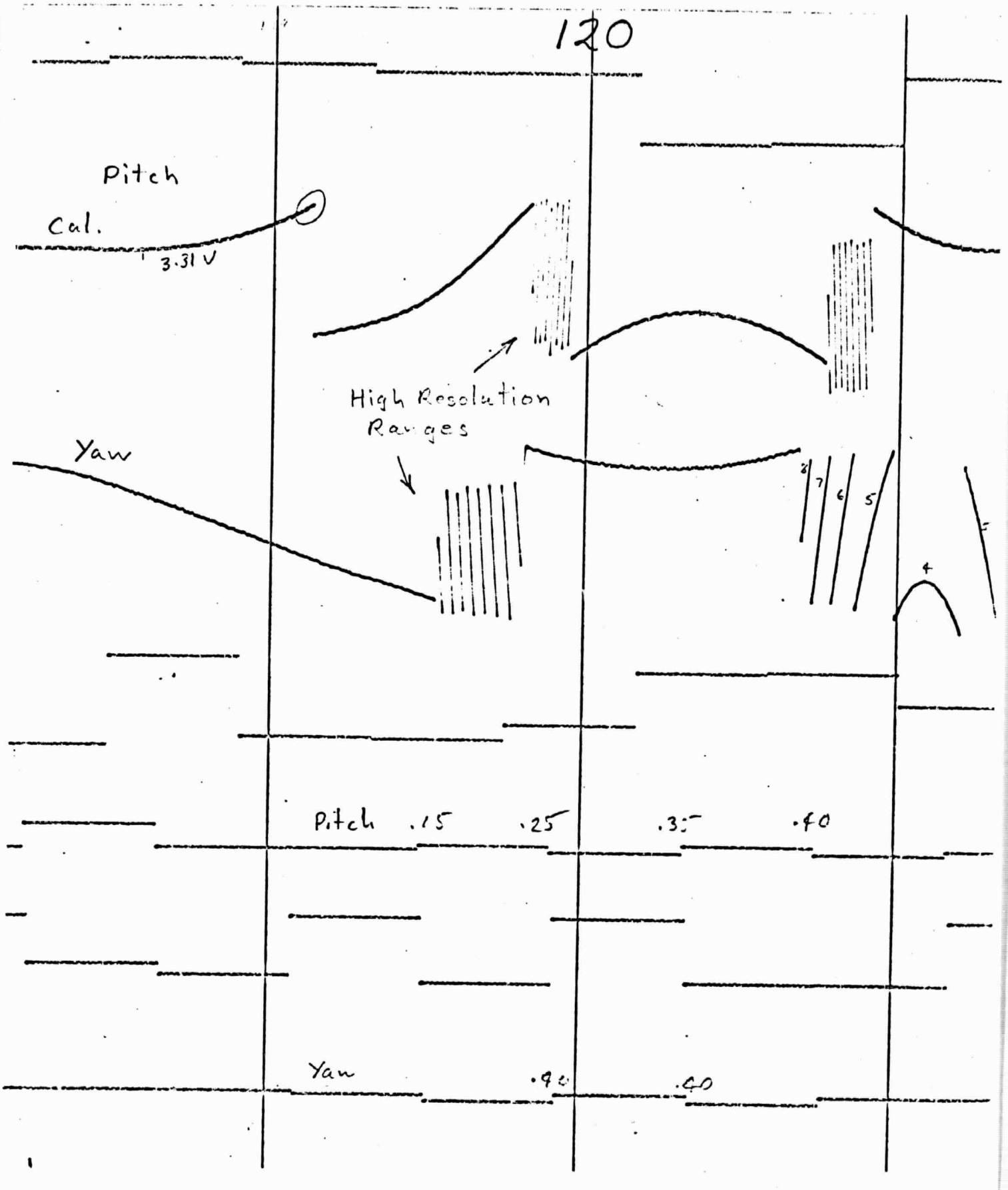
"REPRODUCIBILITY OF THE ORIGINAL PAGE IS POOR."



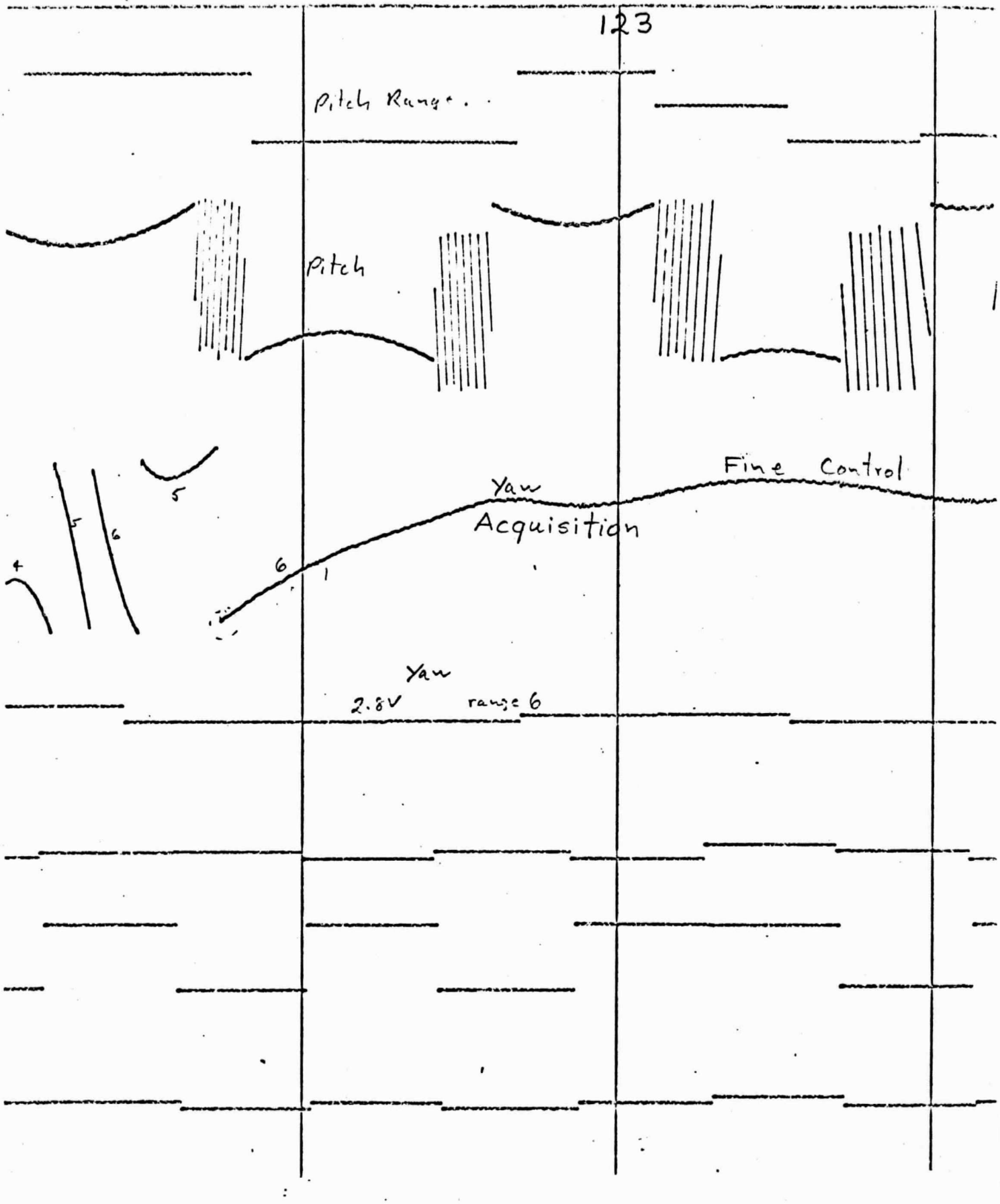
"REPRODUCIBILITY OF THE ORIGINAL PAGE IS POOR."



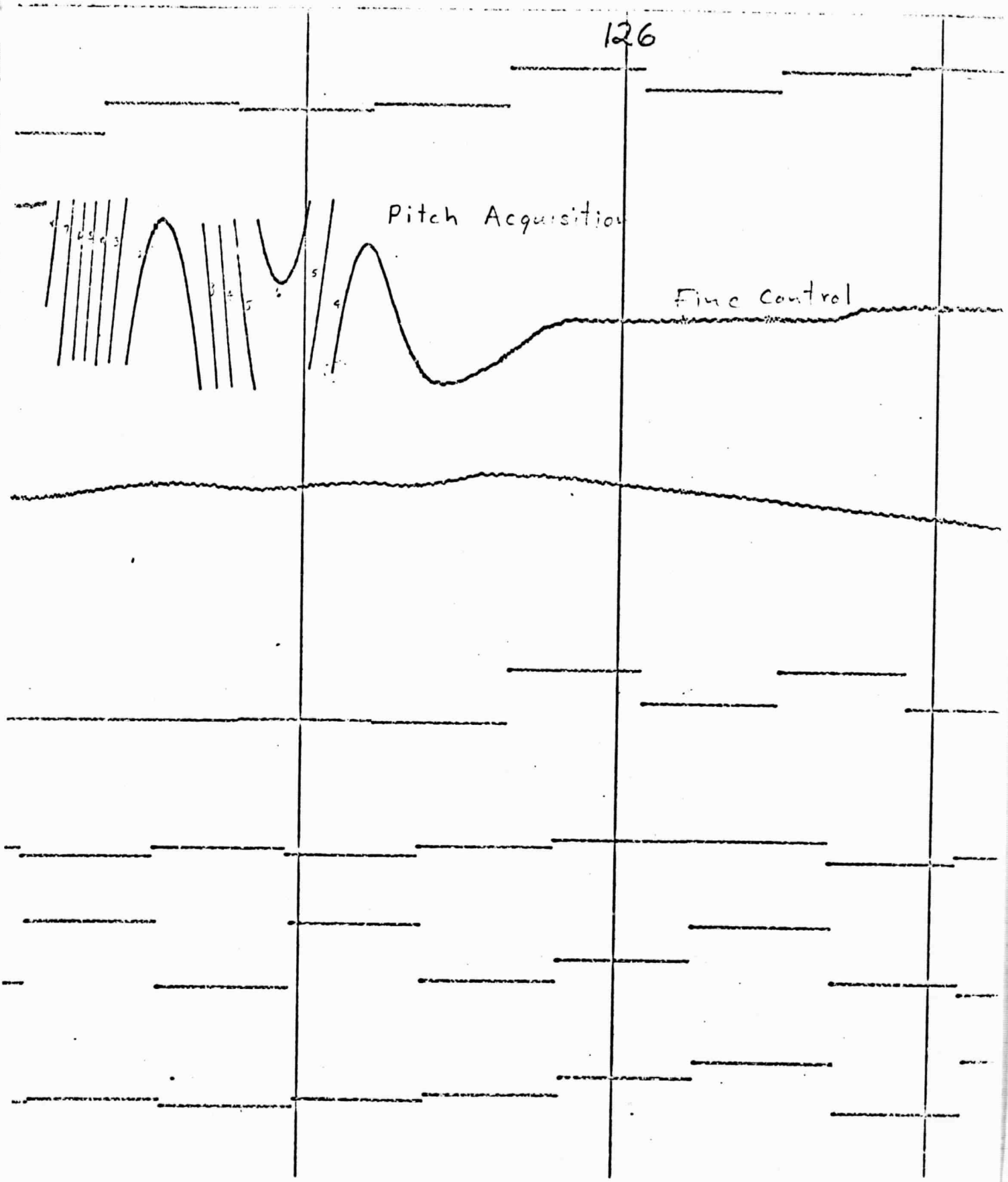
"REPRODUCIBILITY OF THE ORIGINAL PAGE IS POOR."



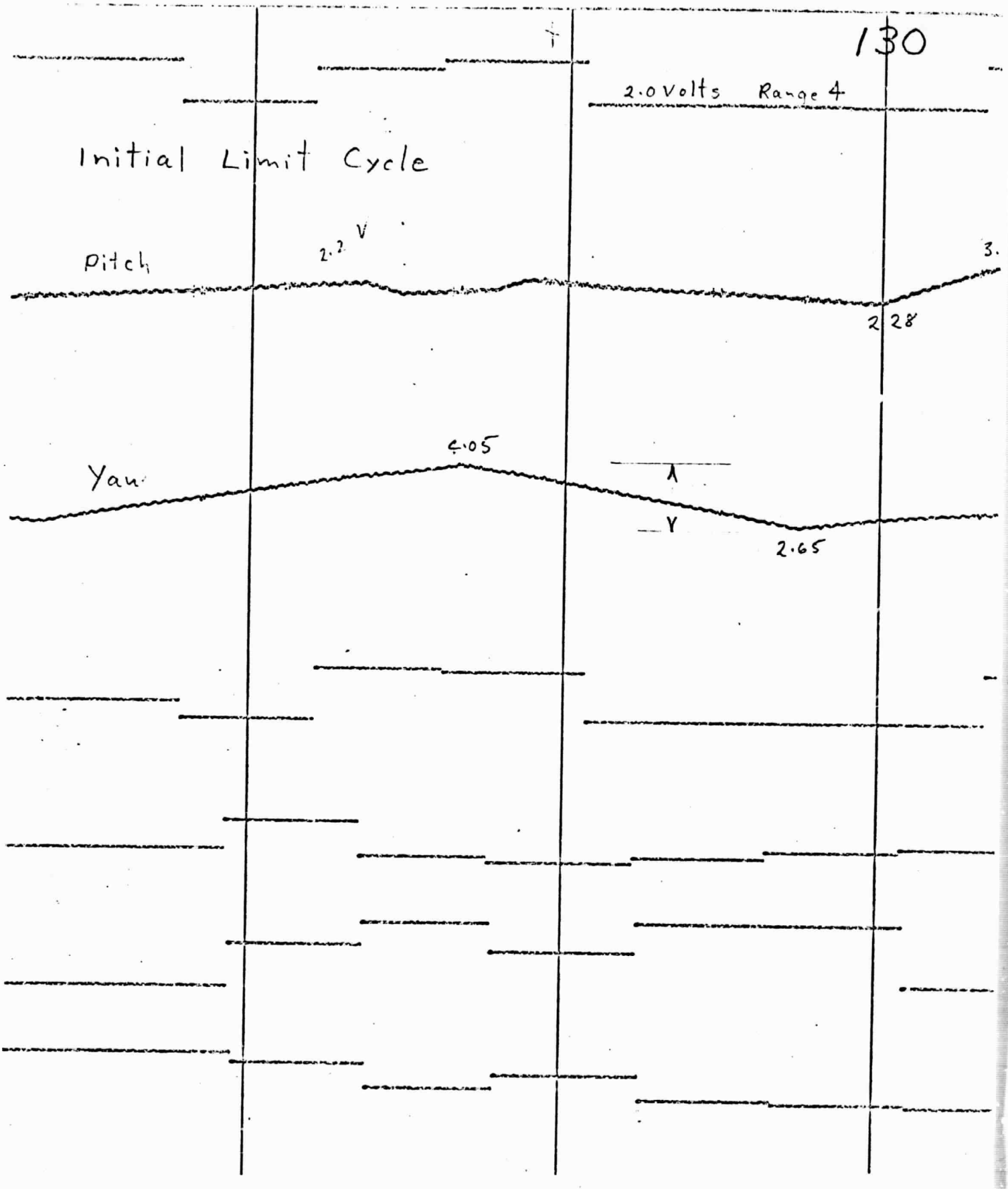
"REPRODUCIBILITY OF THE ORIGINAL PAGE IS POOR."



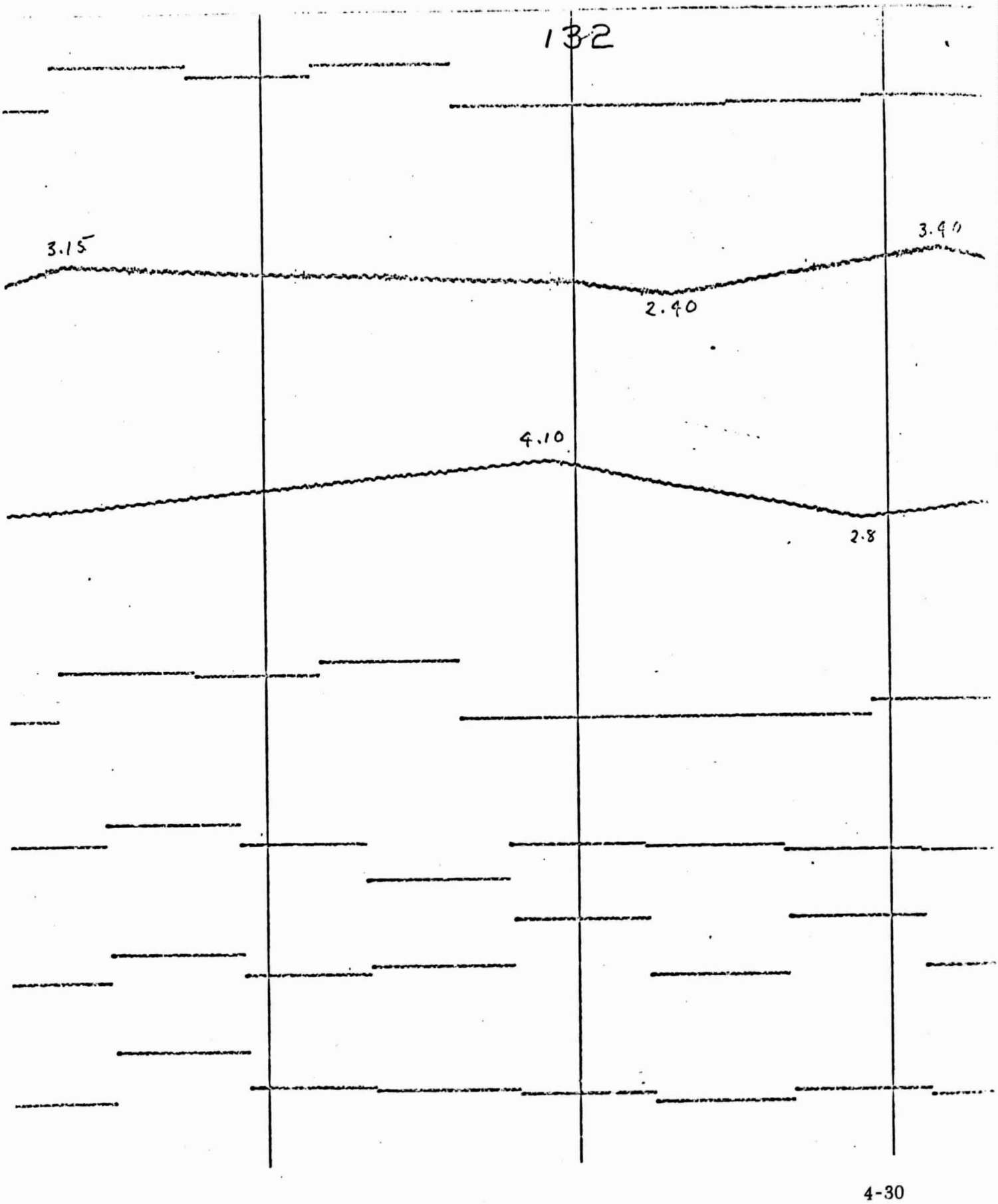
"REPRODUCIBILITY OF THE ORIGINAL PAGE IS POOR."



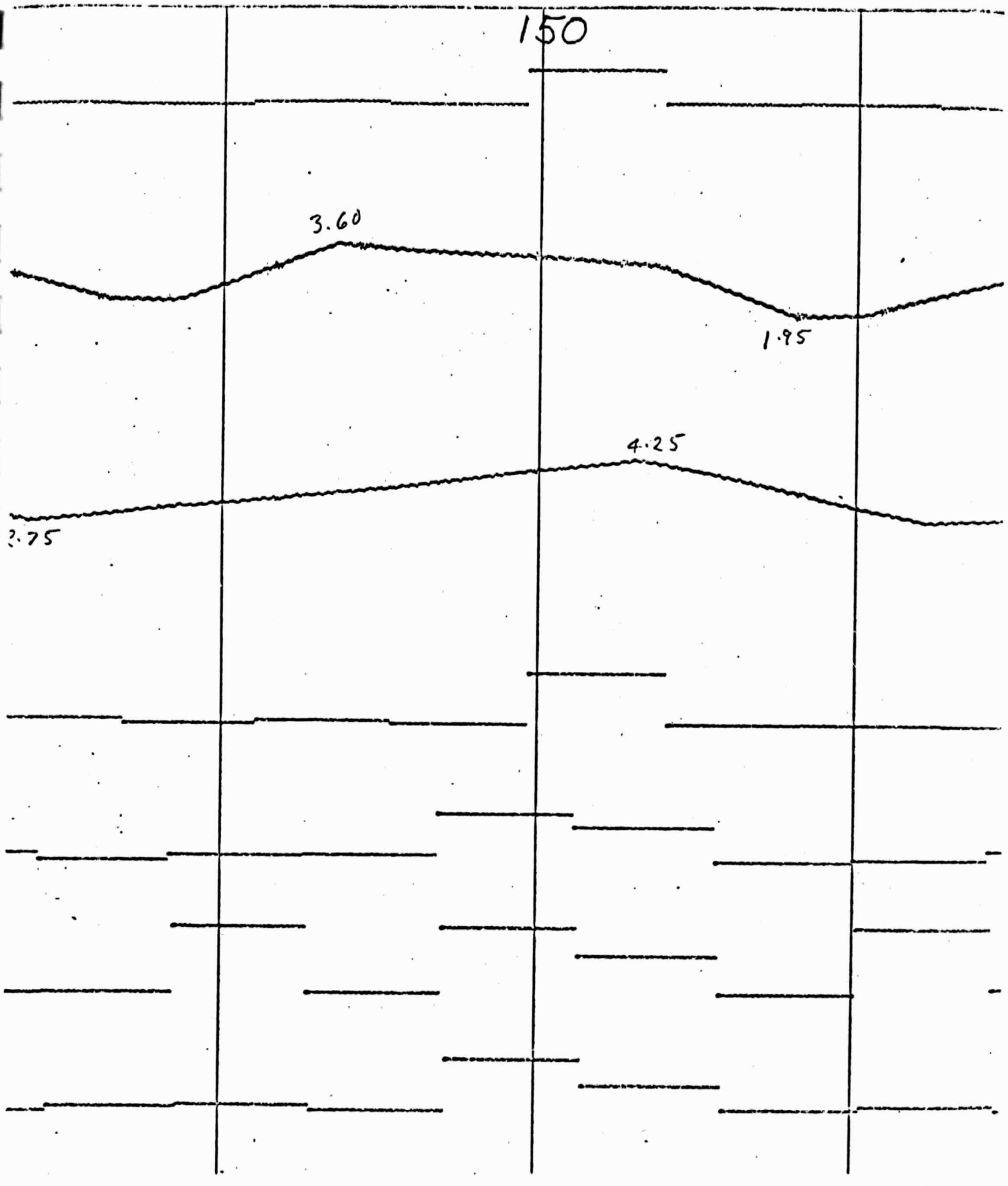
"REPRODUCIBILITY OF THE ORIGINAL PAGE IS POOR."



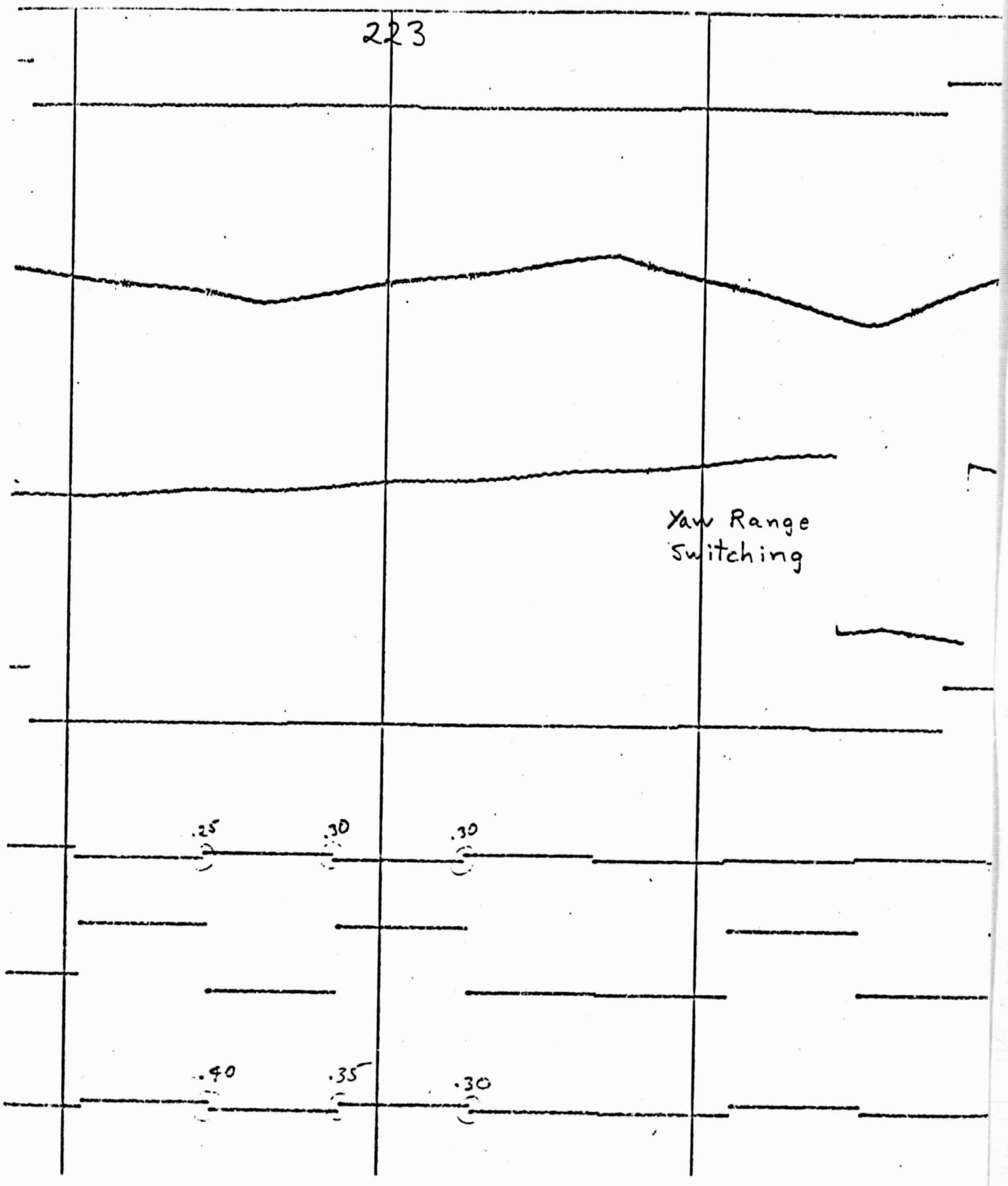
"REPRODUCIBILITY OF THE ORIGINAL PAGE IS POOR."



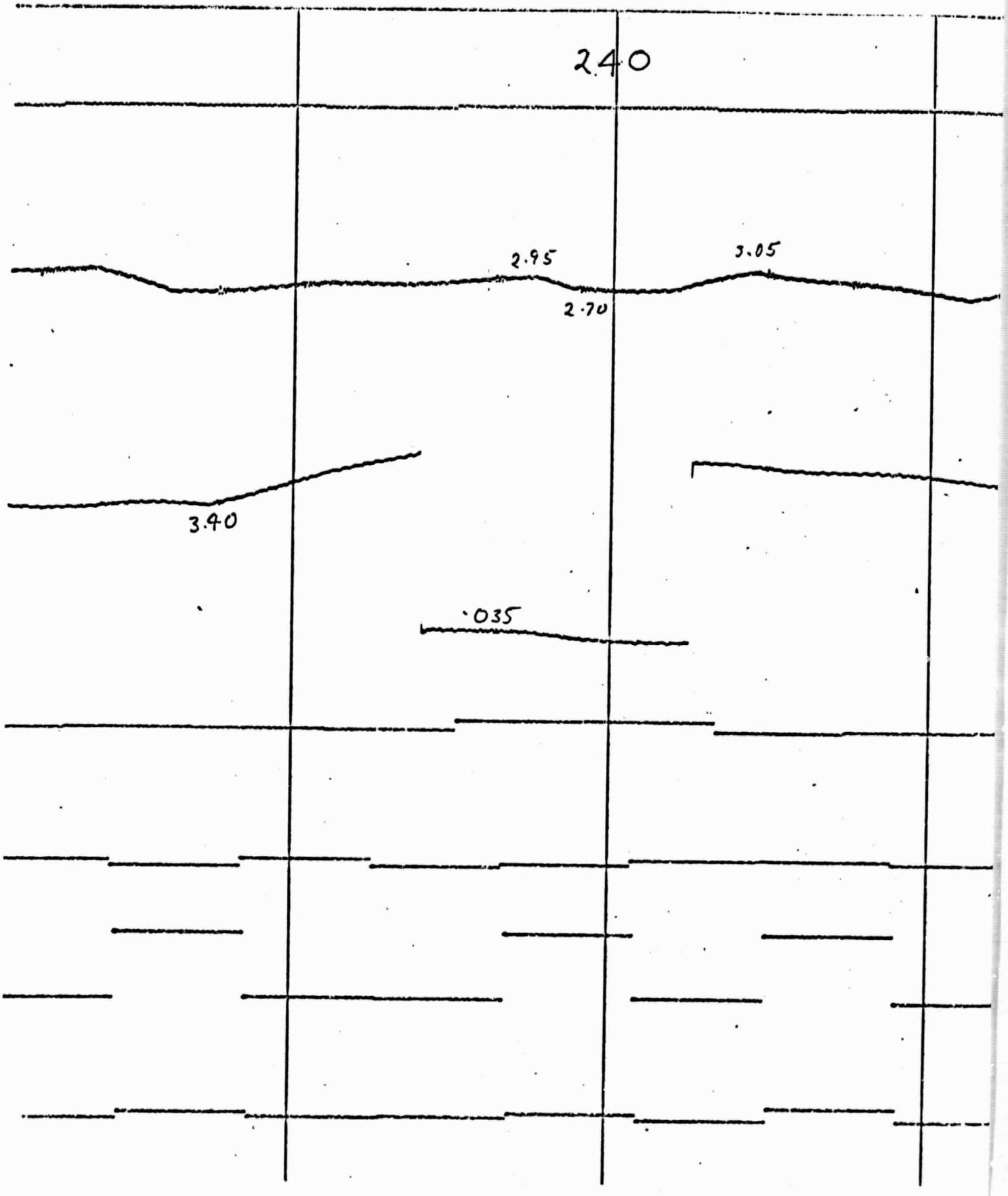
"REPRODUCIBILITY OF THE ORIGINAL PAGE IS POOR."



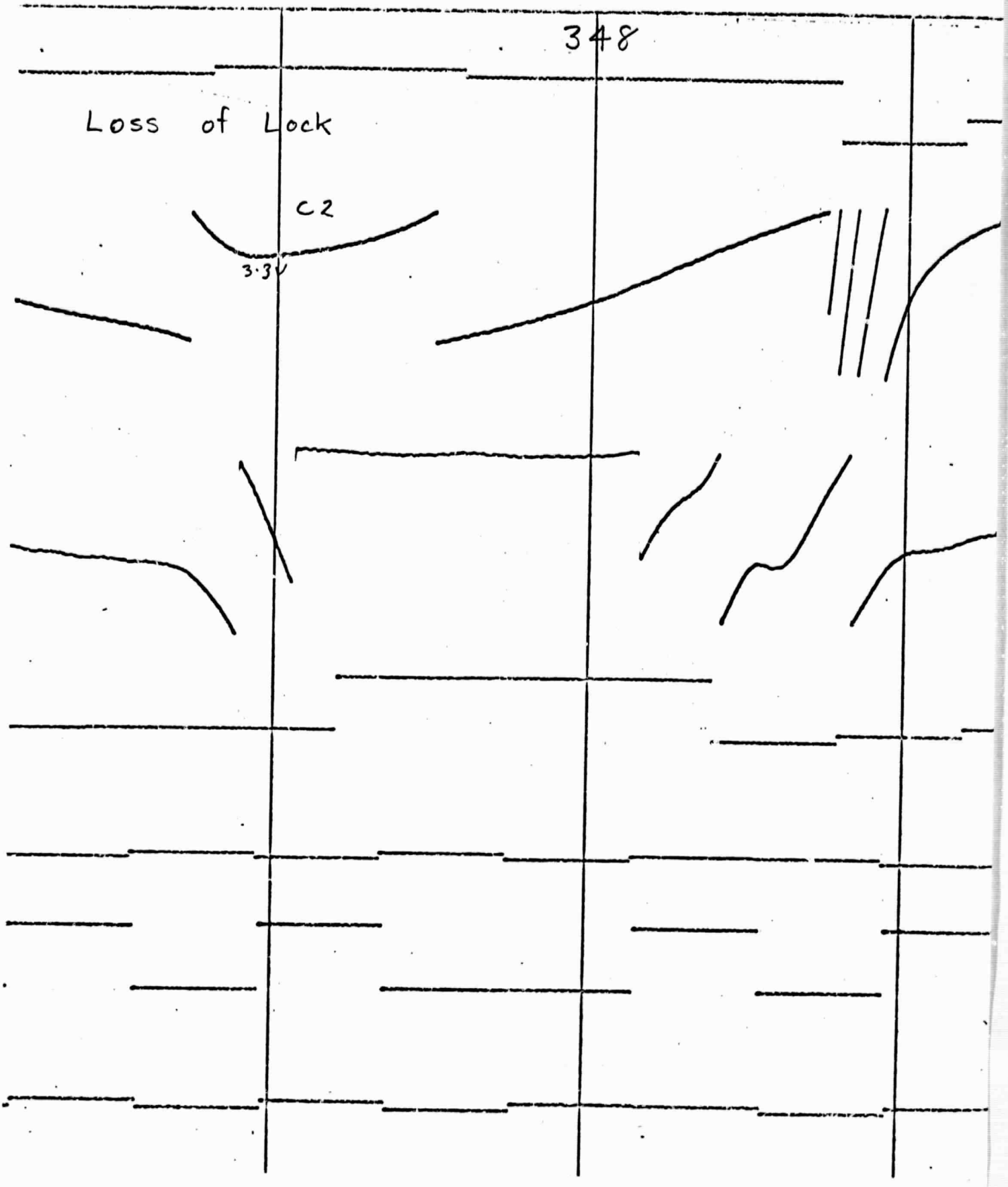
"REPRODUCIBILITY OF THE ORIGINAL PAGE IS POOR."



"REPRODUCIBILITY OF THE ORIGINAL PAGE IS POOR."



"REPRODUCIBILITY OF THE ORIGINAL PAGE IS POOR."



5.0 CONCLUSIONS

The PASS program appears to have been highly successful in terms of its test program, which demonstrated stable performance and in terms of the rocket flight which provided absolute pointing and limit cycle data. In particular, the very high resolution of the solar sensor records permits quantitative observation of control torque and disturbance torque effects. In addition, the solar cell experiment has furnished valuable data concerning solar cell performance in space sun conditions and confirmed the benefits of spectral filtering in terms of stable thermal characteristics. These topics are treated comprehensively in the following discussion.

5.1 Optical Components

The results of the qualification testing on the PASS sensor are summarized in Table 3-1. The alignment shift noted is the change in boresight between the auto-collimator axis and the sun sensor axis. The temperature coefficient noted assumes a best fit straight line temperature variation and accounts for warping in the test reference plate during the thermal excursions.

The flight records shows a shift in the sensor mounting of ten arc seconds in pitch and two arc seconds in yaw during the boost phase. The sensors relaxed after the boost phase to mechanical shift values of 1.0 arc seconds and 1.2 arc seconds, respectively. Mechanical drifts following the boost phase, over the remainder of the flight were 1.4 arc seconds maximum and 1.7 arc seconds maximum in pitch and yaw respectively. These shifts were of course detected and compensated by the PASS sensor, however they indicate very good stability of the sensor in its case.

5.2 Electronics

The electronics system employed to process the basic PASS sensor data for telemetry transmission has proved to be effective, yielding clear, high resolution data from the flight record. The confidence to be placed in the flight results is indicated by performance levels noted in the test program. For example, using the

	Pitch Axis	Yaw Axis
Peak To Peak Limit Cycle	11.0 arc sec	16.5 arc sec
RMS Limit Cycle	3.1 arc sec	4.8 arc sec
Absolute Pointing Error At t = 130	3.3 arc sec	+8.3 arc sec
Absolute Pointing Error At t = 310	+6.7 arc sec	+20.0 arc sec
Drift	-1.4 arc sec	+11.7 arc sec
Pass Uncertainty	± 2 arc sec	± 2 arc sec
Alignment	± 1 arc sec	± 1 arc sec

Table 5-1 Flight Performance Summary

results of Section 3.2 and 3.3, the maximum electronic drift arising from worst case effects of thermal drift, shock, vibration and supply voltage fluctuation, corresponded to one arc second. For this particular flight which had a launch temperature near 25°C and temperature variations of less than 5°C, the anticipated drift would be less than 0.2 arc seconds.

Other uncertainties were introduced by the telemetry accuracy which we will assume to be ±1% or 0.05 volt. In fact, it was probably slightly better since the pre-launch voltage levels were in agreement with those levels set four months previously, to better than 0.05 volts. This corresponds to an uncertainty of about ±0.5 arc seconds. In the case of the autocollimator, the uncertainty in a set of readings is estimated to be about ±0.6 arc seconds based on the spread of readings observed. This gives an overall uncertainty of ±1.3 arc seconds, in the observed values.

5.3 Flight Report

Based on the information computed in Section 4.0, the flight performance is summarized in Table 5-1. Since it was not necessary to align the control sensor to the reference plate for evaluation purposes, initial offset figures of the FSS must be added to the PASS data, which are referenced to the mounting plate to obtain absolute pointing information. According to NASA information, these offsets were: yaw = 13.2 arc seconds and pitch = -9.6 arc seconds.

The overall measurement uncertainty is determined by the contributions of all PASS system elements, plus telemetry and solar sensor gain uncertainty. These are: (1) sensor unit ±4.6 arc seconds, (2) electronics and telemetry ±1.3 arc seconds and, (3) solar sensor calibration of ±1% with a 20 arc second offset for a ±0.2 arc second contribution. These sum to a maximum uncertainty of ±7.1 arc seconds. For the particular flight environment the most probable uncertainty is ± 2 arc seconds.

5.4 Solar Cell Experiment

The results of the solar cell experiment are given in Figures 5-1 and 5-2. The pre-flight data for detectors with filter A is included for comparative purposes and the spectral characteristics of the filters are included as Figure 5-3. From this data it is clear that the matching procedure predicted the flight performance trend accurately though somewhat accentuated any mismatch relative to the actual flight performance. This accentuation is due to the spurious transmission outside the bandpass. Filter A had an undesired transmission rise at 1.05 microns while filger B had a spurious response at 0.45 micron. These zones caused the detectors to have a slight positive and negative temperature coefficient with filters A and B respectively.

A recommended bandpass for the filter is illustrated in Figure 5-3. If more careful attention is given to eliminating any spurious transmission outside this bandpass the cell filter combination should have essentially zero temperature coefficient. This would eliminate or greatly reduce the need for cell matching. The tolerance on the long wavelength cutoff is not critical and the filter cutoff could vary between the limits established by those of filters A and B.

The flight data from the solar cell experiment has permitted the performance characteristics of several standard cells, prepared simultaneously with the cell/filters for this experiment, to be calibrated to space conditions. These standard cells and their accompanying calibration data are stored at Exotech and NASA ARC for use on all future solar sensor programs, thus providing an invaluable tool for cell selection and output level determination based on accurate productions of the cell's performance under space sun illumination derived from comparative laboratory measurements.

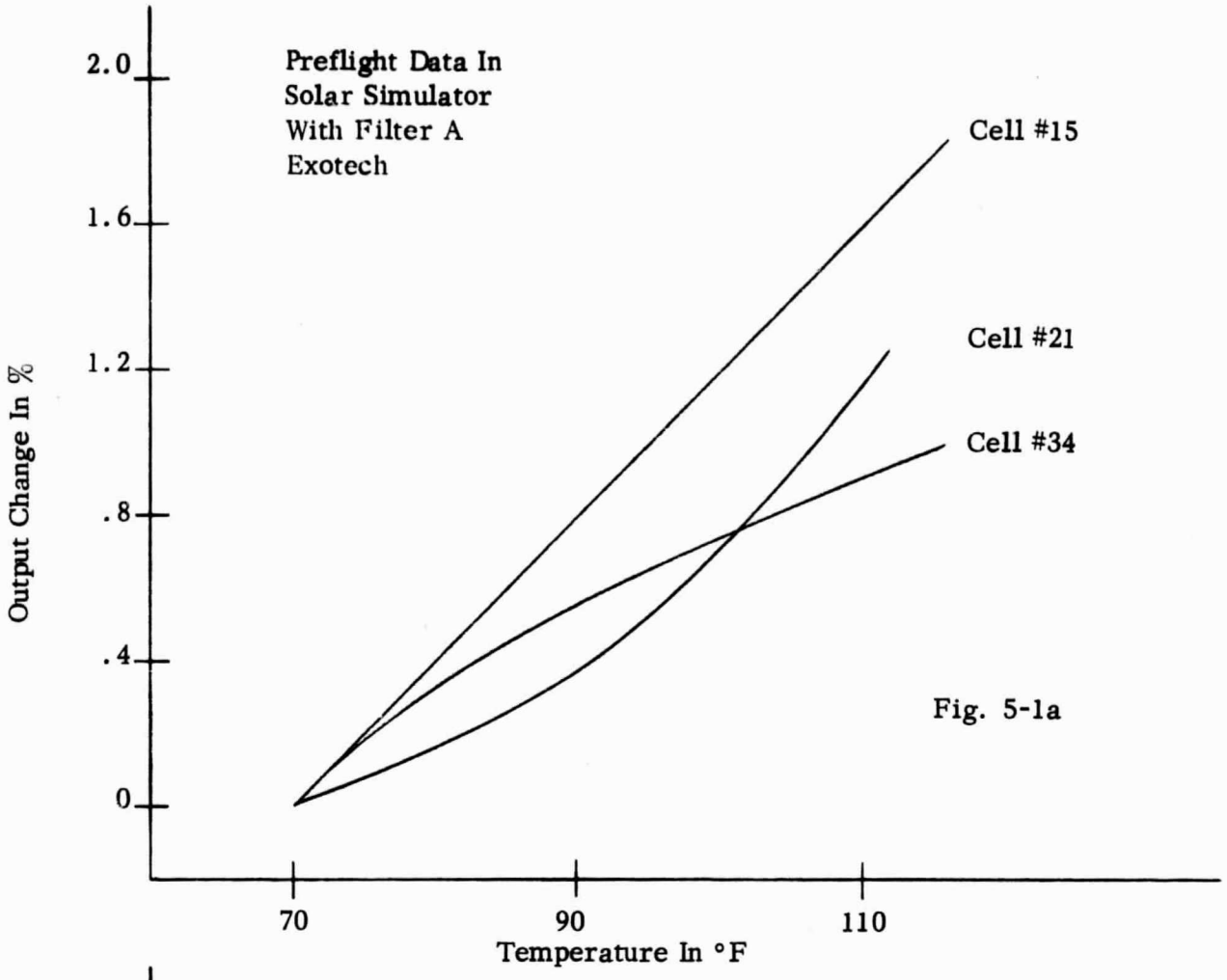


Fig. 5-1a

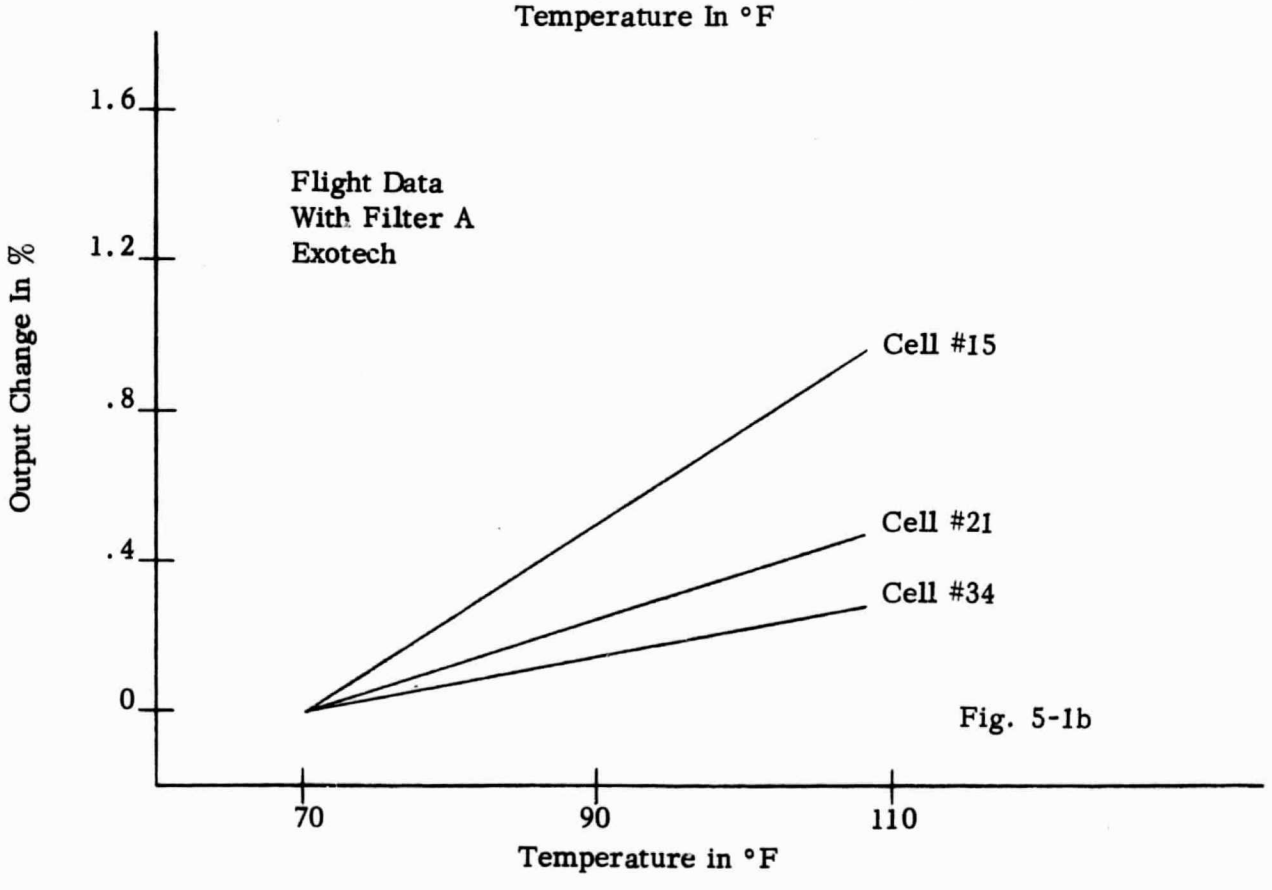


Fig. 5-1b

Figure 5-1 Solar Cell Experiment #1, Flight Data

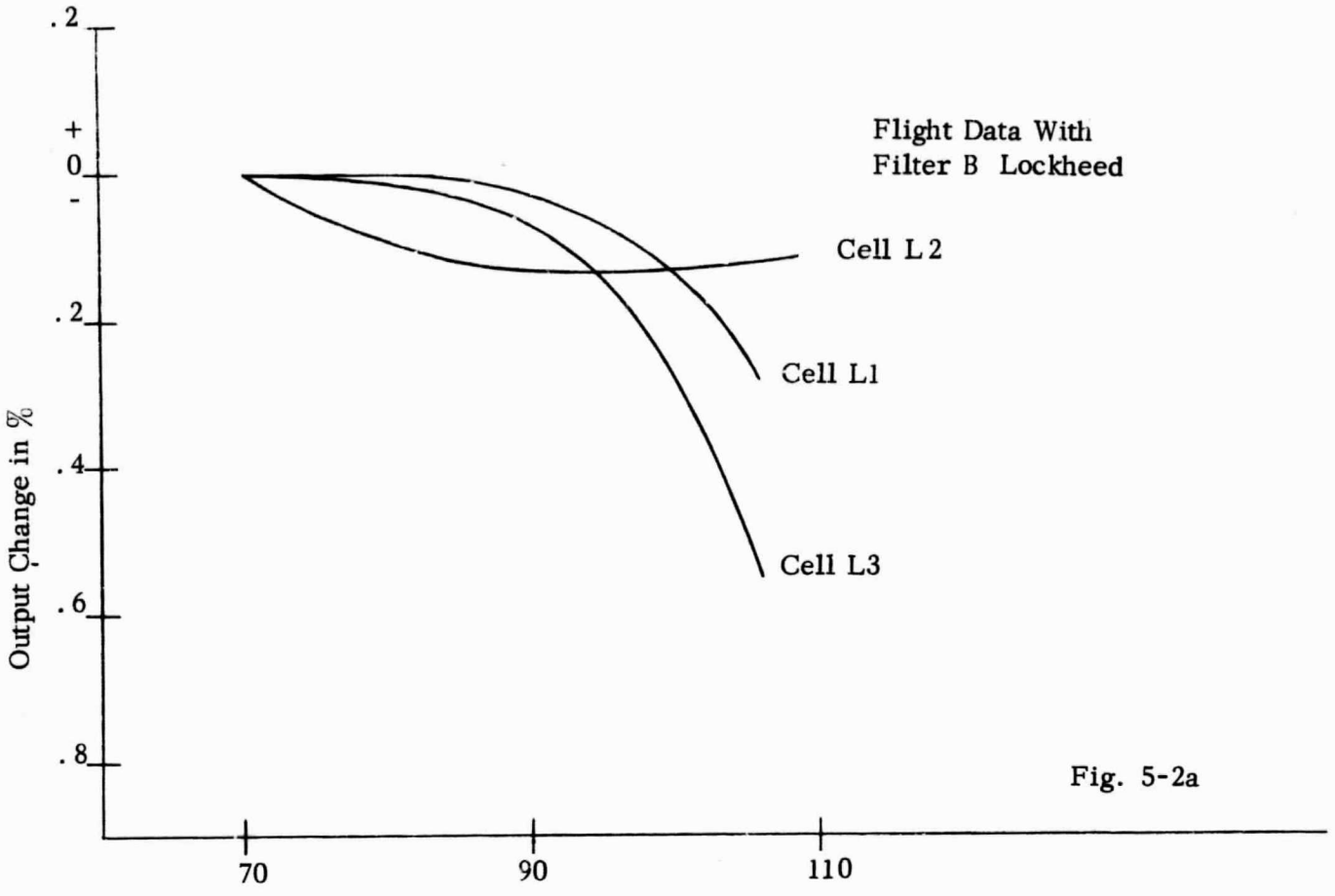


Fig. 5-2a

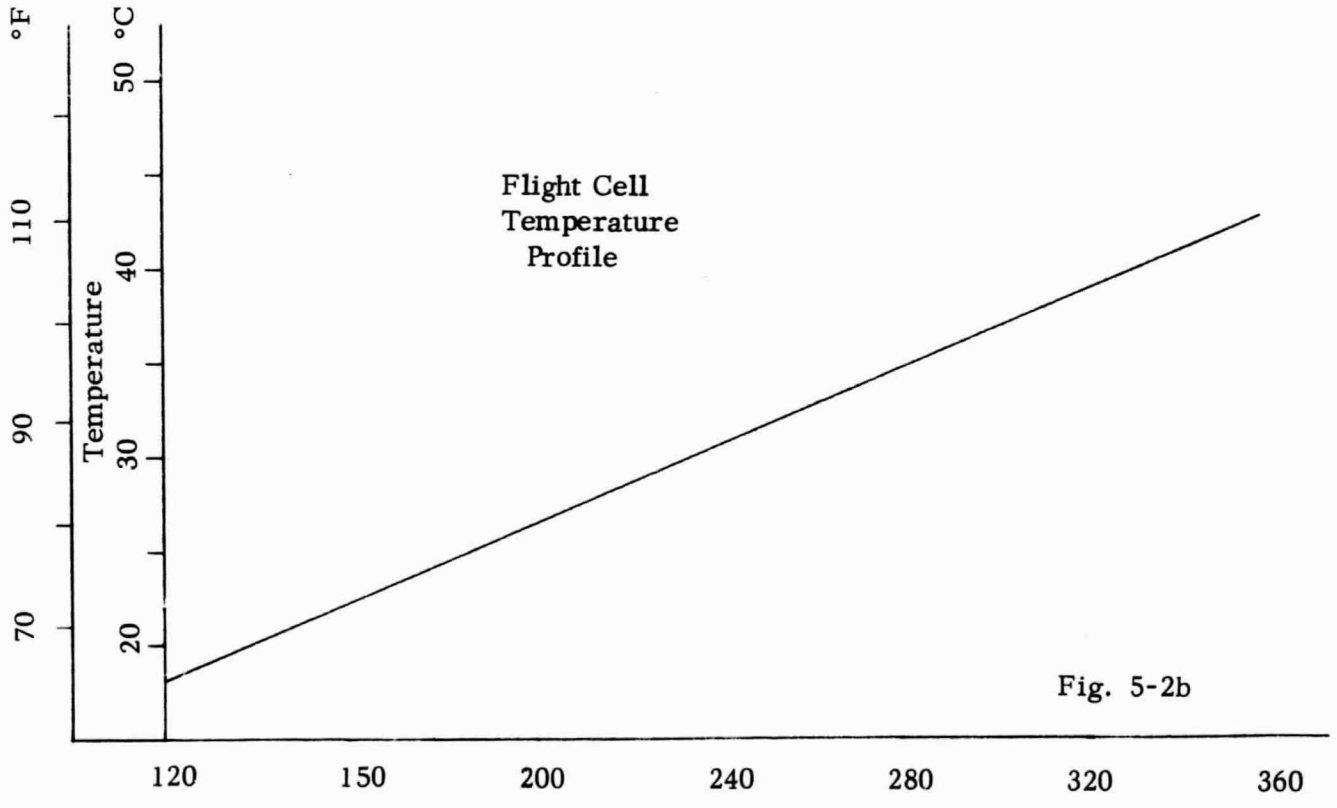


Fig. 5-2b

Figure 5-2 Solar Cell Experiment #1, Flight Data

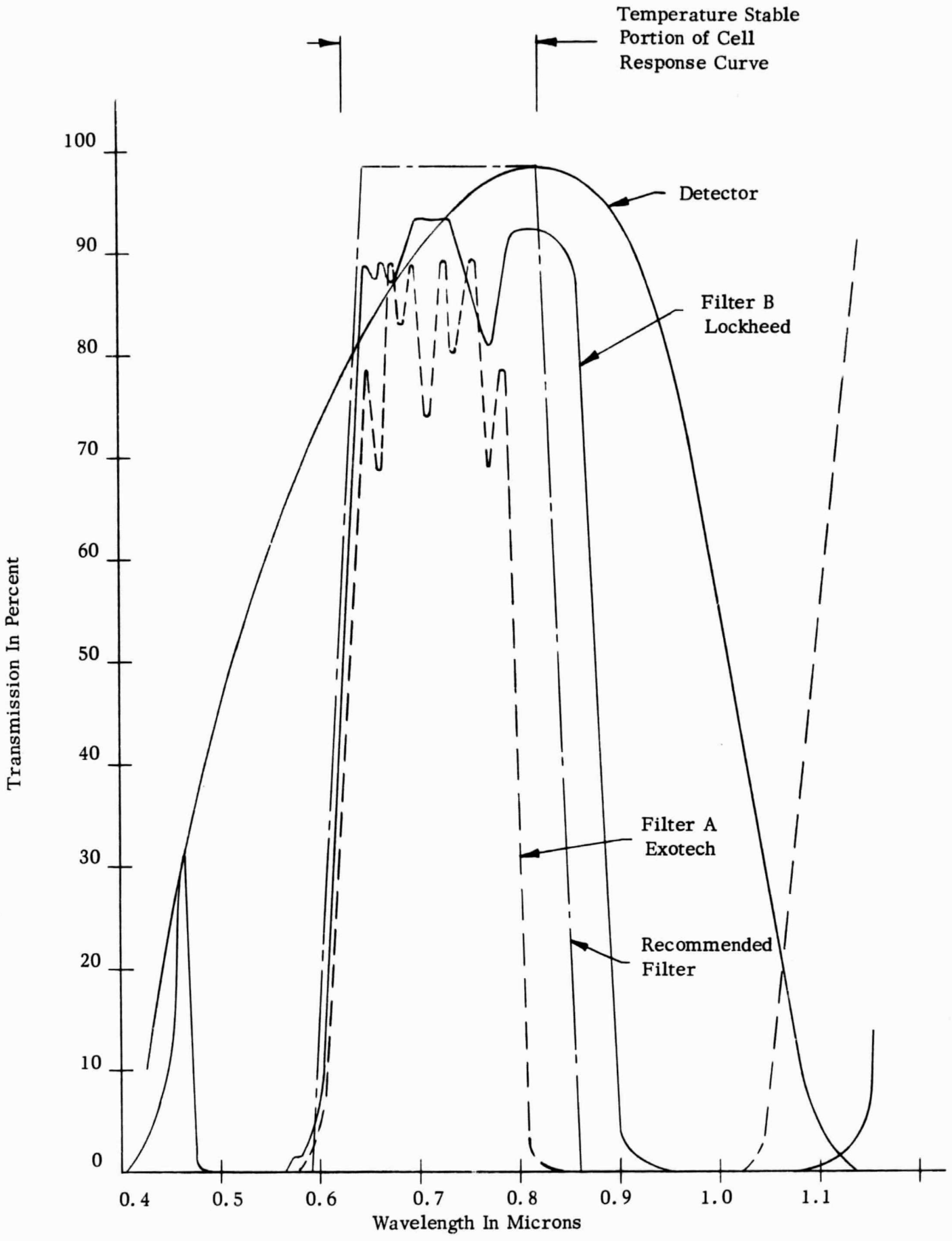
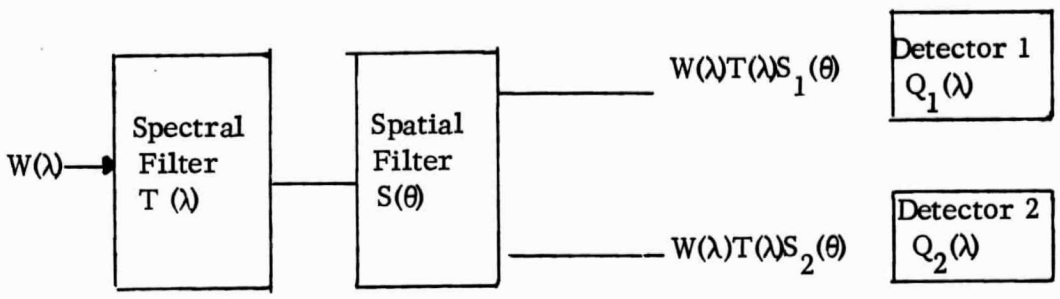


Figure 5-3 Filter Characteristics

APPENDIX

Derivation of the Sensor Transfer Function

If we consider the generalized energy balancing sensor as a combination of a spatial filter, a spectral filter, and two detectors we can base our evaluation of the transfer function on the following block diagram.



Simplified Block Diagram Energy Balancing Sensor

Actually, by using this diagram we have restricted the sensor to those systems in which a single spectral filter and a single spatial filter are used for both detectors. There are notable exceptions to this procedure, however, the basic considerations are similar albeit complicated by possible differences in the filters for each detector.

The spatial filter can be a lens and mask, a combination of two masks, etc; in any case the function is to divide the incoming light between the two detectors according to the part of the field from which the light originated. The spatial filter is assigned a characteristic function, $S(\theta)$ which is some function (depending on the characteristics of the specific filter) of the angle between a reference axis and the line-of-sight to the center of the sun, θ.

The spectral filter is defined by a function, $T(\lambda)$, where the value of the function represents the transmission of the filter.

If each detector has a spectral response characteristic $Q(\lambda)$ the overall response function for the sensor, $R(\theta)$ can be defined as follows:

$$R(\theta) = \int_0^\infty W(\lambda)T(\lambda)S_1(\theta)Q_1(\lambda)d\lambda - \int_0^\infty W(\lambda)T(\lambda)S_2(\theta)Q_2(\lambda)d\lambda$$

This function,commonly referred to as the sensor transfer function, provides a convenient and general basis for analyzing the effects on sensor performance of spectral filtering, detector characteristics, and parameter changes with temperature.

Effects of Detector Parameters

In order to facilitate a discussion of the effects of detector parameters and changes of these parameters with temperature on the sensor transfer function it is expanded as follows:

$$R(\theta) = \left[S_1(\theta) - S_2(\theta) \right] \int_0^\infty W(\lambda)T(\lambda)Q(\lambda)d\lambda$$

$$-S_2(\theta) \int_0^\infty W(\lambda)T(\lambda)\,\Delta Q(\lambda)d\lambda$$

where:

$$Q(\lambda) = Q_1(\lambda)$$

$$\Delta Q(\lambda) = Q_2(\lambda) - Q_1(\lambda)$$

For simplicity the responsivity of the second detector is considered as nearly the same as the first with some incremental difference, $\Delta Q(\lambda)$.

Differential Detector Response and Solar Simulation

The discussion of detector parameters is initiated with an investigation of the effect of detector spectral response on the problem of accurately simulating the sun. Assume a sensor transfer function, $R_T(\theta)$, using a tungsten solar simulator and a space sun function, $R_S(\theta)$. In order to minimize the alignment

and calibration effort it would be preferable if:

$$R_T(\theta) = R_S(\theta)$$

However, in general, the less desirable relationship given below is more descriptive of the situation.

$$R_T(\theta) = \frac{1}{k(t)} \quad R_S(\theta) + \alpha(t)$$

where:

$k(t)$ is a temperature dependent gain

$\alpha(t)$ is a temperature dependent offset (and in general a function of the particular simulator used).

Returning to the expression for the sensor transfer function it is apparent that the conditions for $R_T(\theta)$ and $R_S(\theta)$ to be related by a simple gain constant are:

$$\int_0^\infty W_S(\lambda)T(\lambda)Q(\lambda)d\lambda = k \int_0^\infty W_T(\lambda)T(\lambda)Q(\lambda)d\lambda$$

$$\int_0^\infty W_S(\lambda)T(\lambda)\Delta Q(\lambda)d\lambda = k \int_0^\infty W_T(\lambda)T(\lambda)\Delta Q(\lambda)d\lambda$$

where:

$W_S(\lambda)$ is the spectral irradiance due to the sun

$W_T(\lambda)$ is the spectral irradiance due to a tungsten simulator.

$W_S(\lambda)$ and $W_T(\lambda)$ differ considerably and are not related by any simple constant (as a matter of fact the sunlight at the earth's surface is not simply related to that in space, either).

In order to see more clearly just what is meant by the preceding conditions the expressions are rearranged as follows:

$$\int_0^\infty T(\lambda)Q(\lambda)[W_S(\lambda) - kW_T(\lambda)]d\lambda = 0$$

$$\int_0^\infty T(\lambda)\Delta Q(\lambda)[W_S(\lambda) - kW_T(\lambda)]d\lambda = 0$$

Since $W_S(\lambda)$ and $W_T(\lambda)$ are not linearly related we can replace the term in brackets by $\Delta W(\lambda)$ which is in general non-zero. The two conditions then become:

$$\int_0^\infty T(\lambda)Q(\lambda)\,\Delta W(\lambda)d\lambda = 0$$

$$\int_0^\infty T(\lambda)\,\Delta\, Q(\lambda)\Delta W(\lambda)d\lambda = 0$$

Both $T(\lambda)$ and $Q(\lambda)$ are positive definite. Therefore $\Delta W(\lambda)$ must take on both positive and negative values. For any given $T(\lambda)$ and $Q(\lambda)$ there exists a constant k which results in a $\Delta W(\lambda)$ satisfying the first condition. However, in general, the second condition would not be satisfied. This constant can be determined by measuring the output of a detector-spectral filter combination in each of the two environments. The ratio of the two outputs is the value, k. Thus a mathematical condition and a practical method of negating the error contributions of the first term in the transfer function exists. The problems associated with the second term, i.e., mismatch in the spectral characteristics of the two detectors are yet to be solved.

It might appear that one could simply narrow the region of transmission of the filter thereby tending to force the term:

$$\int_0^\infty T(\lambda)\,\Delta Q(\lambda)\,\Delta W(\lambda)d\lambda$$

to smaller and smaller values, eliminating the problem. Unfortunately, this procedure also reduces the gain of the system since the integral:

$$\int_0^\infty T(\lambda)Q(\lambda)W_S(\lambda)\,d\lambda$$

similarly is reduced.

The criteria to be used for this discussion will be:

$$\frac{\int_0^\infty T(\lambda)\,\Delta Q(\lambda)\,\Delta W(\lambda)d\lambda}{\int_0^\infty T(\lambda)\,Q(\lambda)\,W_S(\lambda)\,d\lambda} \rightarrow 0$$

In order to satisfy this criteria the transmission of the filter is adjusted to attenuate those regions of the spectrum where the ratio of $\Delta Q(\lambda)$ to $Q(\lambda)$ is large. In the case of solar cells this amounts to passing the wavelength region near the peak response (0.8μ) while attenuating both the visible and near infrared regions of the spectrum.

An exact definition of the optimum filter characteristic requires knowledge of the function $\Delta Q(\lambda)$ to a degree of detail not presently available. Further, measurement of the function, even for a particular pair of detectors, to a degree of accuracy meaningful for high accuracy sun sensors (better than one per cent spectral measurements) is a difficult and time consuming task. A more realistic approach to the problem is to make a small number of relative measurements on two detectors being considered as potential mates for a sensor detector pair.

The definition of a reasonable matching program for detector pairs can be aided by specific knowledge of the function $\Delta W(\lambda)$. Consider the character of the functions $W_S(\lambda)$, $W_T(\lambda)$, and $\Delta W(\lambda)$ as illustrated in Fig. A-1. From this figure it may be seen that a solar environment tends to emphasize the short wavelength portion of the detector response while a tungsten simulator tends to emphasize the longer wavelength region of interest by filtering the tungsten illumination with a Corning #1-59 filter. Comparative normalized curves for the solar spectrum and the filtered tungsten are illustrated in Fig. A-2.

The color correction process is accurate enough to guarantee selection of suitable detector pairs. At null the sensor response function is zero, therefore:

$$R(\theta_N) = 0 = [S_1(\theta_N) - S_2(\theta_N)] \int_0^\infty W(\lambda)T(\lambda)Q(\lambda)d\lambda$$

$$-S_2(\theta_N) \int_0^\infty W(\lambda)T(\lambda)\Delta Q(\lambda)d\lambda$$

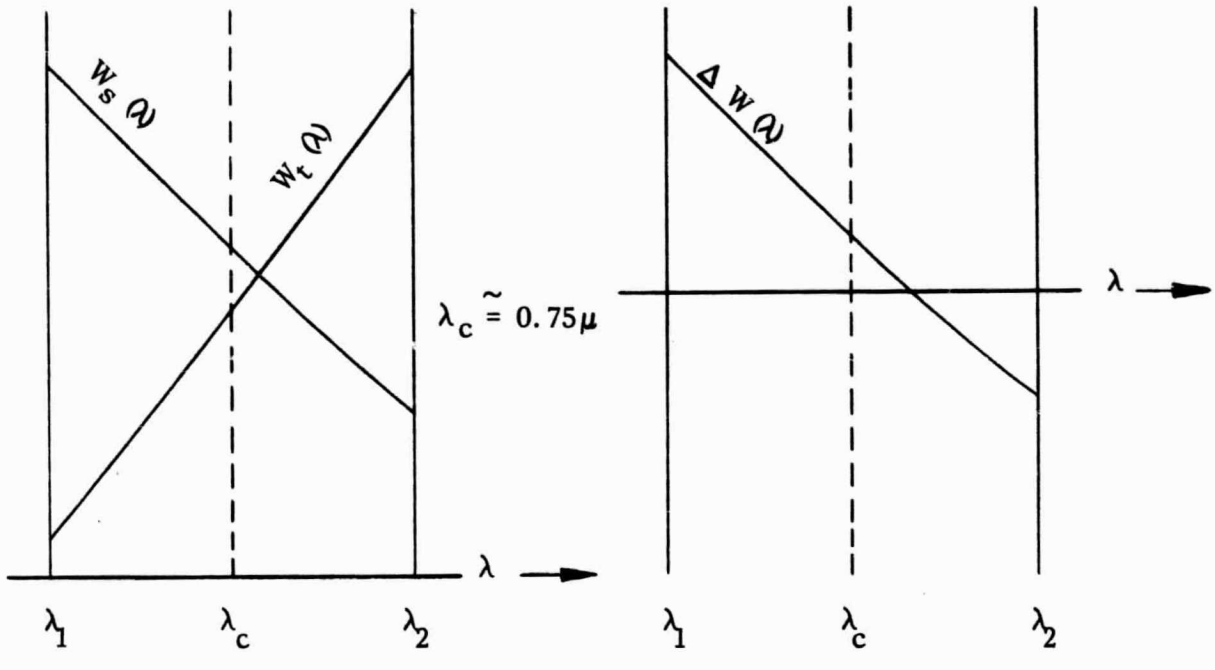


Figure A-1 - General Characteristics of the Spectral Irradiance Function for The Sun and a Tungsten Simulator

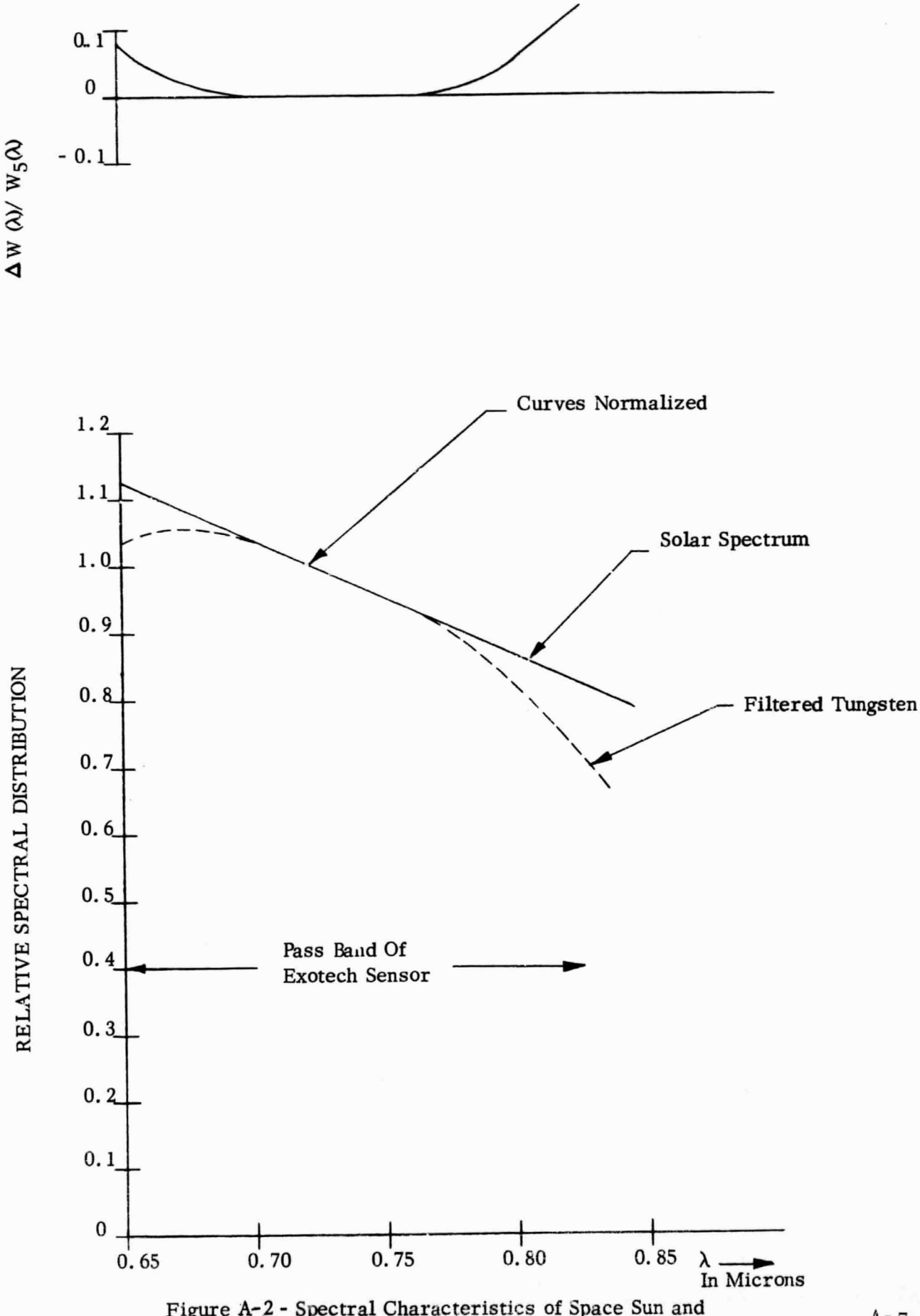


Figure A-2 - Spectral Characteristics of Space Sun and Filtered Tungsten Light

assuming that the second term is small:

$$S_1(\theta_N) \approx S_2(\theta_N)$$

and θ_N will be a small angle.

If the sensor was aligned in a filtered tungsten simulator, thereby defining a null position (θ_N) and a reference surface normal was aligned to the line-of-sight under these conditions and an accurate determination of the constant k had been made the effects on the first term will be negligible leaving an error as follows in a space sun environment.

$$R(\theta_N) = S_2(\theta_N)k \int_o^\infty W_T(\lambda)T(\lambda)\Delta Q(\lambda)d\lambda$$

$$-S_2(\theta_N) \int_o^\infty W_S(\lambda)T(\lambda)\Delta Q(\lambda)d\lambda$$

$$= S_2(\theta_N) \int_o^\infty \Delta W(\lambda)T(\lambda)\Delta Q(\lambda)d\lambda$$

Generally, $S_2(\theta_N)$ is approximately 0.1 for high accuracy sensors, i.e. at null each detector is illuminated with approximately ten per cent of full scale illumination. (For imaging type sensors this results in best linearity through the null region.) Therefore the per cent of full scale offset induced as:

$$\frac{R(\theta_N)}{R(\theta_{FS})} = 0.10 \frac{\int_o^\infty \Delta W(\lambda)T(\lambda)\Delta Q(\lambda)d\lambda}{\int_o^\infty W(\lambda)T(\lambda)Q(\lambda)d\lambda}$$

and since full scale corresponds to an angular error of approximately 2000 arc seconds we have:

$$S = -(2000)(0.10) \frac{\int_0^\infty \Delta W(\lambda) T(\lambda) \Delta Q(\lambda) d\lambda}{\int_0^\infty W(\lambda) T(\lambda) Q(\lambda) d\lambda} \text{ sec.}$$

where: S is the angular error in arc seconds.

In summary, an error of approximately 2 arc seconds occurs if the ratio of the two integrals is one per cent and in order to realize a fractional arc second error contribution from this source the ratio must be less than 0.5 per cent.

If the detector responses are matched to within one per cent over the spectrum of interest (0.65μ to 0.825 μ), the maximum value of the ratio of the two integrals would be:

$$\frac{\int_0^\infty \Delta Q(\lambda) \Delta W(\lambda) T(\lambda) d\lambda}{\int_0^\infty Q(\lambda) W(\lambda) T(\lambda) d\lambda} = \frac{1}{n} \sum_i \frac{\Delta Q(\lambda_i) \Delta W(\lambda_i)}{Q(\lambda_i) W(\lambda_i)}$$

$$= \frac{1}{n} \sum_i (0.01) \frac{\Delta W(\lambda_i)}{W(\lambda_i)}$$

$$= 0.0025 \text{ or } 0.025\%$$

where: n is the number of intervals used in the numerical integration.
This is well within the desired limit of 0.5%.

Changes In Detector Response with Temperature

In general, the detector spectral response is a function of temperature; the near infrared response tends to increase with increasing temperature while the blue response tends to decrease. Since the detectors are expected to operate in sunlight and tungsten illumination, neither of which have equal energies at each wavelength, changes in spectral response will result in output current variations. These variations will be manifested in a temperature dependent gain constant, k, as well as a temperature dependent offset if differential response shifts occur.

During 1965 Heliotek performed an extensive test program to determine the magnitudes of the detector response variations for several filter bandpasses. The results of this program were reported by E. L. Ralph in the "Proceedings of the Fifth Photovoltaic Specialists Conference".[1] A short summary of Heliotek's findings is included in the following paragraph.

A sample of 258 cells was subjected to a rigorous selection procedure which resulted in five groups of matched cells with six detectors in each group. Four of the five groups were placed under narrow-band filters which divided the detector spectral response into four equal parts. The fifth group was used as an unfiltered standard. The spectral transmissions of the filters are illustrated in Fig. A-3. Each of these matched groups was then tested in simulated sunlight as well as outdoor sunlight at Table Mountain, California. Figure A-4 illustrates the reported variations in output for "typical" detectors. Table A-1 is a summary of the actual data.

At first glance, the data shown in Fig. A-4 seems to indicate that the temperature dependence of the detector output for group III is very small, something less than one per cent over the temperature range 10°C to 90°C. However, upon closer examination of the data, comparing the data points at the various temperatures and illumination conditions listed in Table A-1 it is apparent that:

---

1 E. L. Ralph, "Preflight Calibration and Matching of Solar Cells for a Band-Pass Filter Experiment", Proceedings of the Fifth Photovoltaic Specialists Conference, Vol. III, 1965

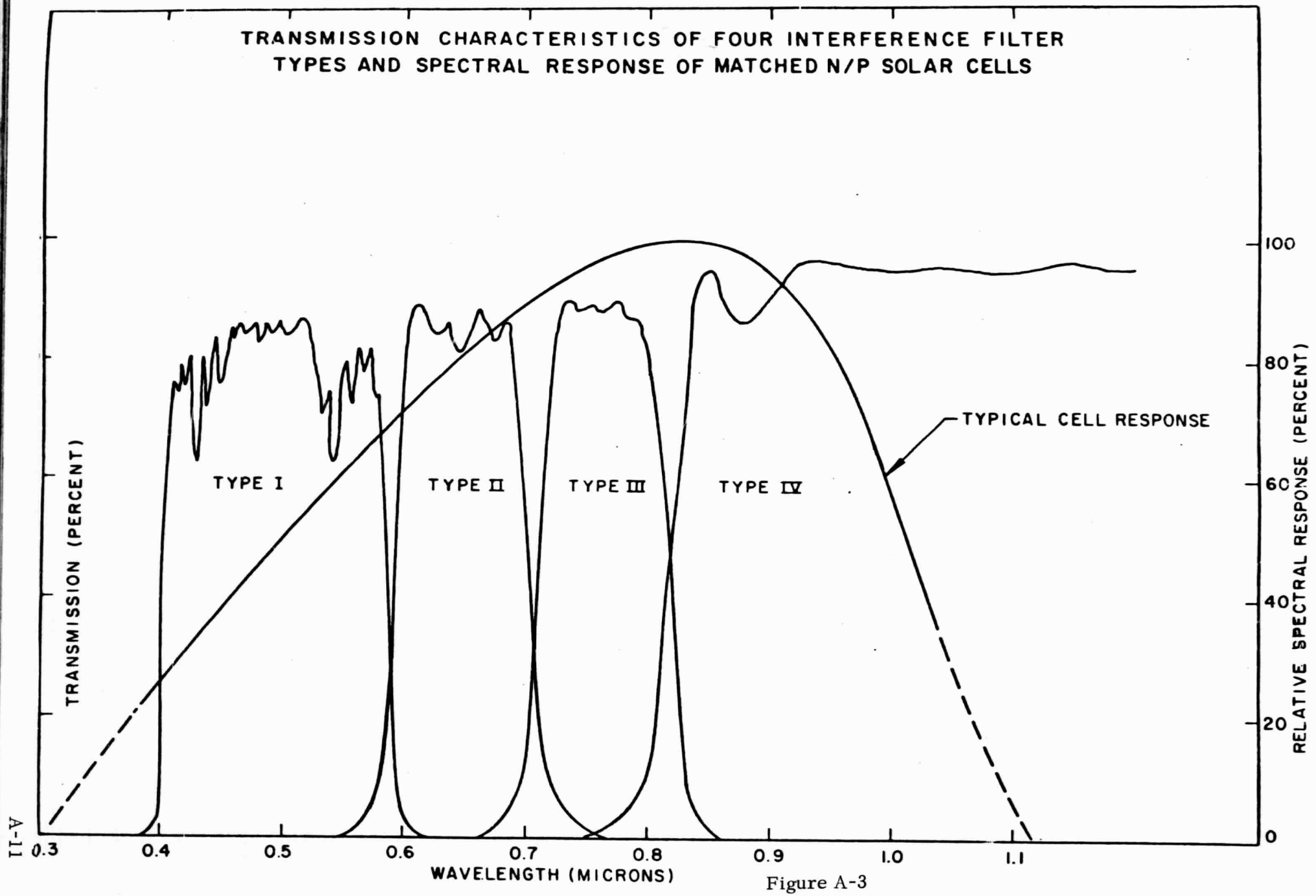

TRANSMISSION CHARACTERISTICS OF FOUR INTERFERENCE FILTER
TYPES AND SPECTRAL RESPONSE OF MATCHED N/P SOLAR CELLS
TRANSMISSION (PERCENT)
RELATIVE SPECTRAL RESPONSE (PERCENT)
TYPE I
TYPE II
TYPE III
TYPE IV
TYPICAL CELL RESPONSE
0.3
0.4
0.5
0.6
0.7
0.8
0.9
1.0
1.1
WAVELENGTH (MICRONS)
0
20
40
60
80
100

Figure A-3

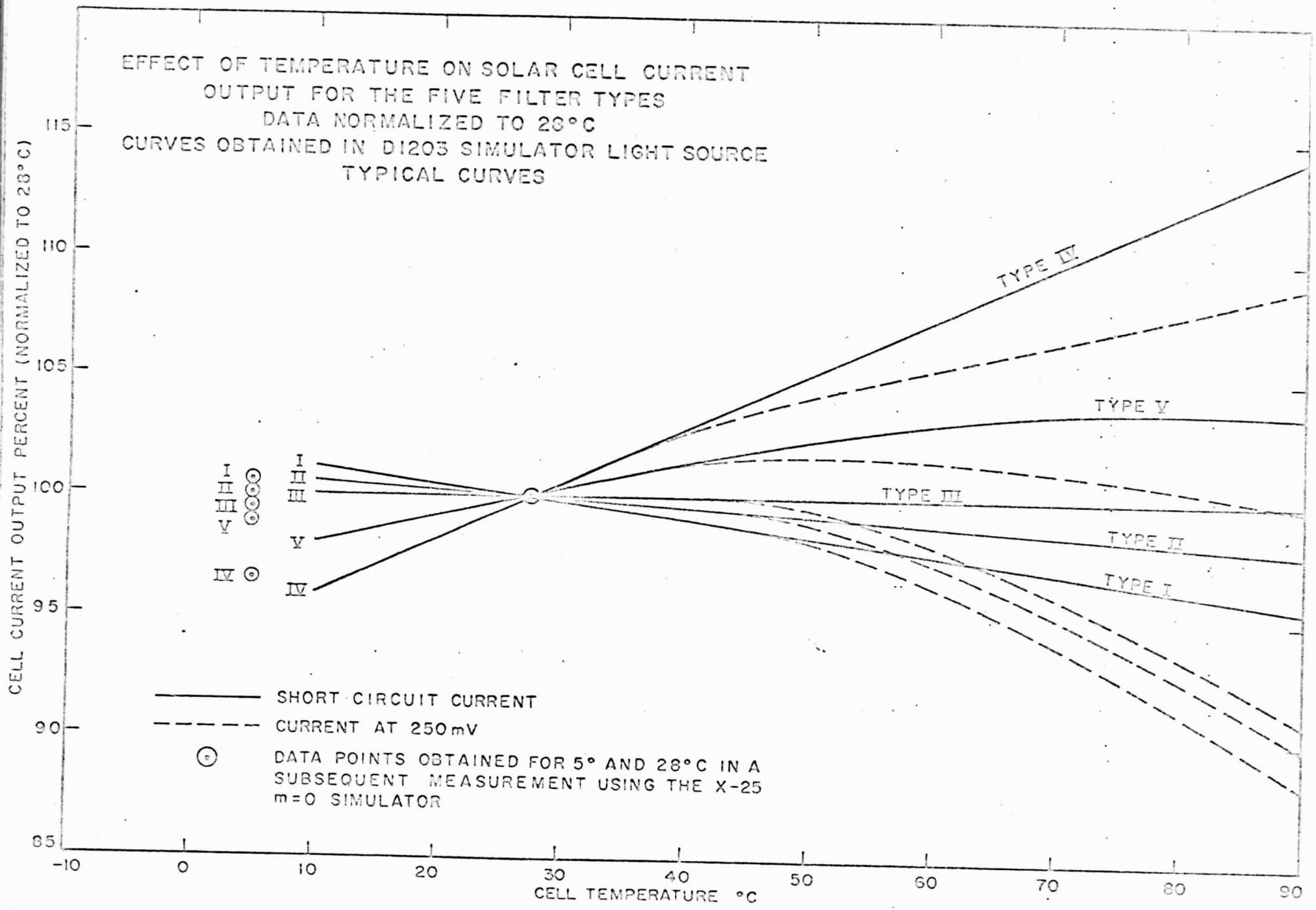


Figure A-4 Effect Of Temperature On Solar Cell Current

"REPRODUCIBILITY OF THE ORIGINAL PAGE IS POOR."

Cells Covered with Filter Type		Voltage At Which I Measured (mV)	Maximum Spread of Current Output in D1203 Solar Simulator (Percent)			Current Spread on Table Mountain (Percent)
I	(6 Cells)	0	3.8	3.0	3.1	0.9
		250	3.8	3.0	3.1	---
II	(6 Cells)	0	2.5	3.7	4.9	0.9
		250	2.5	3.7	7.5	---
III	(6 Cells)	0	0.9	3.6	4.5	1.9
		250	3.6	2.7	11.7	---
IV	(6 Cells)	0	1.9	2.8	3.3	2.9
		250	1.9	2.8	10.7	---
V	(6 Cells)	0	1.5	1.2	1.7	1.1
		250	1.2	1.2	4.0	---

TABLE A-1 -Current Matching in M=0 Simulator and M=1 Sunlight

1. The change with temperature in the maximum spread of current output for the six carefully selected cells of group III was 3.6 per cent, indicating a relative shift between at least two of these detectors of 3.6 per cent.
2. The maximum spread in current output of the detectors in group III changed from 3.6 per cent at 28°C in the DI 203 Solar Simulator to 1.9 per cent under the same environment in Table Mountain sunlight. This indicates that at least two of the six detectors would have given a differential shift of 1.7 per cent had they been used as a matched pair.

Upon a closer examination the data does not bear out a literal interpretation of the conclusions illustrated in Fig. A-4. Furthermore, the data points taken with the X-25 simulator differ by one to two per cent from the data with the DI 203 simulator. In summary, the measurements indicate a trend to the thermal properties of the detectors under the various filtering conditions and represent a marked improvement in knowledge of the behavior of the detectors. However, the reliability of the data appears to be on the order of ±2 per cent which is an order of magnitude or more greater than the accuracy required to reduce the tracking error in a sensor to one arc second.